DISSERTATION

CHARACTERIZING FOREST BIOMASS AND THE IMPACTS OF BARK BEETLES AND FOREST MANAGEMENT IN THE SOUTHERN ROCKY MOUNTAINS, USA

Submitted by

Anthony Grant Vorster

Graduate Degree Program in Ecology

In partial fulfillment of the requirements

For the Degree of Doctor of Philosophy

Colorado State University

Fort Collins, Colorado

Summer 2020

Doctoral Committee:

Advisor: Paul Evangelista

Seth Ex
Catherine Jarnevich
Keith Paustian

ABSTRACT

CHARACTERIZING FOREST BIOMASS AND THE IMPACTS OF BARK BEETLES AND FOREST MANAGEMENT IN THE SOUTHERN ROCKY MOUNTAINS, USA

Overview: Forest carbon sequestration is key in mitigating rising atmospheric carbon concentrations. Recent bark beetle (Curculionidae: Scolytinae) outbreaks have decreased forest carbon stocks across millions of hectares of the western United States (U.S.) since the mid-1990s. Bark beetle outbreaks cause forests to temporarily act as a carbon source and also alter resistance to future disturbances by impacting species composition and forest structure. This dissertation first assesses the quantity and distribution of forest biomass in northern Colorado and southern Wyoming from the tree to landscape scale. In my first chapter, I compare variability and uncertainty in biomass estimates using different allometric biomass equations. In the next chapter, I map tree mortality in lodgepole pine (*Pinus contorta* var. *latifolia* Engelm. ex Wats.) forests of Colorado, Wyoming, Montana, and Idaho to quantify bark beetle impacts and infer bark beetle population dynamics. In the third chapter, I present a new approach for mapping standing dead biomass, summarizes standing aboveground biomass pools by species and forest type, and provides an assessment of potentially accessible biomass for bioenergy scenarios. Lastly, I simulate the impacts of salvage logging beetle killed stands on aboveground biomass and susceptibility to future mountain pine beetle (*Dendroctonus ponderosae* Hopkins) outbreaks and fire.

Chapter 1: Biomass maps are valuable tools for estimating forest carbon and forest planning. Individual-tree biomass estimates made using allometric equations are the foundation for these maps, yet the potentially high uncertainty and bias associated with individual-tree estimates is commonly ignored in biomass map error. I developed allometric equations for lodgepole pine, ponderosa pine (*Pinus ponderosa* Douglas ex Lawson*)*, and Douglas-fir (*Pseudotsuga menziesii* [Mirb.] Franco*)* in northern Colorado. Plot-level biomass estimates were combined with Landsat imagery and geomorphometric and climate layers to map aboveground tree biomass. I compared biomass estimates for individual trees, plots and at the landscape-scale using locally-developed allometric equations, equations applied across the U.S., and the Forest Inventory and Analysis Component Ratio Method (FIA-CRM). Total biomass map uncertainty was calculated by propagating errors from allometric equations and remote sensing model predictions. Two evaluation methods for the allometric equations were compared in the error propagation; errors calculated from the equation fit (equation-derived) and errors from an independent dataset of destructively-sampled trees (n = 285). Tree-scale error and bias of allometric equations varied dramatically between species, while local equations were generally most accurate. Depending on the allometric equation and evaluation method, allometric uncertainty contributed 30%-75% of total uncertainty, while remote sensing model prediction uncertainty contributed 25%-70%. When using equation-derived allometric error, local equations had the lowest total uncertainty compared to the nationwide equations and the FIA-CRM (root mean square error percent of the mean [% RMSE] = 50%). This is likely due to low-sample size (10-20 trees sampled per species) allometric equations and evaluation not representing true variability in tree growth forms. When independently evaluated, allometric uncertainty outsized remote sensing model prediction uncertainty. Biomass across the 1.56 million ha study area and uncertainties were similar for

local (2.1 billion Mg; % RMSE = 97%) and nationwide (2.2 billion Mg; % RMSE = 94%) equations, while FIA-CRM estimates were lower and more uncertain (1.5 billion Mg; % RMSE = 165%). Allometric equations should be selected carefully since they drive substantial differences in bias and uncertainty. Biomass quantification efforts should consider contributions of allometric uncertainty to total uncertainty, at a minimum, and independently evaluate allometric equations when suitable data are available.

Chapter 2: Lodgepole pine has been especially hard-hit by widespread tree mortality over the last two decades, largely due to mountain pine beetle outbreaks triggered by drought conditions and sustained by large swaths of mature host trees. Associated tree mortality has been accurately mapped across relatively small regions using moderate resolution (30 m x 30 m or less) satellite imagery, but accurate estimates of tree mortality across large areas (i.e., multiple states) are needed to assess the impacts and dynamics of these recent outbreaks. In this study, I first mapped mortality severity (i.e., dead canopy area) across the lodgepole pine forests of Colorado, Wyoming, Montana, and Idaho. I then compared modeled mortality severity and extent with U.S. Forest Service Aerial Detection Survey (ADS) observations and field measurements at Forest Inventory and Analysis plots. Attributing summarized ADS data to the models of severity allowed for characterization of outbreak dynamics that would not otherwise be possible using my mortality maps alone, such as the relationship between mortality severity and the timing and duration of events. I found that mountain pine beetle-caused tree mortality dwarfed other insect and disease caused mortality between 2001 and 2013. Colorado and Wyoming experienced higher severity lodgepole pine forest mortality than Idaho and Montana. Mortality severity and variability in severity increased with duration of mountain pine beetle outbreak in a given stand.

Temporal outbreak severity dynamics suggest that host limitation played an important role in the decline of the recent mountain pine beetle outbreaks. I present a promising method of combining the strengths of satellite remote sensing (more accurate assessment of mortality severity and extent) with the strengths of aerial forest insect and disease surveys (identification of the cause and timing of mortality) that can elucidate spatiotemporal forest disturbance dynamics across large geographic extents.

Chapter 3: Tree mortality caused by bark beetle outbreaks have dramatically altered forest carbon cycles. Yet, there are significant uncertainties surrounding estimates of dead tree carbon and biomass resulting from these bark beetle outbreaks. Refining these estimates can improve understanding of how bark beetles impact the forest carbon cycle, and also inform bioenergy and bioproduct industries interested in utilization of beetle-killed wood. The quantification of tree mortality and total biomass are sources of uncertainty in methods to map standing dead biomass. In this study, I use improved estimates of tree mortality severity along with biomass maps and Forest Inventory and Analysis data to map standing dead aboveground biomass in north-central Colorado and southern Wyoming, one of the most severe bark beetle impacted areas of the western U.S. Individual tree dead biomass is calculated by adjusting for structural loss and density reduction. I then tested a number of models to map standing dead biomass; the random forest model performed best (root mean square error = 28.8 Mg ha^{-1}, R^2 = 0.4719). Maps of standing dead biomass were subtracted from total biomass maps to estimate standing live biomass. The plot data showed more live than dead lodgepole pine, the preferred host for the mountain pine beetle outbreaks that impacted this region. According to the biomass maps, about a third of total biomass was dead in lodgepole pine and spruce-fir forests. This approach for

mapping standing dead tree biomass from biotic disturbances, such as bark beetles, relies upon existing, continuing, and free data sources and thus has potential to be repeated elsewhere and scaled up. The biomass maps were used to approximate potentially accessible dead, live, and total aboveground biomass at hypothetical bioenergy and bioproduct production sites for four production scenarios. Higher-elevation sites with more accessible biomass could support 20 years of bioenergy production with between 0.4% and 23.7% of potentially accessible biomass, depending on the bioenergy production scenario. Standing dead biomass accounted for up to a third of this feedstock. At lower-elevation, low-biomass sites, the high feedstock demand scenario is unlikely to be feasible, requiring nearly 70% of accessible biomass over a 20 year period. More accurate dead tree biomass quantification can better characterize disturbance impacts on the forest carbon cycle and can be used to assess the potential for utilization in bioenergy production.

Chapter 4: Post bark beetle outbreak salvage harvesting is common in Rocky Mountain forests. Decisions to salvage harvest will have lasting legacies on forest carbon storage and resistance and resilience to future disturbances. Stand recovery will unfold in the context of climate change impacts to regeneration, growth, and mortality. The objective of this chapter was to simulate the stand-level impacts of harvesting bark beetle-impacted stands and climate change on forest carbon, fuels, and susceptibility to future mountain pine beetle outbreaks. I used the Forest Vegetation Simulator to project growth in 47 mountain pine beetle-impacted lodgepole pine stands in northern Colorado and southern Wyoming for 100 years. I compared salvage harvest to an untreated scenario, with and without climate change. In the absence of climate change, salvage harvesting reduced total stand carbon for roughly 80 years and also lessened

susceptibility to future mountain pine beetle outbreaks. Impacts on canopy fuel characteristics were more nuanced and temporally variable. Climate change substantially reduced suitability of this study area for lodgepole pine, which caused mountain pine beetle susceptibility and live forest carbon stocks to plummet. The impacts of climate change on stand structure, forest carbon, and disturbance susceptibility outsized the effect of salvage treatments. Future work should explore the variability in stand responses to salvage harvesting and account for spatial disturbance interactions. This study underscores the importance of including climate change impacts when evaluating management actions, despite the difficulties and uncertainties it presents.

ACKNOWLEDGEMENTS

This dissertation is the product of a supportive personal and scientific community—I extend my sincere gratitude to all who have supported me in this endeavor. The talented and accomplished researchers at the Natural Resource Ecology Laboratory and the Graduate Degree Program in Ecology have been role models and have shown me what an impactful career as an ecologist can look like. Thank you to my committee—Seth Ex, Catherine Jarnevich, and Keith Paustian. I appreciate the mentorship you have each provided. I also extend tremendous gratitude to my advisor, Paul Evangelista, for the support, mentorship, and the countless opportunities he provided throughout graduate school. Nick Young has also helped me over the years as a colleague always willing to brainstorm ideas, and as a friend always willing to play basketball. Thanks to Brian Woodward for also being an incredible colleague and friend. Special thanks to Bob Sturtevant and Bill Romme for the myriad lessons you have taught me about being top-notch foresters, scientists, and people. I have been lucky to have a great community of fellow graduate students and researchers—Steve Filippelli, Ezequiel Fernandez Tschieder, Atticus Stovall, Ryan Anderson, Peder Engelstad, Kristen Dennis, Ben Bagdon, Trung Nguyen, John Field, Aaron Sidder, Abby Eurich, Allie Rhea, Jody Vogeler, Tim Mayer, Dan Carver, Rebecca Girma, Steve Chignell, Matt Luizza, and Amanda West.

My friends and family may not have always understood what I was doing, but were always supportive. Thank you to my wonderful wife, Avery Vorster, for supporting me through field seasons and long work days, and for helping me balance grad school demands with the joys of life. My daughter, Hazel, also provided joy and perspective to keep me grounded and happy—thank you! Last, but not least, thank you to my parents, brothers, and in-laws. I love you all.

The chapters that follow were accomplished through many collaborations. I recognize the following individuals for their contributions: Paul Evangelista, Atticus Stovall, Seth Ex, Brian Woodward, Nicholas Young, Rebecca Girma, Jillian LaRoe, Steven Filippelli, Timothy Mayer, Julia Sullivan, Emma Bode, Rick Lawrence, Ben Bagdon, John Field, Trung Nguyen, and Keith Paustian.

This work was largely supported by the Bioenergy Alliance Network of the Rockies project through the Agriculture and Food Research Initiative Competitive Grant [Grant number 2013-68005-21298] from the U.S. Department of Agriculture National Institute of Food and Agriculture. Support was also provided by the Colorado Water Center and by the National Aeronautics and Space Administration through contract NNL16AA05C and cooperative agreement NNX14AB60A. Any opinions, findings, and conclusions or recommendations expressed in this material are those of the authors and do not necessarily reflect the views of the National Aeronautics and Space Administration.

TABLE OF CONTENTS

LIST OF KEYWORDS

allometric equations, biomass, *Dendroctonus ponderosae*, forest carbon, forest disturbance, Forest Vegetation Simulator, Google Earth Engine, Landsat, lodgepole pine, mountain pine beetle, *Pinus contorta*, random forest, remote sensing, uncertainty

INTRODUCTION

Forests play an important role in the global carbon cycle. Forest and forest products of the U.S. store 216-313 Tg carbon annually, offsetting about 10-20% of annual U.S. fossil fuel emissions (Mckinley et al., 2011). Forest carbon uptake is spatially and temporally variable; carbon is released through decomposition and combustion, in the case of fire, following disturbances and is then recaptured when forests regrow. As forests cycle through disturbance and recovery, they change between capturing more carbon than they release (carbon sink) and releasing more carbon than they capture (carbon source). These processes tend to balance out, making forest carbon stocks relatively stable over large spatial and temporal scales (Kashian et al., 2006). However, disturbance regime changes and interactions can alter carbon storage (Kashian et al., 2006; Smithwick et al., 2007). North American forests were a carbon source during the 19th century due to extensive timber harvesting, fires, and land use change. These forests then became carbon sinks in the 20th century as the forests recovered. United States forest carbon stocks are increasing by 190 Tg C yr^{-1}, contributing 17% of the global forest carbon increase (Williams et al., 2016).

Harvesting was responsible for the most mean annual tree mortality (23.0 ± 2.8 Tg C yr^{-1}) in the western U.S. between 2003 and 2012, followed by bark beetles (Curculionidae: Scolytinae; 14.6 ± 7.0 Tg C yr^{-1}) and fire (8.2 ± 6.2 Tg C yr^{-1}) (Berner et al., 2017). Forests recover to become carbon sinks for 5-23, 4-34, or 1-15 years after fire, insect outbreak, or timber harvest, respectively, and recover to pre-disturbance carbon stocks after 30-78, 7-76, or 12-88 years (Raymond et al., 2015). The rate of carbon recovery is sensitive to disturbance type, disturbance severity, and pre-disturbance carbon levels (Hicke et al., 2012; Raymond et al.,

2015). Many models of carbon recovery after disturbances make the assumption of an undisturbed recovery (Caldwell et al., 2013; Pfeifer et al., 2011; Raymond et al., 2015). In reality, disturbances affect ecosystem resistance (likelihood, extent, and severity) and resilience (recovery rate or trajectory) to future disturbances (Buma, 2015). Research is needed to understand how recent disturbances have impacted forest carbon, and how the interaction of disturbances may impact carbon storage over time. The uncertainty of how climate change may impact disturbance severity and frequency, and growth rates adds to the challenge of predicting carbon trajectories (Bentz et al., 2010; Crookston et al., 2010; Loudermilk et al., 2013; Westerling et al., 2011).

Rocky mountain forests are in a period of historically high tree mortality from wildfire (Westerling et al., 2006) and bark beetle activity (Raffa et al., 2008). Climate change has, and will likely continue to, contribute to the increasing extent and severity of these disturbances through drought and warmer temperatures (Cudmore et al., 2010; Sidder et al., 2016; Westerling, 2016). While mountain pine beetle outbreaks are temporally cyclical within a given area (Taylor et al. 2006), new areas of intensive mortality have been observed consistently for decades. The mountain pine beetle (*Dendroctonus ponderosae* Hopkins) outbreaks that impacted lodgepole pine (*Pinus contorta* var. *latifolia* Engelm. ex Wats.) forests across western North America between the 1990s and 2010s caused tree mortality across millions of acres of lodgepole pine forest (Raffa et al., 2008).

Consistent data on the extent and severity of biotic disturbances is needed (Kautz et al., 2017). Monitoring of these forest disturbances and tree mortality is critical to the accurate measurement of forest carbon (Hicke et al., 2013; Volkova et al., 2018), and to effectively manage beetle-affected forest systems and timber resources. Images from the Landsat series of

satellites have been used to map the severity of tree mortality caused by bark beetles (Bode et al., 2018; Long and Lawrence, 2016; Vorster et al., 2017; Woodward et al., 2018), but these methods have not been scaled up to multi-state extents. Landsat is moderate-resolution (30m x 30m pixel size), multispectral, free, and has an extensive historical record spanning 1972 to present, making it an ideal candidate for ecological monitoring (Young et al., 2017). Landsat has also been frequently utilized to map forest biomass and structure (Hall et al., 2006; Kelsey and Neff, 2014; López-Serrano et al., 2016; Powell et al., 2010).

With such high attention on forest carbon sequestration, it is critical to understand current forest carbon stocks and how these stocks respond to disturbance, management, and climate changes (Williams et al., 2016). There are many sources of error when estimating forest biomass such as error from the allometric equations used to estimate individual tree biomass and error from the remote sensing models used to extrapolate biomass estimates across the landscape (Chave et al., 2004; Chen et al., 2015; Stovall and Shugart, 2018). Research is needed to understand the total and relative contributions of these error sources. Methods to advance mapping of bark beetle-killed biomass are also needed (Ghimire et al., 2015). Such refinements to forest carbon accounting methodologies are improving our understanding of the forest carbon cycle. For example, taking a field-based approach to estimating standing dead tree carbon rather than a model-based approach used in the U.S. National Greenhouse Gas Inventory revealed that model-based methods were over-estimating dead tree carbon by nearly 100%, which was inflating total forest carbon estimates for the U.S. (Woodall et al., 2012).

The use of forests to mitigate climate change has received considerable attention in science and policy discussions (Keith et al., 2015; Schulze et al., 2012). Policies, such as the recent Clean Energy Plan (among many others), classify forest bioenergy as carbon neutral

because forests recapture carbon when they regrow. The literature shows this to be false, however, because it does not consider the growth in the absence of bioenergy production, carbon emissions needed to harvest, transport, and produce the bioenergy and the elevated atmospheric carbon concentrations while the forest is recovering (Keith et al., 2015; Schulze et al., 2012; Ter-mikaelian et al., 2015). Forest bioenergy production results in a carbon debt for decades to centuries (Holtsmark, 2012; Schulze et al., 2012) and in some cases it may never be favorable (Hudiburg et al., 2011). The carbon footprint of forest bioenergy depends on many factors, such as the fossil fuel being replaced and the local forest carbon cycle. The comparison of bioenergy harvested forest stands to the untreated alternative need to extend for long time periods (>100 years), and thus should account for the uncertain impacts of climate change.

It is possible that one system where bioenergy production would have climate change mitigation benefits is bark beetle-impacted, fire-prone forests (Hudiburg et al., 2011). Bioenergy produced from these forests may have a favorable carbon footprint because carbon that would be released by decomposition or fire is instead used to displace fossil fuels. Interest in utilizing beetle-killed wood goes beyond carbon storage considerations; concerns about public safety from falling dead trees, forest health, fire behavior, and loss of timber value have motivated utilization. These concerns contributed to the 2.5-fold increase in timber harvesting from the 1990's to 2000's in northern Colorado (Collins et al., 2010). The use of beetle-killed wood for bioenergy production has been proposed (Campbell et al., 2018; Field et al., 2018). Producing bioenergy from beetle-killed biomass is attractive because it requires no cultivation, would create a market for low-value biomass, avoids the food versus fuel debate, and potentially has a favorable carbon balance compared to fossil fuels. However, the feasibility and carbon consequences of using beetle-killed wood as a biofuel are poorly understood. Information about

the quantity, distribution, and condition of beetle-killed biomass is needed to assess the feasibility and sustainability of such an industry. This work will contribute to this feasibility and sustainability assessment.

In the four chapters that follow, I address these knowledge gaps through the following objectives:

Chapter 1 Objectives

- Develop local allometric biomass equations for lodgepole pine, ponderosa pine (*Pinus ponderosa* Douglas ex Lawson), and Douglas-fir (*Pseudotsuga menziesii* [Mirb.] Franco) and use them to estimate biomass in forest inventory plots.
- Combine field data and remote sensing to map standing aboveground forest biomass for montane and subalpine forests in northern Colorado and southern Wyoming.
- Analyze the biomass differences at the tree, plot, and landscape scale between locally-developed allometric equations and two widely-used allometric biomass equations.
- Propagate the allometric error measured against an independent validation dataset and the remote sensing modeling error to quantify biomass map total uncertainties and the relative importance each error source.

Chapter 2 Objectives

- Model dead canopy area (mortality) across lodgepole pine forests in four Rocky Mountain states impacted by severe mountain pine beetle outbreaks between 2000 and 2013.
- Compare modeled mortality severity and extent with Aerial Detection Surveys (ADS) and field observations.

- ❖ Fuse ADS and modeled mortality severity to characterize mortality severity relative to timing, duration, and region.

Chapter 3 Objectives

- ❖ Test new methods for mapping aboveground standing dead biomass in a landscape impacted by numerous bark beetle outbreaks.
- ❖ Evaluate the distribution of dead and live standing aboveground biomass by species and forest type.
- ❖ Use live, dead, and total biomass maps to quantify potentially accessible biomass for hypothetical bioenergy production scenarios and facility locations.

Chapter 4 Objectives

- ❖ Simulate the stand-level impacts of harvesting bark beetle-impacted stands on forest carbon, fuels, and susceptibility to future mountain pine beetle outbreaks.
- ❖ Project the potential impacts of climate change on forest development after salvage harvest.

CHAPTER 1 — VARIABILITY AND UNCERTAINTY IN FOREST BIOMASS ESTIMATES FROM THE TREE TO LANDSCAPE SCALE: THE ROLE OF ALLOMETRIC EQUATIONS

Introduction

Spatially explicit aboveground biomass estimates are critical for monitoring forest carbon storage and for strategic forest planning (Dilling et al., 2016; Graham et al., 2017; McRoberts et al., 2019). They provide baseline inventories that capture the legacy of past land use and disturbance while serving as a reference point for studying the impacts of subsequent disturbances (Baccini et al., 2012). Forest biomass maps are also a critical tool for measuring, reporting, and verifying forest carbon stocks (Baker et al., 2010). Programs such as Reducing Emissions from Deforestation and forest Degradation (REDD+) and California cap-and-trade seek to mitigate rising greenhouse gas concentrations by storing carbon in forests. The financial incentives tied to forest carbon in these programs have led countries and forest landowners to closely track their forest carbon. Individual-tree biomass calculated from allometric equations are the foundation for these estimates, but can have high uncertainty and bias that propagate to biomass/carbon estimates (Chave et al., 2004; Mitchard et al., 2014). Widely-used allometric equations must be independently evaluated using tree biomass datasets to identify error and bias (Duque et al., 2017).

Allometric equations provide biomass estimates from tree measurements, such as diameter at breast height (DBH), height, and/or wood density. These equations capture the scaling relationships between tree form and function to predict total and component (e.g., branch, needle, bark, bole, root) biomass (West et al., 1999). Allometric relationships are commonly developed from trees sampled across large areas (Chojnacky et al., 2014; Jenkins et al., 2003; Ter-Mikaelian and Korzukhin, 1997). In the U.S., two widely-applied allometric equations are

the Forest Inventory and Analysis Component Ratio Method (FIA-CRM) (Heath et al., 2009; Woodall et al., 2011) and from Jenkins et al. (2003). The FIA-CRM is used to calculate forest carbon for the U.S. Environmental Protection Agency's (EPA) annual greenhouse gas inventory (Environmental Protection Agency, 2018) and for California cap-and-trade projects. The Jenkins et al. (2003) equations were used for the EPA annual greenhouse gas inventory in the past, are part of the FIA-CRM, and are an option in the Fire and Fuels Extension of the Forest Vegetation Simulator (Rebain et al., 2010).

Allometric equations are frequently applied outside populations from which they were developed, potentially leading to significant biomass estimation errors (Weiskittel et al., 2015). Allometric relationships vary spatially with differences among trees (i.e., species and genetics) and growing conditions (i.e., site productivity arising from nutrient availability, soil type, and climate, competition and tree age) (Feldpausch et al., 2011; Peichl and Arain, 2007; Yang et al., 2019). Where available, locally-developed equations offer an alternative to more generic equations and can be better tuned to local species, growth forms, and environments. However, locally-developed allometric equations are typically developed from small sample sizes, potentially rendering them biased, unreliable, and prone to measurement error (Chave et al., 2004; Weiskittel et al., 2015). Some studies suggest locally-developed allometric equations are more accurate (Daba and Soromessa, 2019; van Breugel et al., 2011; Zhao et al., 2012), while other studies have found that generic allometric equations perform better (Feldpausch et al., 2011; Montagu et al., 2005; Rutishauser et al., 2013). Another method for developing more robust allometric equations is to tune generic allometric equations to better represent local growth forms. For example, the FIA-CRM uses regional stem volume equations to rescale biomass predictions made by generic allometric equations (Heath et al., 2009). Ultimately, those

conducting biomass inventories are left with the choice of selecting allometric equations, or must take on the time-consuming, expensive, and difficult task of building their own allometric equations. The choice of allometric equation can have significant impacts on biomass estimates (Phillips et al., 2016; van Breugel et al., 2011).

To map biomass across landscapes, allometric biomass equations are applied to individual tree measurements, which are summed across forest inventory plots that calibrate larger-scale remote sensing datasets (e.g., Phillips et al., 2016). Biomass and forest structure are frequently mapped using freely-available images from Landsat satellites (Hall et al., 2006; Kelsey and Neff, 2014; López-Serrano et al., 2016; Powell et al., 2010). Landsat satellites acquire moderate resolution (30m x 30m pixel size) multispectral data that have an extensive historical record spanning 1972 to present, making these sensors ideal candidates for ecological monitoring and estimating forest productivity (Boisvenue et al., 2016). Landsat spectral bands, vegetation indices, and texture metrics are useful predictors of forest biomass (Eckert, 2012; Kelsey and Neff, 2014; Lu, 2005; Lu and Batistella, 2005; Zhao et al., 2016). Since Landsat and other optical sensors rely on detectable changes in canopy closure, one issue is underestimation, or saturation, of predictions at high biomass values and in closed-canopy forests. Landsat-based biomass mapping may, however, be aided in the western U.S. by the strong biophysical gradients of forest type and biomass and the open canopies of some of the forests (Powell et al., 2010). Biomass predictions can be improved by supplementing remote sensing imagery with climate, topography, and landform data that are correlated with forest biomass (Swetnam et al., 2017). Active sensors, such as LiDAR (Light Detection and Ranging), can also improve Landsat-based biomass estimates by providing accurate information about forest structure and height (Zolkos et al., 2013), but spatial and temporal data coverage is limited and collection is expensive.

There are many sources of uncertainty when mapping biomass, such as tree measurements, allometric models, plot representativeness, and remote sensing model fitting and prediction (Chave et al., 2004; Chen et al., 2015). Biomass maps are commonly evaluated by comparing predicted pixel biomass to observed plot biomass values, treating the plot biomass as "truth." This approach only captures one source of error; variability or errors in the remote sensing model. While this is certainly a major error source, failing to account for other error sources underlying tree and thus plot-level biomass calculations underestimates uncertainty (Chen et al., 2015; Mitchard et al., 2014). Allometric model uncertainty accounts for the majority of the tree-level uncertainty, and can be biased (Chave et al., 2004; Stovall and Shugart, 2018). Tree measurement errors of attributes, such as DBH and height, can also be significant (Chen et al., 2015). Since allometric error is generally calculated from the same trees used to develop the equations (i.e. lacking independent validation), issues such as sampling bias may not be captured in uncertainty measures. Although it is rare to have an independent dataset of destructively sampled trees, allometric error and bias are best captured by comparing predictions to trees within the study area that are independent of the allometric equation generation.

In this study, I estimate standing aboveground forest biomass using multiple allometric equations for montane and subalpine forests in the southern Rocky Mountains. I developed local allometric biomass equations for lodgepole pine, ponderosa pine, and Douglas-fir, and use them to estimate biomass in Forest Inventory and Analysis (FIA) plots. With these plot-level biomass estimates, Landsat Enhanced Thematic Mapper Plus (ETM+) imagery, and geomorphometric and climate layers I use a machine learning algorithm to calibrate several biomass maps covering 1.56 million ha. I analyzed the magnitude and patterns of biomass differences at the tree, plot, and landscape scale between locally-developed allometric equations and two widely-used

allometric biomass equations: Jenkins et al. (2003) and the FIA-CRM (Heath et al., 2009; Woodall et al., 2011). Using an independent validation dataset (Radtke et al., 2015), I evaluated accuracy and bias of the three allometries. Finally, I propagated allometric error to the final remote sensing calibration model to quantify biomass map uncertainties and the relative importance each error source.

Methods

Study Area

This study was conducted across 1.56 million ha of forest in northern Colorado and southern Wyoming bound by Landsat scene path 34, row 32 (Figure 1.1). Mean temperature and precipitation vary along an elevation gradient from 52 °C and 31 cm at lower elevation montane forests to -3 °C and 180 cm at higher elevation subalpine forests (Wang et al., 2016). Forest species composition also changes with elevation and aspect. Montane forests dominated by ponderosa pine start between 1,540 m and 1,845 m above sea level (asl) and become more mixed with Douglas-fir and quaking aspen (*Populus tremuloides* Michx.) as elevation increases (Huckaby et al., 2003). Douglas-fir is particularly common on north-facing slopes. Lodgepole pine and limber pine (*Pinus flexilis* James) join the species mix at about 2,460 m asl. Lodgepole pine is the dominant tree species above 2,770 m, mixed with quaking aspen, limber pine, subalpine fir (*Abies lasiocarpa* [Hook.] Nutt.) and Engelmann spruce (*Picea engelmannii* Parry ex Engelm.). These lodgepole pine forests experienced extensive mountain pine beetle induced tree mortality starting at low levels in the early 2000s, peaking between 2006 and 2009, and declining in 2010 (Walter and Platt, 2013). Subalpine fir and Engelmann spruce take over as the predominant tree species between 3,077 m and treeline (~ 3,540 m asl) (Huckaby et al., 2003).

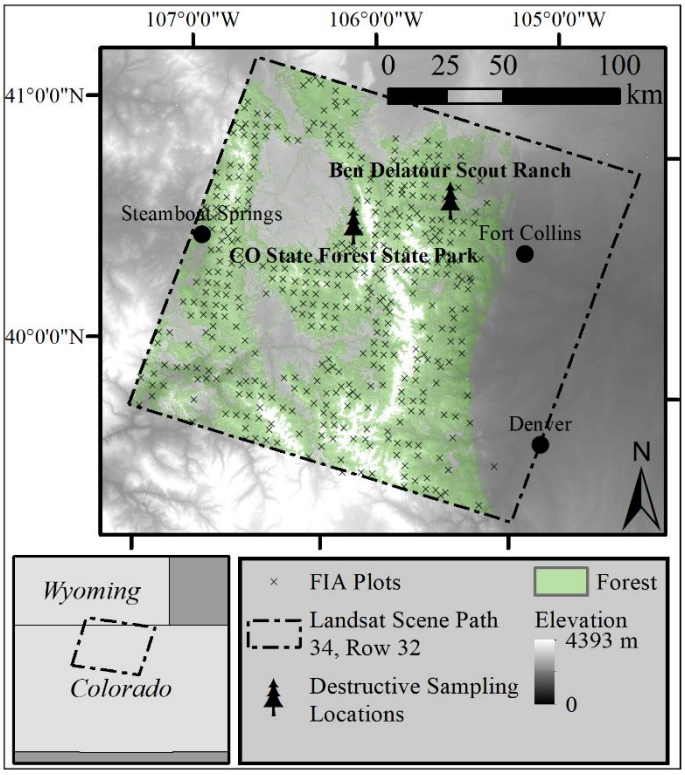

Figure 1.1. Study area map showing the destructive sampling sites, the approximate locations of Forest Inventory and Analysis (FIA) plots, and the forest extent within Landsat scene path 34, row 32.

Allometric Equations

Destructive Sampling

The destructive biomass sampling required to build the local allometric biomass equations was conducted at two sites (Figure 1.1). Lodgepole pine was sampled at the Colorado State Forest and the ponderosa pine and Douglas-fir trees were sampled at the Ben Delatour Boy Scout Ranch. I selected trees free of deformities that represented the diameter range in each area: 20 lodgepole pine, 10 ponderosa pine, and 10 Douglas-fir. The larger-diameter lodgepole pine (n = 14) were sampled in a mature, even-aged stand at 2,700 m asl that was impacted by a mountain pine beetle outbreak around 2007 which killed 75% of the basal area, as measured by inventory plots around the destructively sampled trees. The smaller trees (<14 cm; n = 6) were sampled

near the mature lodgepole pine sampling site in a regenerating clearcut at 2,800 m asl that was pre-commercially thinned a year prior to destructive sampling. Both stands were lodgepole pine-dominated. The ponderosa pine trees were sampled from a mixed-age forest at 2,300 m asl that had irregular structure consisting of patches of trees as well as open-grown trees. While ponderosa pine was the dominant tree in this area, Rocky Mountain juniper (*Juniperus scopulorum* Sarg.) were interspersed. The Douglas-fir were sampled from a Douglas-fir-dominated stand at 2,300 m asl that also contained ponderosa pine and Rocky Mountain juniper.

The destructive sampling procedure (Chung et al., 2017; Stovall et al., 2017) was designed to measure dry biomass of the bole, bark, branch, and foliage components, as well as total aboveground biomass of each tree. The bole is the main stem (without bark) between the 1-foot stump and where the bole reaches a 10.2 cm (4 inch) diameter, hereafter referred to as the 10.2 cm top. The bark component is all bark on this same portion of the main stem. Foliage represents all needles on the tree. Branch biomass includes wood and bark of the main stem above the 10.2 cm top and all other branches. In the destructive sampling procedure, the wet mass of the whole tree was weighed as components in the field and then subsamples were retained to determine moisture contents. These methods are described in detail in Stovall et al. (2017) and Appendix 1.1. Methods for calculating the biomass of each component are also detailed in Appendix 1.1.

Allometric Equation Calculation

Allometric biomass equations for the components of each tree were generated using nonlinear seemingly unrelated regression. Seemingly unrelated regression is well-suited for allometric biomass equations because it allows for dependencies between error terms of the component equations and the equations can be constrained to ensure tree components sum to

total aboveground biomass (Carvalho and Parresol, 2003; Chung et al., 2017; Parresol, 2001; Poudel and Temesgen, 2016). I used the logarithmic model form,

(1) $Biomass = \exp(a_{11} + a_{12} * \ln(DBH))$

which is commonly used for tree biomass estimation (Jenkins et al., 2003; Nay and Bormann, 2014; Poudel and Temesgen, 2016) and appeared to fit scatterplots of the biomass data for all three species. I implemented the nonlinear model form rather than the log–log transformed linear model to avoid back-transformations and to allow for the inclusion of component zero values for trees too small to have bole and bark biomass under the component definitions. Nonlinear seemingly unrelated regression was implemented in SAS OnDemand software (SAS Institute Inc, 2017) to estimate parameters for the following set of equations for lodgepole pine, ponderosa pine, and Douglas-fir:

(2) $Bole = \exp(a_{11} + a_{12}X)$

(3) $Bark = \exp(a_{21} + a_{22}X)$

(4) $Foliage = \exp(a_{31} + a_{32}X)$

(5) $Branch = \exp(a_{41} + a_{42}X)$

(6) $Total = \exp(a_{11} + a_{12}X) + e\,\exp(a_{21} + a_{22}X) + \exp(a_{31} + a_{32}X) + \exp(a_{41} + a_{42}X)$

where a_{ij} are the regression parameters (j = 1,2) to be estimated for each component (i = 1,2,3,4) and X is the natural logarithm of DBH in cm. Biomass values are in dry kg. Parameter start values were estimated by solving the linear version of each component model using ordinary least squares (Parresol, 2001).

Allometric Equation Comparison

I estimated aboveground biomass for trees in FIA plots within the study area using three sets of allometric equations. The three sets of allometric equations tested were: (1) the equations presented in Jenkins et al. (2003), (2) the FIA-CRM and (3) a local set of equations. The allometric biomass equations presented by Jenkins et al. (2003) for U.S. tree species were developed using pseudodata generated from published allometric equations. These equations predict total aboveground biomass and component biomass (i.e., foliage, coarse roots, stem bark, stem wood, and branches) as a proportion of aboveground biomass for species groups (e.g., pine, spruce, true fir/hemlock, etc.) from tree DBH. The FIA-CRM method estimates biomass using a fusion of Jenkins et al. (2003) equations and regional stem volume equations compiled in Woodall et al. (2011). Regional equations are used to estimate volume of the merchantable stem, which is then converted to biomass using specific gravity values found in Miles and Smith (2009). Volume estimates account for species, diameter, height, and atypical tree form to deduct missing or rotten bole mass (Heath et al., 2009). The FIA-CRM equations do not estimate foliage biomass. Additional information about how biomass is calculated using FIA-CRM can be found in Appendix 1.1.

Local biomass estimates were made from a variety of allometric equations depending on species. As described above, I developed equations for three dominant tree species in the study area: lodgepole pine, ponderosa pine, and Douglas-fir. For other species, I used equations from the literature that were developed as near as I could find to the study area. I applied equations from Landis and Mogren (1975) for Engelmann spruce and Johnston and Bartos (1977) for aspen. Species covered by the allometry presented in this paper and local equations from the literature accounted for 77% of the basal area in the FIA plots used in this study. I estimated

biomass for all other species (23% of plot basal area) using the FIA-CRM biomass since the FIA-CRM estimates are designed to be more tuned to local conditions.

Biomass estimation

Forest Inventory Data

I used FIA plot data to evaluate biomass variability between allometric equations at the plot scale and to map standing aboveground tree biomass. The FIA program is responsible for systematically monitoring U.S. forests on a 5-10 year cycle (Tinkham et al., 2018). Each FIA plot consists of four 7.3 m radius circular subplots where trees with a DBH of 12.70 cm or greater are measured. Saplings, defined as having a DBH between 2.54 and 12.70 cm, are measured in 2.1 m radius microplots nested within the subplots. Sapling biomass was included in this analysis, but biomass of trees less than 2.54 cm diameter was excluded. I calculated and compared standing aboveground tree biomass at FIA plots measured between 2002 and 2015 (n = 418) using Jenkins et al. (2003), FIA-CRM and the local set of allometric equations. FIA remeasures plots in Colorado about every ten years—only data from the measurement closest to the satellite imagery capture date (2001) were used. I also only used plots designated as a single condition (i.e., forest or land cover type) to avoid spectral confusion that could be caused by heterogeneous plots (Ohmann et al., 2014).

Plots sampled between 2002 and 2015 and satellite imagery from 2001 were used to map total aboveground standing biomass before the mountain pine beetle epidemic caused widespread lodgepole pine mortality in the study area. Plot measurements captured tree mortality not reflected by the 2001 imagery, especially for plots sampled at the latter end of this sampling timeframe. I mitigated differences between image and sampling conditions by including all standing trees, both living and dead, in plot biomass estimates. While some localized areas may

have had significant treefall by 2015, a study in this same area found no change in downed woody material seven years after this outbreak (Klutsch et al., 2009). Most plots were measured towards the beginning of this sample period when dead trees were likely to still be standing. Between 35 and 46 plots were sampled annually between 2002 and 2011 for a total of 393 plots, while only 25 total plots were sampled between 2012 and 2015. Another discrepancy between plot data and the imagery is that the plots continued to grow between image capture and the date-of-sampling. This discrepancy was minor considering the relatively slow growth in this region (e.g., average of 0.94 cm decade^{-1} diameter increment for lodgepole pine) [Bagdon, B., Nguyen, T., Vorster, A.G., Paustian, K., Field, J., unpublished observations] and the other, larger sources of uncertainty. Errors resulting from the temporal mismatch between imagery and plot measurement were deemed worth the tradeoff for more plots to train the remote sensing models.

Mapping Aboveground Forest Biomass

I used a combination of geomorphometric, topographic, climatic, and spectral predictor variable layers to map biomass. Spectral bands, vegetation indices, and image textures were all generated from a Level 1 Terrain-corrected (L1T) Landsat 7 ETM+ image captured on September 24, 2001. The image was accurately geometrically registered (Root Mean Square Error [RMSE] = 3.2m). Areas flagged by the C Function of Mask (CFMask) algorithm as water, cloud shadow, snow, or cloud overlapped with 0.04% of the forested area and were removed from the study. I used digital number for the ETM+ bands, texture, and most vegetation indices since the study encompassed a single scene and point in time (Young et al., 2017). Some vegetation indices required top-of-atmosphere reflectance (second modified soil-adjusted vegetation index, Tasseled Caps, soil-adjusted vegetation index) or surface reflectance (enhanced vegetation index). For these indices, the top-of-atmosphere reflectance and Landsat Climate Data

Record surface reflectance products were used. I used the least processed imagery necessary for each predictor variable (Young et al., 2017). In addition to ETM+ bands, vegetation indices, and texture (Kelsey and Neff, 2014; Lu, 2005; Lu and Batistella, 2005; Zhao et al., 2016), I also generated topographic, geomorphometric, and climatic predictor variables that correlate with tree species and biomass distributions (Evans and Cushman, 2009; Swetnam et al., 2017). See Appendix 1.1 for more information about how these predictor variables were generated and Table A1.1.4 for a list of all predictor variables generated. I had 302 total predictor variables between all band (n = 7), index (n = 16), texture (n = 240), climate (n = 16), and topography and geomorphology layers (n = 23). Values of each predictor variable were extracted for FIA plots using a 3x3 pixel mean since the four FIA subplots cover an area roughly this size (Ohmann et al., 2014).

I mapped biomass only within forested pixels in the study area, as defined by a forest mask developed for this area (Bode et al., 2018). This mask only includes pixels with greater than or equal to ten percent canopy cover as defined by the LANDFIRE Existing Vegetation Cover (LANDFIRE, 2008) product. This aligns with the ten percent canopy cover requirement component of the FIA forest definition.

I mapped standing aboveground tree biomass using a random forest model which is commonly used for remote sensing applications and biomass mapping (Liu et al., 2017; Pflugmacher et al., 2014; Powell et al., 2010). Random forest models are efficient, non-parametric, have strong prediction accuracy, can handle large numbers of predictor variables, and are robust to noise and outliers (Breiman, 2001). In this approach, a regression tree is trained with a random subset of training data and with a random selection of predictor variables at each node. This process is repeated many times to build a “forest” of unpruned decision trees.

Predictions are made as the average of the predictions from all trees (Liaw and Wiener, 2002). Users define the number of trees (ntree) and number of parameters considered at each node (mtry), although the models are relatively stable to parameter adjustments. Data withheld from each tree (out-of-bag data) are used to calculate reliable estimates of error and variable importance, reducing the need to withhold test data (Breiman, 2001). I evaluated the random forest models using pseudo R^2, RMSE, and bias. These three evaluation metrics are indicative of model fit: pseudo R^2 indicates the proportion of the variability explained by the model, RMSE reflects the magnitude of errors between predicted and observed values, and bias shows the degree to which models tend to over- (positive bias) or under-predict (negative bias). Bias and RMSE are also reported as percentages of the observed mean.

I had a large number of predictor variables, so I implemented a data-driven variable selection technique suitable for applications such as this study where prediction is the goal (Table A1.1.5) (Genuer et al., 2015). This method, Variable Selection Using Random Forest (VSURF) (Genuer et al., 2015), is described in Appendix 1.1. After implementing VSURF, I removed variables from variable pairs correlated by 0.7 or more, keeping the variable with the higher variable importance from a random forest model run with all variables in the VSURF prediction set. I measured predictor variable importance by the average decrease in the mean squared error attributable to a particular variable across all trees (Liaw and Wiener, 2002). Several variables correlated by up to 0.75 were retained if the correlated variables contained unique information and retaining both improved model performance.

I repeated this variable selection routine for each set of biomass values (local, Jenkins et al., 2003, and FIA-CRM) and used the selected predictor variables in the randomForest package (Liaw and Wiener, 2002). I tested a range of mtry (1-# of predictors) and ntree (500, 1000, 1500,

2000, 3000, 4000, 5000) values in 10 iterations and selected the parameters that most frequently lead to the smallest out-of-bag errors.

Biomass variability and uncertainty

Biomass variability across tree, plot, and landscape scales

At the tree-, plot-, and landscape-scales, I compared the magnitude and patterns of differences in biomass estimates between the three sets of allometric equations. At the tree-scale, component biomass and total biomass excluding foliage were compared for the species destructively sampled: lodgepole pine, ponderosa pine, and Douglas-fir. Only total biomass excluding foliage was compared for Engelmann spruce, subalpine fir, and aspen. At the plot- and landscape-scales, I compared aboveground biomass for all species.

Some component definitions differed between the three sets of allometric equations so I made the necessary adjustments. Jenkins et al. (2003) and local equations estimated biomass for the same components: bole, bark, branch, and foliage. When comparing local to Jenkins et al. (2003) component biomass estimates, the only adjustment needed was to subtract stump biomass as calculated by FIA-CRM (Raile, 1982) from the Jenkins et al. (2003) branch biomass estimates. This branch component aligned with the FIA-CRM branch biomass definition (sometimes called the top component). The FIA-CRM bole component spanned the same portion of the tree as the local and Jenkins equations but included the bark. So, bole and bark together were compared across all three sets of allometric equations at the tree scale. Another difference in components between estimation methods is that FIA-CRM does not calculate foliage biomass. For tree-scale total biomass comparisons, foliage biomass is excluded from both local biomass estimates and Jenkins et al. (2003) estimates. However, foliage is included for local and Jenkins et al. (2003) estimates, but not FIA-CRM estimates, in plot and landscape-scale comparisons.

For the subset of tree species where local biomass estimates were generated from FIA-CRM equations, foliage biomass as estimated by Jenkins et al. (2003) was added to each tree for plot and landscape-scale local biomass estimates. Aboveground biomass included the stump for FIA-CRM and Jenkins et al. (2003) estimates, but not for the local equations. I remedied this by adding stump biomass as estimated by FIA-CRM (Raile, 1982) to each tree when calculating local total biomass for tree, plot, and landscape scale analyses.

At all scales (tree, plot, and landscape), I measured variability between biomass estimates by calculating the mean difference and mean relative difference. The difference between each set of allometric equations was calculated at each scale: (1) local – Jenkins et al. (2003), (2) local – FIA-CRM, and (3) Jenkins et al. (2003) – FIA-CRM. I calculated relative differences by dividing differences by the minuend. I analyzed tree, plot, and landscape scale differences by calculating the mean and relative differences across all trees in the FIA plots, FIA plots (i.e., the sum of trees within each plot), and pixels. To better understand patterns in variability between allometric equations at the tree scale, I calculated biomass differences for each species I sampled (lodgepole pine, ponderosa pine, and Douglas-fir) for each component and in 20 cm diameter bins.

At the plot scale, I identified the stand characteristics most correlated with biomass estimate differences between different sets of allometric equations. This was done using a random forest model to predict the plot biomass difference between allometric equations using stand structure and composition predictor variables. Details about this analysis can be found in Appendix 1.1. At the landscape scale, I evaluated patterns in allometric equation differences by summarizing biomass differences and relative differences by forest type in 2001 as defined by LANDFIRE version 1.0.5 Existing Vegetation Type (LANDFIRE, 2001).

Allometric error

Allometric biomass error is not reported in some cases (e.g., FIA-CRM) and, when it is reported, the error is simply the error or variability in the model fit (e.g., Jenkins et al., 2003 and the local equations). To better understand the representativeness of allometric equations in the study area, I evaluated all three equations using an independent dataset of destructively sampled lodgepole pine, ponderosa pine, and Douglas-fir trees from the Legacy Tree Database (Radtke et al., 2015). Calculating precision and bias with an independent set of trees allowed us to compare allometric model performance in the study region, while also enabling error estimates for the FIA-CRM predictions.

I used 285 lodgepole pine, ponderosa pine, and Douglas-fir trees located in Colorado from the Legacy Tree Database (Table A1.1.6). No trees from Wyoming were available for these species. I used dry weights of all above-stump bark and wood for 73 lodgepole and ponderosa pine trees from near Red Feather Lakes in northern Colorado (Reid, 1974; Tossey, 1982) which is within the study area and is near the ponderosa pine and Douglas-fir sampling sites (Table 1.1). Reid (1974) destructively sampled 19 lodgepole pine trees at around 3,000 m elevation. Tossey (1982) sampled seedlings and saplings across a range of site qualities, topographic positions, and habitat types between elevations of 1,700 m and 3,700 m. The other 212 Legacy trees used were sampled in National Forests within and just outside of the study area, but only green mass was reported (Sánchez Meador, 2007). For these trees, I converted above-stump green mass to dry mass using the steps described in Appendix 1.1. Comparing biotic and abiotic growth conditions (e.g., trees ha^{-1}, basal area, site index, precipitation) between my sites and Legacy Tree sites could help explain differences between biomass observations and predictions, but comparable information was not available across studies.

Table 1.1: Destructively sampled trees used in this study (Legacy Trees and trees destructively sampled for this study), the number of trees sampled for each species, location, and study and a summary of the diameter at breast height (DBH). NF = National Forest, CO = Colorado

Species	Study	Location	n	Mean DBH (cm)	Min DBH (cm)	Max DBH (cm)
Lodgepole pine	This study	CO State Forest	20	16.3	2.5	29.9
	Reid et al., 1974	Near Red Feather Lakes, CO	19	13.3	2.5	28.7
	Sánchez Meador, 2007	Pike, San Isabel, and Aarapaho NF	69	13.2	1.5	32.0
	Tossey, 1982	Near Red Feather Lakes, CO	26	5.4	1.0	11.4
Ponderosa pine	This study	Ben Delatour Boy Scout Ranch	10	34.0	4.9	61.8
	Sánchez Meador, 2007	Pike, San Isabel, and Aarapaho NF	80	15.3	1.8	36.6
	Tossey, 1982	Near Red Feather Lakes, CO	28	5.3	0.8	11.7
Douglas-fir	This study	Ben Delatour Boy Scout Ranch	10	24.9	2.4	46.6
	Sánchez Meador, 2007	Pike, San Isabel, and Aarapaho NF	63	14.1	1.5	39.6

For each Legacy tree, I estimated biomass using each set of allometric equations. I adjusted local, Jenkins et al. (2003), and FIA-CRM estimates to match components measured for the Legacy trees by subtracting foliage mass from local and Jenkins et al. (2003) estimates and by subtracting stump mass from Jenkins et al. (2003) and FIA-CRM estimates. For FIA-CRM, I did not have all information needed to calculate biomass of Legacy trees so I employed an alternative method. FIA-CRM biomass was estimated as the biomass of the tree in the FIA plot data most similar to the Legacy tree. I matched Legacy trees to a tree in the FIA plot data by extracting the 20 FIA trees most similar in DBH to the Legacy tree and then selecting the tree closest in height to the Legacy tree from this list of 20. The DBH of trees for which the FIA-CRM biomass values were used matched Legacy trees within 0.1 cm DBH height on average (sd = 0.6 cm) and < 0.1 m height (sd = 0.5 m). I report relative and absolute RMSE and bias between Legacy tree biomass and predictions from each set of allometric equations.

Uncertainty propagation

I propagated error from two important contributors to total biomass prediction uncertainty (Chave et al., 2004; Chen et al., 2015; Stovall and Shugart, 2018): error from allometric biomass equations (hereafter "allometric error") and from the remote sensing model predictions used to map biomass (hereafter "prediction error"). I calculated uncertainty at the tree, plot, and pixel scale and compared the relative contributions of allometric error and prediction error using methods from Chen et al. (2015) and Stovall and Shugart (2018). I do not account for errors in the predictor variable measurement (i.e., DBH or spectral, topographic, and climatic layers) or model parameters of the allometric and remote sensing models and, thus, underestimate total uncertainty. Past work has highlighted allometric and prediction errors as the primary sources of biomass prediction error (Chen et al., 2015). Moreover, my primary goal was to better understand the relative contribution from each of these error sources, as opposed to quantifying total uncertainty in each scenario. I hypothesize adding the additional sources of error would scale the overall results, increasing the total amount of uncertainty, but relative contributions from allometry and remote sensing model-based predictions would likely remain similar.

I propagated allometric error from two scenarios—one with the errors from the equation fit (equation-derived) and one using errors calculated from comparisons with the independent Legacy Tree Data. Both error scenarios were propagated for local and Jenkins et al. (2003) allometric equations, but I only propagate Legacy Tree Data allometric error for FIA-CRM since error is not reported for FIA-CRM equations. I only had error for the three focal species when propagating allometric error from Legacy Tree Data evaluations, so errors reported in Jenkins et al. (2003) were used for all other species across all three sets of allometric equations. For

equation-derived evaluation of local biomass estimates, allometric error (σ_{tree}) for the three focal species was the total tree biomass relative RMSE from my equations (Figure 1.2). I used the standard error reported in Landis and Mogren (1975) for Engelmann spruce in the local equation-derived evaluation. The aspen biomass equations used in the local estimates (Johnston and Bartos, 1977) only reported R^2, so I utilized Jenkins et al. (2003) uncertainty for these trees and for all other species. Jenkins et al. (2003) errors are reported as RMSE in natural log units. I calculated Jenkins et al. (2003) allometric error (σ_{tree}, kg) for each tree using the following equation.

$$(7) \quad \sigma_{tree} = \frac{e^{(\beta_0+\beta_1 \ln DBH)+1.96*RMSE} - e^{(\beta_0+\beta_1 \ln DBH)-1.96*RMSE}}{2*1.96}$$

Where β_0, β_1, and RMSE are species group-specific regression parameters and errors from Table 4 of Jenkins et al. (2003). Allometric uncertainty is propagated to the plot level (σ_{plot}, Mg ha^{-1}) using the following equation (Chen et al., 2015; Stovall and Shugart, 2018)

$$(8) \quad \sigma_{plot} = \sqrt{\sum_{i=1}^{n_{tree,plot}} \frac{\sigma_{tree,i}{}^2}{s}}$$

where s is the area of the plot in hectares.

This plot-level allometric uncertainty was combined and propagated with remote sensing model prediction error ($\sigma_{\epsilon,\hat{B}_{plot}}$) using the following equation. The model prediction error was the RMSE for the random forests model built with the respective set of allometric biomass equations.

$$(9) \quad \sigma_{pred} = \sqrt{\sigma_{\epsilon,plot}{}^2 + \sigma_{\epsilon,\hat{B}_{plot}}{}^2}$$

where σ_{pred} is the total uncertainty from allometric and prediction error in Mg ha^{-1}. I calculated percent uncertainty by dividing by the mean plot-level biomass density and evaluate the relative contribution of each error source as the percentage of σ_{pred}.

Results

Destructive sampling and local allometric equations

Destructively sampled trees spanned the diameter range observed at each site (Table 1.2). The lodgepole pine tended to have the smallest DBH and grow at the highest density, while the ponderosa pine had the largest DBH and grew in the lowest densities. I calculated dry total and component biomass for each destructively sampled tree. The multiple regression equations (Table A1.1.2) developed for predicting single branch length, foliage mass, and wood mass performed strongly, with adjusted R^2 values averaging 0.84 and ranging from 0.63 to 0.98 (Table A1.1.3). Predictions from these equations were used in combination with other in-field measurements to calculate component biomass (Table 1.2). For all species, the majority of aboveground biomass was in the bole and branch components, and trees had more biomass in the foliage than the bark (Figure A1.2.1). Moisture content for each component and species are presented in Table A1.2.1. Specific gravity of the bole increased from lodgepole pine (0.39) to ponderosa pine (0.42) to Douglas-fir (0.43). Table 1.3 presents regression coefficients for Equations 2-6 predicting component biomass from a tree's DBH for each species. Parameter estimates were stable to variations in their start values. Allometric equations fit the data well, with all but two components having adjusted R^2 values greater than 0.90 (Figure 1.2). Absolute RMSE values were highest for ponderosa pine, but lodgepole pine tended to have the highest relative errors (Figure 1.2). Across species, allometric equations over-estimated bark and bole biomass, but under-estimated foliage biomass (Figure 1.2).

Table 1.2. Height, diameter at breast height (DBH), and stand structure of destructively sampled trees and from 7.32 m radius plots measured around each tree and total and component biomass of the destructively sampled trees. PSME= Douglas fir (*Pseudotsuga menziesii;* n = 10*)*; PICO= lodgepole pine (*Pinus contorta;* n = 20); PIPO= ponderosa pine (*P. ponderosa;* n = 10)

	Species	Mean	Standard Deviation	Min	Max
DBH (cm)	PSME	24.9	15.4	2.4	46.6
	PICO	16.3	8.0	2.5	29.9
	PIPO	34.0	18.5	4.9	61.8
Height (m)	PSME	12.7	5.3	3.2	19.7
	PICO	12.2	6.5	3.2	21.1
	PIPO	11.3	4.3	3.0	16.8
Tree density (trees ha^{-1})	PSME	386	176	119	535
	PICO	921	414	238	2139
	PIPO	172	162	0	416
Basal area (m^2 ha^{-1})	PSME	15.6	6.5	7.2	30.3
	PICO	18.6	14.9	0.5	44.9
	PIPO	13.4	10.4	0	29.7
Average plot DBH (cm)	PSME	21.2	7.4	12.2	35.9
	PICO	15.3	7.2	4.9	27.0
	PIPO	26.6	17.6	0.0	65.0
Total biomass* (kg)	PSME	286.3	290.1	3.2	809.1
	PICO	117.6	114.7	1.7	358.4
	PIPO	710.4	751.7	5.7	2188.1
Stem wood biomass** (kg)	PSME	152.6	166.1	0	434.2
	PICO	72.1	83.5	0	247.2
	PIPO	270.4	268.1	0	738.5
Stem bark biomass (kg)	PSME	33.1	31.3	0	81.8
	PICO	5.3	5.6	0	15.8
	PIPO	35.5	32.3	0	89.7
Foliage biomass (kg)	PSME	28.2	25.4	1.2	72.1
	PICO	10.2	7.3	0.8	24.1
	PIPO	49.2	49.9	1.5	153.9
Branch biomass (kg)	PSME	72.4	70.5	2.0	220.9
	PICO	30.1	23.7	0.9	82.0
	PIPO	355.3	410.8	4.2	1206.0

* Includes foliage

** Stem wood does not include bark

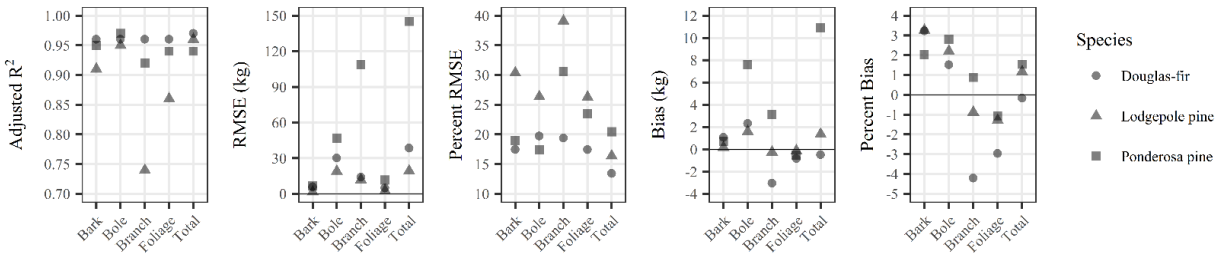

Figure 1.2. Evaluation metrics for allometric equations generated in this study for each component and species.

Table 1.3. Allometric biomass equation regression coefficients for Equations 2-6 for lodgepole pine, ponderosa pine, and Douglas-fir. Equations were fit using nonlinear seemingly unrelated regression to estimate component biomass (kg) from a tree's diameter at breast height (cm). Values in parentheses are standard errors of the parameter values. Total biomass can be calculated as the sum of these four components.

Species	Component	a_{i1}	a_{i2}
Douglas-Fir	Bole (i=1)	-2.9162 (0.9896)	2.3437 (0.2647)
	Bark (i=2)	-2.0888 (0.7021)	1.6911 (0.1903)
	Foliage (i=3)	-3.3489 (0.8356)	1.9822 (0.2249)
	Branch (i=4)	-3.7741 (1.0634)	2.3588 (0.2845)
Lodgepole Pine	Bole (i=1)	-4.3642 (0.8611)	2.9255 (0.2634)
	Bark (i=2)	-5.2333 (0.8573)	2.3723 (0.2646)
	Foliage (i=3)	-2.0830 (0.6570)	1.5402 (0.2075)
	Branch (i=4)	-1.0172 (0.9174)	1.5475 (0.2897)
Ponderosa Pine	Bole (i=1)	-2.5513 (0.8855)	2.2322 (0.2231)
	Bark (i=2)	-3.5399 (0.9608)	1.9588 (0.2432)
	Foliage (i=3)	-5.75806 (1.2645)	2.6110 (0.3168)
	Branch (i=4)	-5.2127 (1.6641)	2.9843 (0.4149)

Tree-Scale Biomass Variability

The 285 Legacy Tree Data trees used in this study were smaller in terms of DBH and height than the trees that I destructively sampled and there were more low than high biomass Legacy trees (Table 1.1; Figure 1.3; Table A1.1.6). Local equations had the lowest error and bias across all three species, although the bias was similar between local and Jenkins et al. (2003) equations (Table 1.4). In general, error and bias for each set of allometric equations differed dramatically for each species. Error values were as high as 113.7% of the mean (Jenkins et al. [2003] equations for Douglas-fir) and as low as 23.1% (local equations for ponderosa pine), while predictions were as biased as 54.0% (Jenkins et al. [2003] equations for Douglas-fir) and had as little bias as -4.5% (Jenkins et al. [2003] equations for ponderosa pine; Table 1.4). The Jenkins et al. (2003) equations predicted lodgepole pine biomass most accurately and performed similarly to the local equations for ponderosa pine. Local equations performed best for Douglas-fir. The FIA-CRM equations underpredicted biomass for all species, while local and Jenkins et al. (2003) equations were less biased, but tended to overpredict biomass (Table 1.4; Figure 1.3).

Table 1.4. Comparison of biomass estimates measured in the Legacy Tree Database and predictions by three allometric biomass equations for the Legacy trees: local allometrics presented in this study, Jenkins et al. (2003), and the Forest Inventory and Analysis Component Ratio Method (FIA-CRM). Negative bias values indicate that the allometric equations are under-predicting biomass compared to the Legacy Database biomass.

	All Species (n = 285)				Lodgepole pine (n = 114)				Ponderosa pine (n = 108)				Douglas-fir (n = 63)			
	RMSE		Bias		RMSE		Bias		RMSE		Bias		RMSE		Bias	
	kg	%	kg	%	kg	%	kg	%	kg	%	kg	%	kg	%	kg	%
Local	27.9	46.3	9.1	15.1	30.7	71.3	16.0	37.1	16.6	23.1	3.8	5.2	36.6	51.7	5.8	8.2
Jenkins et al. (2003)	40.6	67.4	9.3	15.4	16.1	37.5	5.2	12.0	17.3	23.9	-3.3	-4.5	80.5	113.7	38.2	54.0
FIA-CRM	37.3	62.0	-16.1	-26.8	23.0	53.5	-7.9	-18.3	45.4	62.9	-27.1	-37.6	42.5	60.0	-12.3	-17.4

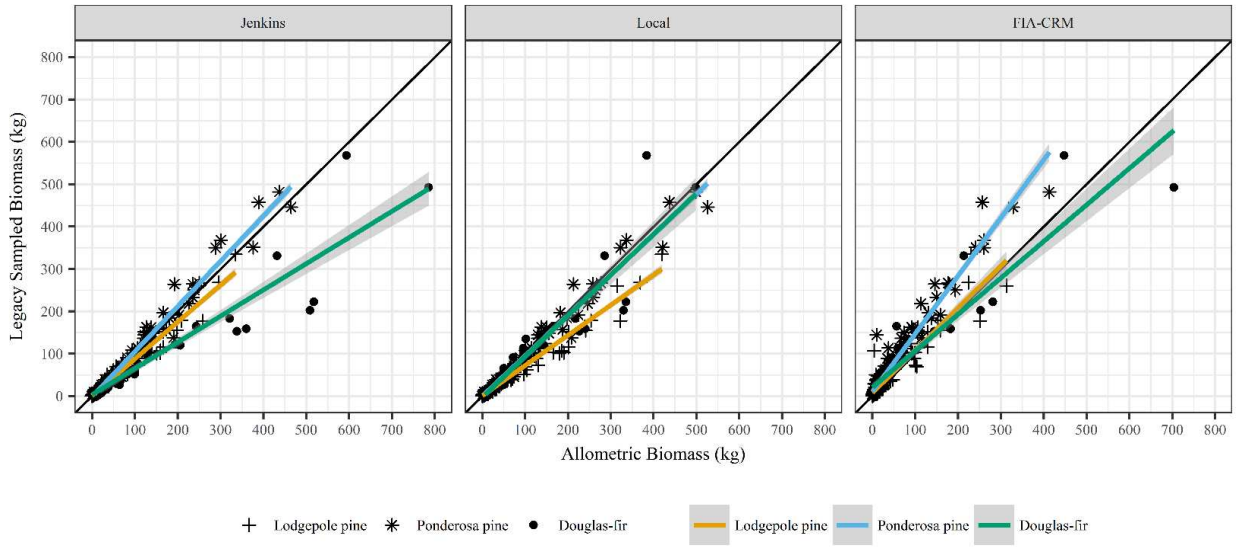

Figure 1.3: Scatter plots with regression lines and 95% confidence intervals comparing destructively-sampled biomass estimates from the legacy database to the three allometric equations used in this study (Jenkins et al., [2003], local, and FIA-CRM). Comparisons are made for three species, as shown in the legend. The 1:1 line of exact agreement between Legacy sampled biomass and allometric biomass is shown by the black line for reference. All biomass estimates shown in the figure exclude foliage and stump biomass to align with the Legacy measurements used.

Differences between allometric equations at the tree scale varied by species, component, and diameter (Figure 1.4). Disagreement between allometric equations was minor for some species and components (e.g., total ponderosa pine biomass predicted by local and Jenkins) and large for others (e.g., total ponderosa pine biomass predicted by local and FIA-CRM; Figure 1.4

and Table A1.3.1). The FIA-CRM biomass estimates have a range for a given tree diameter (the spread of gray points in Figure 1.4) as opposed to a single line of biomass estimates like Jenkins et al. (2003) and local equations because FIA-CRM biomass estimates are based on more factors than just diameter, such as height and tree breakage or rot. Jenkins et al. (2003) allometric equations tend to predict the highest biomass values for Douglas-fir, while local equations predict the highest biomass for ponderosa and lodgepole pine. However, there is variability in this order by components. For example, local equations predict dramatically more ponderosa pine branch biomass than the other allometric equations, but Jenkins et al. (2003) predicts the highest ponderosa pine bole and bark biomass. The absolute difference between allometric equations tended to increase with diameter and the relative difference had mixed trends (Figure 1.4 and Table A1.3.1). The relative difference sometimes increased with diameter but for other species and components, the relative difference decreased with diameter or remained relatively steady.

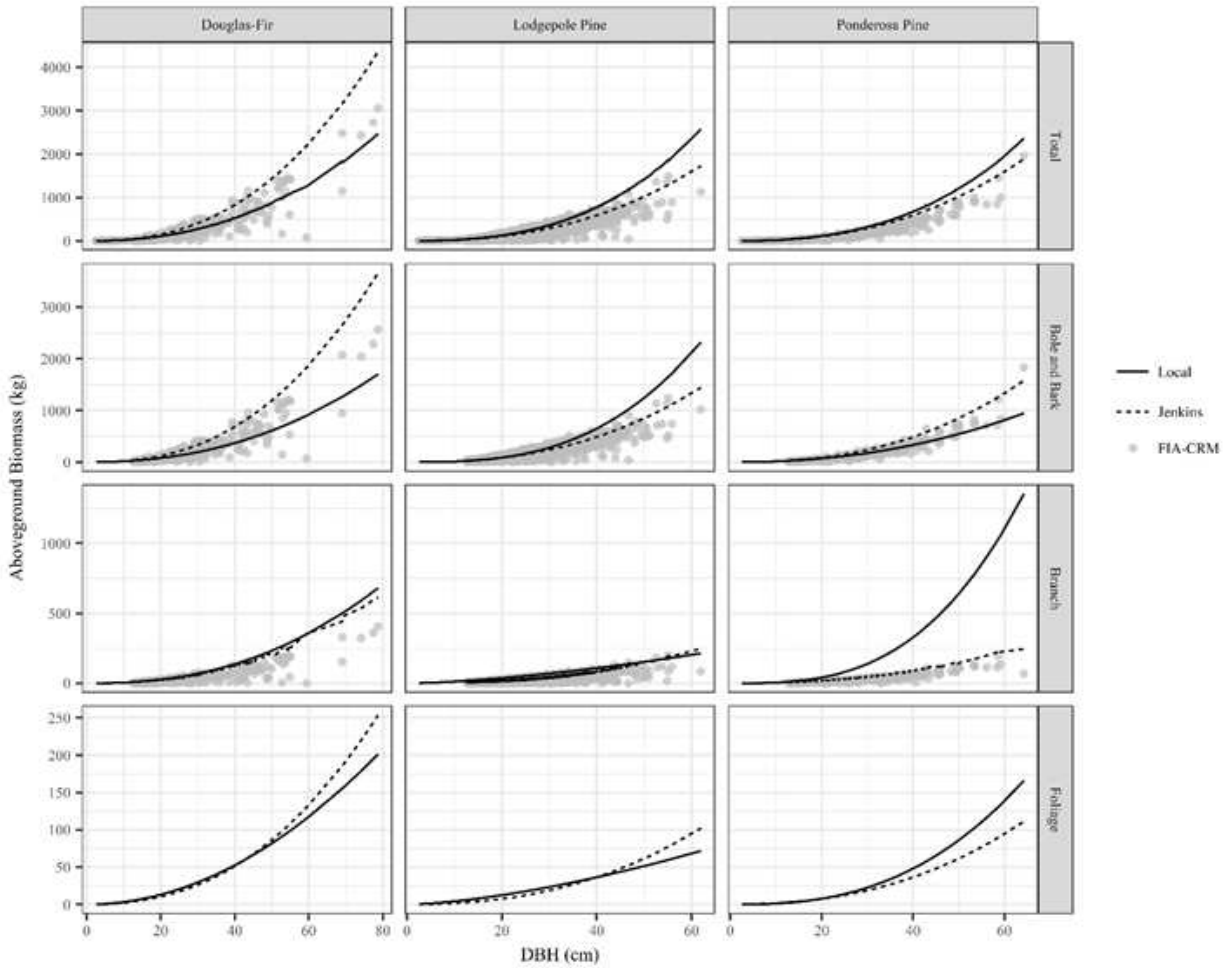

Figure 1.4. Comparison of the three sets of allometric equations used in this study (local equations presented in this study, Jenkins et al. (2003), and Forest Inventory and Analysis Component Ratio Method [FIA-CRM]). Comparisons are made for the three species that were destructively sampled in this study (Douglas-fir, lodgepole pine, and ponderosa pine), the total tree biomass and three components. The figure shows biomass for the trees in the FIA plots used in this study. Total biomass includes stump biomass, but excludes foliage since FIA-CRM does not estimate foliage biomass. Bole and bark biomass are combined for the sake of direct comparison since FIA-CRM does not separate these components. This component represents bole and bark of the merchantable portion of the tree between the 1-foot stump and 4-inch top.

Engelmann spruce, subalpine fir, and aspen were all common in the plots, but were not destructively sampled in this study. Other allometric biomass equations were used for these species in the local biomass estimates for scaling to the plot and landscape-level. Engelmann spruce biomass from Landis and Mogren (1975) and aspen biomass from Johnston and Bartos (1977) both predicted higher biomass than FIA-CRM, but lower biomass than Jenkins et al.

(2003) (Table 1.5). The largest tree-level mean biomass difference for the non-focal species of this study was for Engelmann spruce between Jenkins et al. (2003) and FIA-CRM (83.4 kg) and the largest mean relative difference was for subalpine fir (-116.3%) between local (same as FIA-CRM for subalpine fir tree-scale comparisons) and Jenkins et al. (2003).

Table 1.5. Comparison of aboveground tree biomass (stump included, foliage excluded for all allometric equations) for tree species common in the study area, but not destructively sampled. Local biomass estimates for Engelmann spruce, subalpine fir, and aspen were made using allometric equations from Landis and Mogren (1975), FIA-CRM, and Johnston and Bartos (1977), respectively. The relative differences were calculated by dividing each tree biomass difference by the minuend. FIA-CRM was used to estimate tree-level biomass in both the local and FIA-CRM scenario, so their difference is not applicable.

	Local - Jenkins		Local – FIA-CRM		Jenkins – FIA-CRM	
Species	Mean Diff (kg)	Mean Relative Diff (%)	Mean Diff (kg)	Mean Relative Diff (%)	Mean Diff (kg)	Mean Relative Diff (%)
Engelmann spruce	-20.2	-15.6	67.8	33.4	83.4	41.2
Subalpine fir	-60.8	-116.3	NA	NA	60.8	44.2
Quaking aspen	-35.1	-30.0	12.4	23.3	47.9	41.2

Plot-Scale Biomass Variability

I calculated biomass at 418 FIA plots with each set of allometric equations. Plots ranged from dense (max basal area = 95.2 $m^2 ha^{-1}$, max trees ha^{-1} = 11,411) to sparse (min basal area = 0.5 $m^2 ha^{-1}$, min trees ha^{-1} = 30), with an average basal area of 33.0 $m^2 ha^{-1}$ and 1,608 trees per hectare (Figure 1.5). Lodgepole pine accounted for 40.5% of the basal area, making it the most abundant species in these plots. Engelmann spruce (20.6%) and subalpine fir (17.1%) were also common, while aspen (7.6%), Douglas-fir (4.3%), ponderosa pine (3.5%), limber pine (2.0%), Utah juniper (1.4%), and pinyon pine (1.0%) made up small percentages of the plot basal area. Of the three species that I destructively sampled, ponderosa pine in the FIA plots tended to be the largest (mean average diameter = 23.2 cm, max = 64.3 cm, min = 2.5 cm), Douglas-fir in the middle (mean average diameter = 21.5 cm, max = 78.7 cm, min = 2.5 cm), and lodgepole pine the smallest (mean average diameter = 19.9 cm, max = 62.0 cm, min = 2.5 cm).

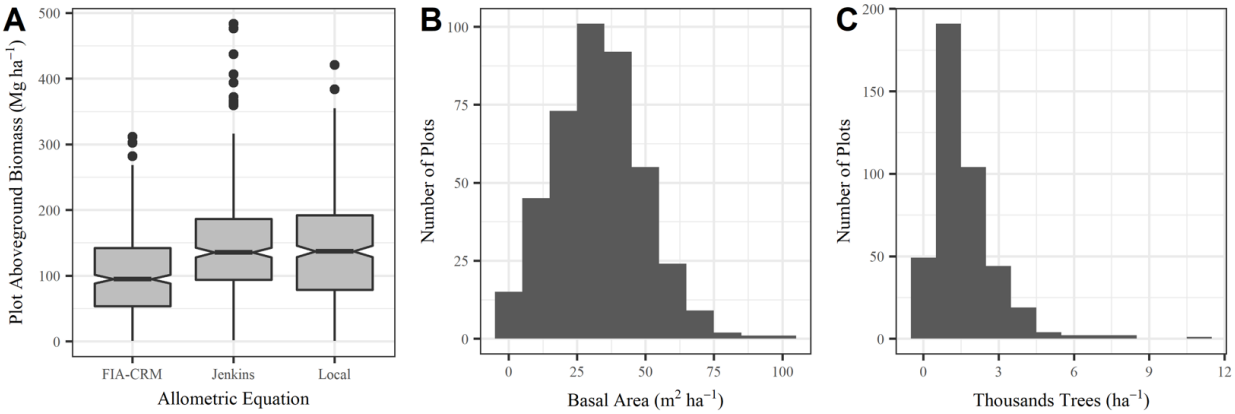

Figure 1.5. A) Summary of aboveground tree biomass at Forest Inventory and Analysis (FIA) plots as estimated by three allometric equations. FIA-CRM = FIA Component Ratio Method (does not estimate foliage mass); Jenkins = Jenkins et al. (2003); local = equations presented in this study. B and C) Histograms of basal area and the number of trees per hectare at the FIA plots.

Biomass at the FIA plots tended to be highest when using Jenkins et al. (2003) equations (mean biomass = 144.4 Mg ha^{-1}), followed by local equations (mean biomass = 137.5 Mg ha^{-1}) and then FIA-CRM (mean biomass = 100.2 Mg ha^{-1}, Figure 1.5). The differences between plot estimates made using Jenkins et al. (2003) and FIA-CRM were the largest, followed by local equations and FIA-CRM differences (Table 1.6). Local equations and Jenkins et al. (2003) plot biomass estimates were most similar, however differences between these two were larger when presented in terms of the absolute value of the biomass differences (Table 1.6). This reflects that plot biomass estimates made by local equations were sometimes higher and sometimes lower than Jenkins et al. (2003) estimates. Differences between local and FIA-CRM and Jenkins et al. (2003) and FIA-CRM changed little when the absolute values of the differences were considered, reflecting the consistent under-estimation of biomass by FIA-CRM. Random forests models of these differences in plot biomass estimates as a function of forest structure attributes showed that differences between allometric equations were larger in stands with higher basal area (Figures A1.3.1-A1.3.4). Forest structure attributes explained between 56.7% and 86.1% of the variance in plot biomass differences (Table A1.3.2). When the relative biomass between allometric

equations was modeled, less of the variance was explained by stand structure and composition (39.0% - 55.3%).

Table 1.6. Summary of differences in plot biomass when calculated using different allometric equations: local (presented in this study), Forest Inventory and Analysis Component Ratio Method (FIA-CRM), and Jenkins et al. (2003). The mean of both the differences and the absolute value of the differences are presented as well as the mean relative difference.

Allometric Equations Compared	Mean Difference (Mg ha $^{-1}$)	Mean of Absolute Differences (Mg ha $^{-1}$)	Mean Relative Difference (%)
Local – Jenkins et al. (2003)	-6.9	25.9	-13.0
Local – FIA-CRM	37.3	37.9	28.7
Jenkins et al. (2003) – FIA-CRM	44.2	44.8	32.9

Plot-scale allometric uncertainty was lower when utilizing equation-derived allometric errors and was higher when propagating the independent Legacy evaluation (Figure 1.6). The equation-derived local allometric equation error values resulted in the lowest plot-level uncertainty (mean plot RMSE = 41.5 Mg ha^{-1}). However, when evaluated against the independent Legacy Tree data, Jenkins et al. (2003) was lowest (mean plot RMSE = 90.9 Mg ha^{-1}), followed by local equations (mean plot RMSE = 108.4 Mg ha^{-1}) and FIA-CRM (mean plot RMSE = 135.7 Mg ha^{-1}).

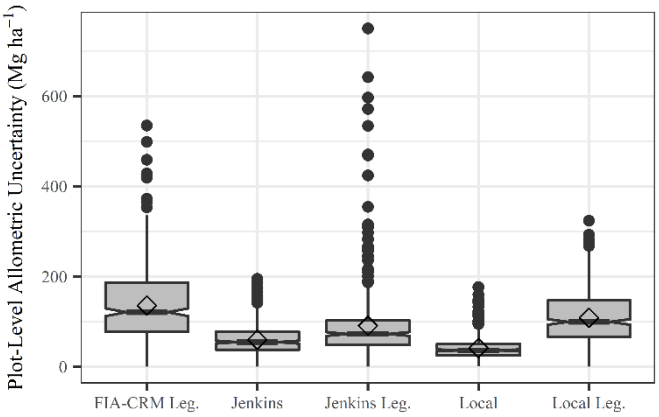

Figure 1.6. Boxplots showing plot-level allometric uncertainty for local equations (those presented in this study), Jenkins et al. (2003), and the Forest Inventory and Analysis Component Ratio Method (FIA-CRM). Allometric error was evaluated in two ways for Jenkins et al. (2003) and local equations: equation-derived evaluation and independent evaluation against Legacy Tree Data ("Jenkins Leg." and "Local Leg."). The FIA-CRM model was only evaluated against

Legacy tree data ("FIA-CRM Leg."). Notches on the boxplots show roughly a 95% confidence interval for the medians. Diamonds are the mean.

Landscape-Scale Biomass Variability

I developed three maps of standing aboveground tree biomass in 2001 using random forests models—one map for each set of allometric biomass equations. The three models performed similarly with 53.77- 59.36 percent variation explained and RMSEs ranging from 40.8 Mg ha^{-1} to 54.8 Mg ha^{-1} and low bias (Table 1.7). The Normalized Difference Infrared Index (NDII) was an important variable in all models, and the Landsat 7 blue band (band 1) and digital elevation model were also important predictor variables (Table 1.7). Consistent with other studies that map biomass using passive remote sensing, the biomass predictions saturate in all three maps (Figure 1.7A). Models built from allometric equations that predict higher biomass in the FIA plots (local and Jenkins et al. [2003]) saturate at slightly higher levels than FIA-CRM, which estimated lower biomass at the FIA plots.

Table 1.7: Out-of-bag model evaluation metrics (pseudo R^2 and RMSE) from the Random Forest aboveground biomass models. These values are the prediction errors only, and do not include allometric error. FIA-CRM = Forest Inventory and Analysis Component Ratio Method, RMSE = root mean square error, NDII = normalized difference infrared index, DEM = digital elevation model, PAS = precipitation as snow, mtry = number of predictor variables randomly sampled at each split in model, ntrees = number of trees grown in model

Allometric Equation	RMSE	RMSE percent of mean	Pseudo R^2	Percent Bias	Number of Predictors (Top 3 Predictors)	mtry	ntrees
Local	48.1	35.0	0.5936	0.9	11 (Band 1, NDII, DEM)	8	2000
Jenkins et al. (2003)	54.8	37.9	0.5377	0.9	10 (NDII, DEM, Band 1)	5	1500
FIA-CRM	40.8	40.8	0.5463	1.1	9 (NDII, Band 2 texture_5x5 mean, PAS)	4	1000

I evaluated the contribution of two main sources of uncertainty to the biomass predictions: allometric error and prediction error from mapping biomass (Figure 1.7B). Total uncertainty was lowest for models constructed using equation-derived evaluation of local allometric equations (49.9%) and was highest for independently evaluated FIA-CRM models

(164.5%; Figure 1.7B). Model prediction error was relatively consistent across all models. The variability in total uncertainty was driven by allometric uncertainty, which ranged from 29.9% to 75.2% of the total uncertainty (Figure 1.7B). Allometric errors were less than prediction errors only when equation-derived allometric errors were used.

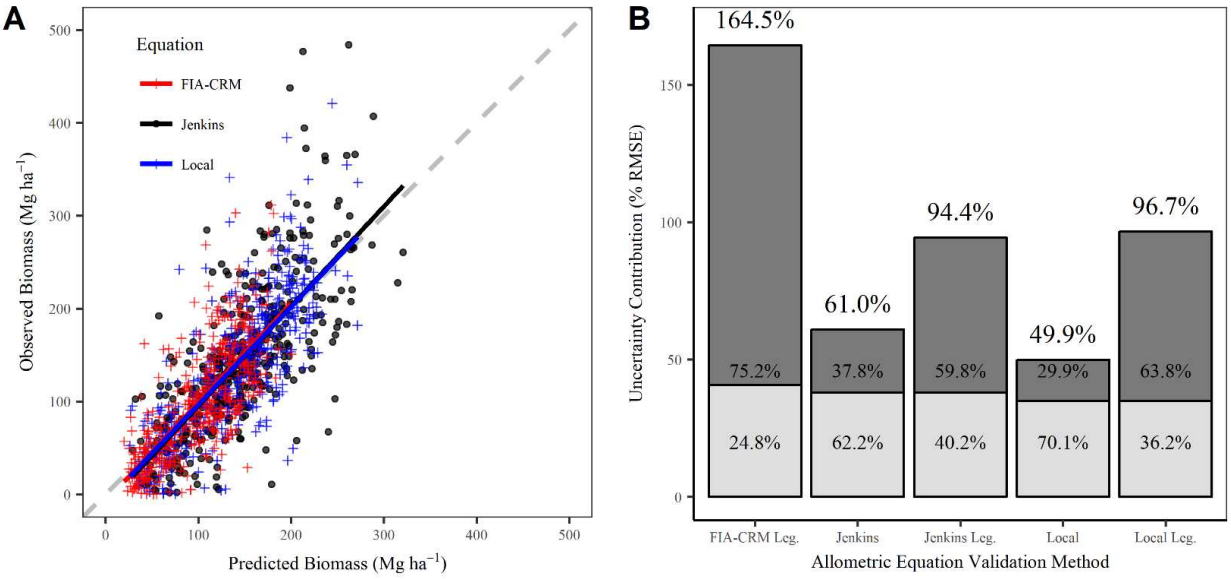

Figure 1.7. A) Observed plot aboveground biomass values and those predicted by the random forest models for generating biomass maps in three allometric biomass equation scenarios: local equations (those presented in this study), Jenkins et al. (2003), and the Forest Inventory and Analysis Component Ratio Method (FIA-CRM). Dashed grey line is the 1:1 line representing perfect model fit. B) Uncertainty contributions from the allometric model (dark grey) and random forest prediction (light grey). The printed percentages within each bar are the allometric and prediction uncertainties relative to total uncertainty. Total uncertainty is printed at the top of each bar. Allometric error was evaluated in two ways for Jenkins et al. (2003) and local equations: equation-derived and independent evaluation against Legacy tree data ("Jenkins Leg." and "Local Leg."). The FIA-CRM model was only evaluated against Legacy tree data ("FIA-CRM Leg.") because I was unable to locate FIA-CRM equation-derived errors.

Across all forested areas in the study area, maps generated using local allometric biomass equations estimate 2.066 billion Mg of standing aboveground biomass, while maps based on Jenkins et al. (2003) and FIA-CRM equations estimate 2.224 billion Mg and 1.502 billion Mg, respectively. The maps based on Jenkins et al. (2003) showed 7.6% more biomass than the local maps, while FIA-CRM maps showed 27.3% less biomass than local maps. These three biomass

maps were differenced to highlight areas of agreement and disagreement in the predicted amount of aboveground forest biomass (Figure 1.8). Differences between biomass in a given pixel were as large as 236.6 Mg ha^{-1}. The largest differences between "Jenkins – FIA-CRM" and "local – FIA-CRM" were in spruce-fir forests (Figure 1.9). Local and Jenkins et al. (2003) predictions were remarkably similar for lodgepole pine forests and were most different for aspen forests (Figure 1.9).

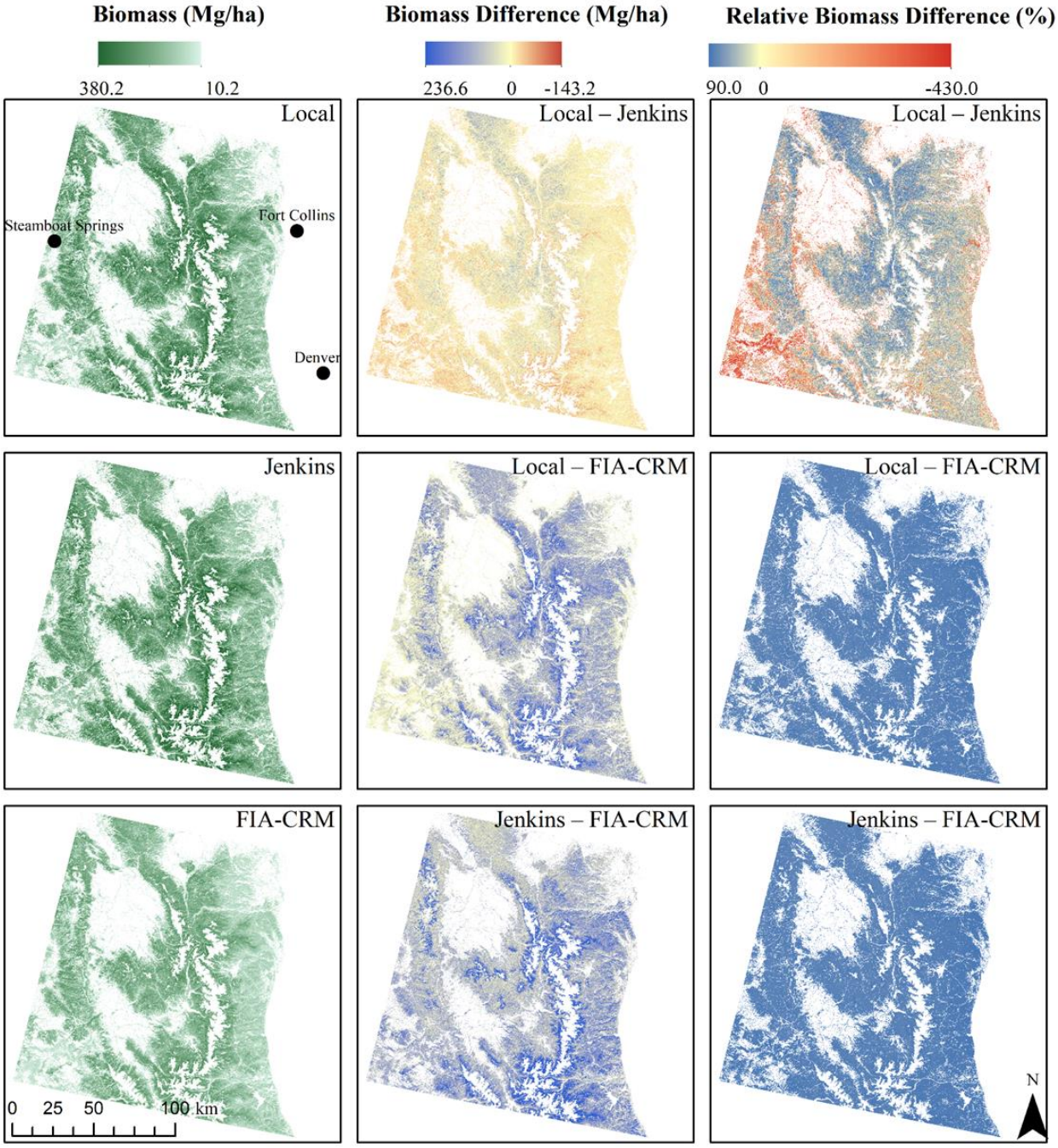

Figure 1.8. Left column: Biomass maps created using three sets of allometric biomass equations: local equations presented in this study, Jenkins et al. (2003), and the Forest Inventory and Analysis Component Ratio Method (FIA-CRM). Middle and right columns: Maps of the difference and relative difference between the biomass maps, respectively. Note that FIA-CRM biomass estimates do not include foliage mass, but local and Jenkins et al. (2003) maps do.

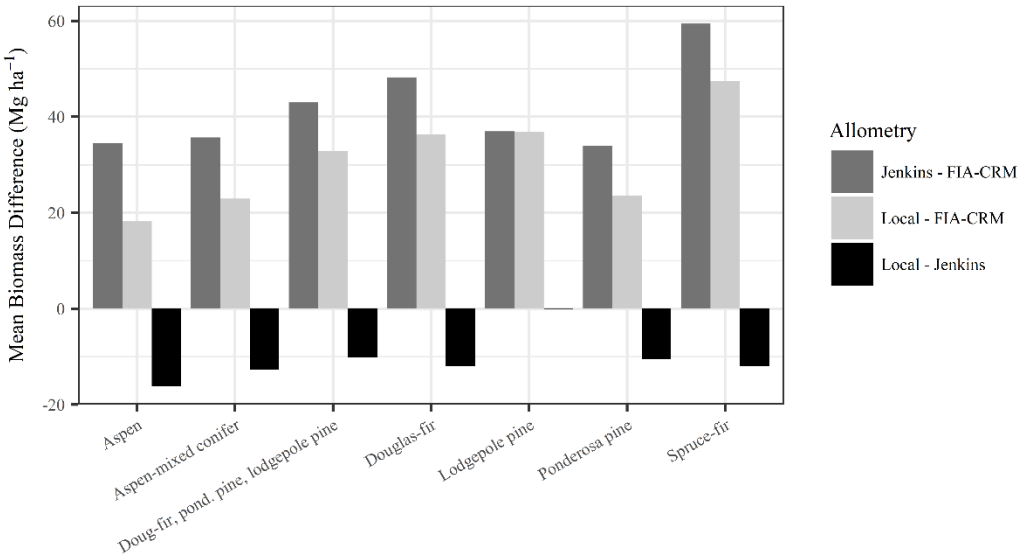

Figure 1.9. Mean difference in biomass between maps produced from three sets of allometric biomass equations for the most common forest types in the study area. The mean was taken of all pixels within each forest type. Forest types are derived from LANDFIRE Existing Vegetation Type version 1.0.5—forest type names are simplified for this figure. Note that mapped Forest Inventory and Analysis Component Ratio Method (FIA-CRM) biomass estimates do not include foliage, but local and Jenkins et al. (2003) estimates do include foliage.

Discussion

Allometric equation selection is critical for accurately estimating regional biomass stocks. I evaluated the variability and accuracy of aboveground forest biomass estimates from three sets of allometric equations at the tree, plot, and landscape scale. Destructive sampling of even as few as ten trees per species generated relatively reliable allometric equations for the study area compared to existing equations. In an independent evaluation of these local equations, Jenkins et al. (2003), and FIA-CRM, the local equations performed best for Douglas-fir and comparably to Jenkins et al. (2003) for ponderosa pine. The local lodgepole pine equations had the highest error and bias of the allometric equations tested. While it is reasonable that the local equations would perform strongly in the areas near the destructive sampling sites, I was also surprised given the low sample sizes and potential for high bias (Duncanson et al., 2015). Due to

the low sample size sampled across small areas, the allometric equations presented in this study should be used cautiously if applied in other regions. More accurate local allometries could be developed by sampling additional trees representing a variety of genetic, abiotic, and biotic conditions and by incorporating more predictor variables in the allometric equations such as height and crown ratio.

Accuracy of each of the equations differed substantially between species. For example, Jenkins et al. (2003) performed well compared to the Legacy Tree Data for lodgepole pine (RMSE = 16.1 kg; Table 1.4), but poorly for Douglas-fir (RMSE = 80.5 kg). Allometric performance should be tested for each species of interest when possible. The variability in biomass estimates across diameters (i.e., higher differences between allometrics at some diameters) suggests that equations should also be tested across the diameter range being used.

The FIA-CRM equations, which are commonly used for forest carbon accounting (e.g., Environmental Protection Agency, 2018), consistently under-estimated biomass and generated the lowest estimates at the tree, plot, and landscape scales. Other studies have also found FIA-CRM to under-estimate biomass (e.g., Duncanson et al., 2015; Heath et al., 2009). The FIA-CRM plot and landscape-level estimates did not include foliage biomass, while estimates from the other allometric equations included foliage. Foliage accounted for an average of 14% of total aboveground biomass for the trees I destructively sampled. Differences between equations at the plot scale (28.7% mean difference between local and FIA-CRM and 32.9% difference between Jenkins and FIA-CRM) and across the entire study area (27.3% difference between local and FIA-CRM and 32.5% difference between Jenkins et al. (2003) and FIA-CRM) are influenced by the exclusion of foliage in FIA-CRM estimates. However, biomass differences exceeded what can be attributed to the exclusion of foliage, indicating that FIA-CRM underestimates the

biomass of other components. Foliage was excluded for the comparison of all allometric predictions to Legacy Trees to reduce impacts of the lack of foliage on FIA-CRM uncertainty propagation.

Biomass differences between equations varied widely across species, DBH, and component, indicating that total tree biomass errors can't be assumed to represent errors for a single component, or errors for another species or size class. For example, branch biomass predictions varied between equations (75% difference between local and Jenkins et al. [2003]) much more than total biomass (14% difference) for large ponderosa pine (40-60 cm DBH; Figure 1.4; Table A1.3.1). This also highlights the potential pitfalls and strengths of local allometric equations. The local equations predict high branch biomass compared to other equations, potentially reflecting true differences in growth form between the study area and the areas from which trees were sampled to develop these other equations. However, the high branch estimates could also be the result of sampling bias. I sampled ponderosa pine in a variety of stand densities, but several of the large trees were more open grown and thus had more branch biomass, contributing to the high branch biomass predictions.

The differences between allometric equation biomass predictions were frequently, but not always, largest for the biggest (60 – 80 cm DBH) trees (Table A1.3.1). This reflects an issue common for biomass allometry: large trees have the most biomass and greatest variation in growth form, but are rarely measured because they are the most difficult and expensive to sample (Stovall et al., 2018a). I had only one destructively sampled ponderosa pine tree in this upper diameter range, and lacked any trees this size for lodgepole pine or Douglas-fir. While it is problematic to predict outside the diameter range of sampled trees, this practice is commonplace in biomass assessments because few alternatives exist for most species and locations. Improved

allometric equation accuracy for large trees is needed to improve forest biomass estimates (Stovall and Shugart, 2018). The inclusion of large trees in the Jenkins et al. (2003) equations likely make the large tree biomass predictions more reliable than the local equations. However, allometric equations that don't utilize tree height can overpredict large diameter tree biomass (Heath et al., 2009).

Plot-level biomass estimates diverged with increasing basal area. Engelmann spruce-subalpine fir forests are some of the higher basal area forests in the study area. The maps (Figure 1.8) and summaries of biomass differences by forest type (Figure 1.9) both show high disagreement in these spruce-fir forests between all equations, highlighting it as a forest type where allometric equation selection is particularly important. Independent evaluation of the allometric equations for these species is needed to determine which allometric equation is best suited for this forest type. Allometric choice is also important in the lower elevation montane forests due to the high relative biomass difference between Jenkins and local equations (Figure 1.8). The use of the local equations is advised for these montane forests in the study area based on the favorable performance of the local equations relative to the Legacy Tree data for Douglas-fir and ponderosa pine.

The tree biomass measurements needed to independently evaluate allometric accuracy are rare and valuable. These data are typically unavailable for a particular area or species, or are used in the development of the allometric equations themselves. Resources such as the Legacy Tree Database (Radtke et al., 2015) and efficient non-destructive biomass sampling methods (Stovall et al., 2017, 2018b) make independent allometric validation more feasible. Independent tree biomass datasets come with their own difficulties and biases due to the potential for biased sampling and inconsistent destructive sampling methodologies and component definitions. For

example, I converted green mass to dry mass and adjusted which components were included in the independent evaluation dataset. I also had a disproportionately high number of small trees in the Legacy Data (Table A1.1.6) that likely had the effect of underestimating allometric uncertainty of all allometric equations since allometric error tends to be less for smaller trees. I encourage biomass studies to openly share data (Table A1.4) to enable improved evaluation of existing allometric biomass equations and for updating or building new equations. Even if independent data are not available for all species within a study area, the most common species can be prioritized as they have a larger influence on biomass uncertainty than less abundant species.

Independently evaluating tree-level allometry increased uncertainty estimates. Errors reported with allometric equations reflect allometric performance relative to samples used to build the equations, not necessarily for the application area. These samples may be a small, localized dataset (local equations) or from a large geographic area containing multiple species (Jenkins et al., 2003). When using equation-derived errors, local allometric equations had 11% lower total uncertainty than the Jenkins et al. (2003) equations (Figure 1.7B). However, evaluating both allometric equations with independent data resulted in similar and higher overall uncertainties. The increase in plot and landscape level uncertainty resulting from independent evaluation is likely an underestimate since I only had data to independently evaluate three species. To my knowledge, allometric errors are not reported for FIA-CRM equations, so independent evaluation is the only appropriate way to quantify FIA-CRM allometric error. Comparing allometric biomass predictions to independent biomass observations from the application area enables improved estimates of allometric uncertainty, and guides selection of the best allometric equations for a particular region or application.

Reporting remote sensing model prediction error alone, as is common in many studies, insufficiently represents biomass estimation uncertainty. Allometric error should be considered, and, if possible, should be based on independent evaluation of the allometric equations from the population of interest. The accuracy of each biomass map in this study appeared similar if only considering remote sensing model prediction error, but differed widely once allometric uncertainty was propagated (Figure 1.7B). Ignoring allometric uncertainty and only reporting model prediction uncertainty would have represented as little as a quarter of the total uncertainty, reflecting a false confidence in the biomass maps. Just as FIA-CRM had the highest tree-level errors, biomass maps built using FIA-CRM had the highest total uncertainty. Propagation of allometric uncertainty from an independent dataset revealed very high biomass estimate uncertainties, and improved accuracy by informing the selection of the most accurate allometric equations.

Conclusion

Allometric equation selection is a dominant influence on forest aboveground biomass estimates at the tree, plot, and landscape scale. Unless allometric uncertainty is propagated, total error in biomass estimates will be underestimated and uncertainty of estimates made with different allometric equations may look deceivingly similar, giving false confidence in mapped estimates of biomass. Allometric uncertainty can exceed the remote sensing model prediction uncertainty. Furthermore, regional evaluation is needed to quantify allometric performance in the study area. I found reported allometric equation error to underestimate error compared to an independent, regional, tree-level biomass validation dataset. Total uncertainty was comparable between estimates made using nationwide allometric equations (Jenkins et al., 2003) and local, low sample size equations. Both outperformed FIA-CRM equation uncertainty. Future efforts

should incorporate other sources of uncertainty not considered here (e.g. diameter and height measurements). Remote sensing model prediction uncertainty will be reduced as algorithms improve and LiDAR and synthetic aperture radar become more widely available (e.g., Stovall et al., 2018a), increasing the relative contribution of allometric uncertainty to total uncertainty (Stovall and Shugart, 2018). Efforts to quantify and reduce allometric uncertainty are also needed. Data repositories of individual tree biomass data (such as the Legacy Tree Database used in this study) will be key in building more robust and independently evaluated allometric equations at regional-scales. Additional destructive sampling and refinement of nondestructive sampling methods will help quantify and reduce allometric uncertainty.

CHAPTER 2 — FUSING SATELLITE MONITORING WITH AERIAL FOREST HEALTH SURVEYS TO CHARACTERIZE LODGEPOLE PINE FOREST MORTALITY DUE TO BARK BEETLE OUTBREAKS ACROSS THE INTERMOUNTAIN WEST, USA

Introduction

Climate change and susceptible forest stand conditions have created ideal conditions for reproduction, range expansion, and population growth of multiple bark beetle species native to the forests of western North America's Rocky Mountains (Berg et al., 2006; Carroll et al., 2003; Cudmore et al., 2010; Sidder et al., 2016). The coniferous tree species these bark beetles utilize for shelter, food, and reproduction, however, have responded less favorably to these environmental changes (Mantgem et al., 2009; Williams et al., 2013). Drought events and temperature stress have weakened the ability of many vulnerable coniferous tree species to resist the effects of bark beetle occupation (Bentz et al., 2010). This, in combination with an abundance of host tree availability, has resulted in widespread and well-documented tree mortality across millions of acres of Rocky Mountain forests (Hicke and Jenkins, 2008; Raffa et al., 2008). Monitoring tree mortality from these disturbances informs our understanding of disturbance impacts (e.g., Kautz et al., 2017), disturbance dynamics (e.g., Meigs et al., 2015), and forest management (e.g., Vorster et al., 2017). The progression and severity of this historically unparalleled scale of mortality is difficult to monitor across large areas, and as a result, the associated ecosystem, economic, and social impacts are challenging to precisely quantify (Kurz et al., 2008; Patriquin et al., 2007).

Lodgepole pine has experienced particularly high rates of mortality over the past two decades, largely as the result of landscape-scale mountain pine beetle outbreaks (Meddens and Hicke, 2014; Raffa et al., 2008). As a dominant tree species in many of western North America's

iconic forests, lodgepole pine has long been valued for its aesthetic, ecological, recreational, and timber value across its range from southern Colorado, U.S. to the northern reaches of British Columbia, Canada. Often said to be "pole-like" in structure, the species regenerates from seed following intensive disturbance, particularly fire (Anderson and Romme, 1991; Turner et al., 1999), but also harvest (Collins et al., 2011) and bark beetle attack (Kayes and Tinker, 2012). Although mountain pine beetles can impact many conifer tree species, lodgepole pine is a preferred host.

Bark beetles are native to western North America, where they cycle through endemic population levels and large population eruptions that cause widespread disturbance (Raffa et al., 2008). Mountain pine beetle outbreaks most recently arose across the western U.S. Rocky Mountain region between the mid-1990s and early 2010s, aided by drought and high temperatures (Chapman et al., 2012; Sidder et al., 2016). Populations concomitantly grew from multiple epicenters that commonly overlapped outbreak locations from previous decades (Chapman et al., 2012). Mountain pine beetle populations have since returned to endemic levels as the beetles exhausted their supply of suitable host trees (Creeden et al., 2014). Today, dead trees can be seen across large areas, which can remain standing for 10 or more years (Schoennagel et al., 2012). However, surviving trees and advanced regeneration are typically sufficient for these forests to recover (e.g., Nelson et al., 2014). Despite their initial disturbance, bark beetle outbreaks can lead to more heterogeneous forests that may reduce the impact of future insect outbreaks, although these forests may not necessarily be better suited to future drought conditions (Perovich and Sibold, 2016).

The severity of tree mortality caused by mountain pine beetles ranges from low, where a few trees are dead, to stands where nearly all of the trees are dead (e.g., Vorster et al., 2017). The

ecological and hydrological impacts of bark beetle outbreaks vary along this severity gradient (Diskin et al., 2011; Hansen et al., 2015; Ivan et al., 2018; Perovich and Sibold, 2016; Pugh and Small, 2012; Rhoades et al., 2016, 2013). Forest susceptibility to bark beetles and resulting severity patterns are influenced by a number of factors, such as host abundance, stand density, tree size, topographic position, and beetle population pressure (Kaiser et al., 2013; Shore and Safranyik, 1992; Vorster et al., 2017). Forests with high numbers of larger, older pine trees in dry topographic positions are most susceptible during outbreaks, although susceptibility can change throughout an outbreak (Nelson et al., 2014). During the recent outbreaks in northern Colorado, beetles expanded into new stands in the earlier years, while their impacts intensified during the latter outbreak years (Bode et al., 2018; Meddens and Hicke, 2014). Beetles may impact stands for multiple years, and this duration decreases with high beetle pressure (Meddens and Hicke, 2014). Continued research is needed to evaluate bark beetle severity dynamics over time and across large extents.

Broad-scale insect and disease monitoring of U.S. forests is conducted through the U.S. Forest Service's Aerial Detection Survey (ADS). The program conducts annual forest monitoring via fixed wing aircraft that can be used for early detection of insect and disease outbreaks, and to track progression over space and time. Interpreters manually delineate the cause, host species, and severity of tree damage, defoliation, and mortality across millions of forested acres at an extremely fast pace from an airplane using a process called "sketch mapping" (Johnson and Wittwer, 2008). This program has proven cost-effective and generates data that are available soon after surveying. Errors in aerial surveys can arise from a number of factors including, but not limited to, observer differences, differentiating current from past year's impacts, spatial accuracy, weather and viewing conditions during surveys, the timing of surveys relative to

phenology and pest impacts, and variability of the patch size, damage type (e.g. defoliation compared to tree mortality) and severity of forest pest impacts (Backsen and Howell, 2013; Coleman et al., 2018; Johnson and Ross, 2008; Taylor and Maclean, 2008). Aerial Detection Survey data captures trends, but may not be reliable for a specific point location; particularly because homogenous polygons are drawn to represent heterogeneous insect and disease patterns (G.W. Meigs et al., 2015). Evaluations of the accuracy of ADS data have found timing information to be reliable (Meigs et al., 2015) and damage type to be accurate (Coleman et al., 2018), but severity (dead trees per ha) to be considerably underestimated (Backsen and Howell, 2013; Meddens et al., 2012; Meigs et al., 2011) or overestimated (Coleman et al., 2018). The extent can be underestimated in some cases (Bode et al., 2018) and over-estimated in other cases (Meigs et al., 2015). Meigs et al. (2011) found dead trees per hectare recorded by ADS and field measurements to be positively correlated, but ADS underestimated mortality by an order of magnitude. Prominent and common damage agents, particularly those that have visible impacts (e.g., mountain pine beetle), are more accurately classified in ADS surveys than other damage agents (e.g., defoliators like western spruce budworm [*Choristoneura occidentalis* Freeman]); and estimates of dead trees per acre can be less accurate in areas of high mortality (Coleman et al., 2018; Johnson and Ross, 2008).

Estimates of area impacted by insects and diseases often sum ADS polygons, including area covered by live trees or other cover types. Meddens et al. (2012) refined estimates of area impacted in western North America by estimating just the area covered by dead trees. Estimates of mortality area caused by mountain pine beetles in the western U.S. ranged by a factor of 16 (201,582 ha to 3,384,471 ha) due to underestimation of severity by ADS, with the authors emphasizing more confidence in the higher estimate (Meddens et al., 2012). Recent research has

improved bark beetle monitoring and our understanding of outbreak dynamics through the integration of ADS data with satellite-based forest monitoring (G.W. Meigs et al., 2015; Meigs et al., 2011). Satellite monitoring can provide improved estimates of tree mortality extent and severity, while ADS data can describe causal agents and timing.

Satellite remote sensing is a viable tool for monitoring biotic forest disturbances (i.e., insects and diseases; Bode et al., 2018; Long and Lawrence, 2016; Meddens et al., 2013; Woodward et al., 2018), and can be conducted using a range of sensor technologies across spatial and spectral resolutions (Wulder et al., 2006). These efforts to map forest insect and disease impacts are typically limited to specific case studies and need to be developed across larger geographic extents (Senf et al., 2017). Remote sensing methods are well established for monitoring disturbances that result in high magnitude tree mortality, such as fire and harvest, and have been successfully applied across large regions and national scales (e.g., Eidenshink et al., 2007; Hermosilla et al., 2016; Vogeler et al., 2020). However, biotic disturbances resulting in less severe tree mortality have less spectral change and can be difficult to detect (Cohen et al., 2018). Recent advancements in remote sensing software, data storage and transfer, and cloud based image calibration and processing (Gorelick et al., 2017) have enabled improved broad-scale monitoring and detection of vegetation and disturbance (Vogeler et al., 2018; Woodward et al., 2018). These tools can integrate ADS products with remotely sensed maps of mortality severity across large areas, reducing uncertainty, improving our ability to measure forest mortality, and allowing us to better understand patterns of disturbance over time (Bode et al., 2018a; Ghimire et al., 2015; Meigs et al., 2015). Improved estimates of mortality severity and spatial extent have considerable potential to refine estimates of the impacts of bark beetles on a

range of landscape-scale ecosystem processes (Ghimire et al., 2015; Hicke et al., 2016, 2013; Volkova et al., 2018).

The goal of this study was to fuse ADS data and satellite remote sensing to monitor and understand mortality in lodgepole pine forests across four Rocky Mountain states impacted by severe mountain pine beetle outbreaks between 2000 and 2013. My objectives were to 1) model dead canopy area (mortality) across lodgepole pine forests; 2) compare modeled mortality severity and extent with ADS and field observations, and; 3) characterize mortality severity relative to timing, duration, and region by attributing summarized ADS data to the modeled mortality. I used this information to provide refined area estimates of dead lodgepole pine forests and investigate how severity of mountain pine beetle caused mortality varied with timing and duration of the outbreak across multiple spatial scales.

Methods

Study Area

This analysis covered the four state Intermountain West region of Idaho, Montana, Wyoming and Colorado (Figure 2.1). I restricted this analysis to lodgepole pine forests within this region as defined by the Landscape Fire and Resource Management Planning Tools Program (LANDFIRE, 2017). Within the Existing Vegetation Type LANDFIRE layer, the "Rocky Mountain Lodgepole Pine Forest" and "Rocky Mountain Poor-Site Lodgepole Pine Forest" classes were combined to delineate the study area of lodgepole pine dominated forests. I excluded areas that burned between 1984 and 2013, as defined by the Monitoring Trends in Burn Severity dataset (Eidenshink et al., 2007), resulting in a study area covering 248,642 ha. Montana contained the largest area of lodgepole pine forest, followed by Colorado, Wyoming,

and Idaho (Table 1). Lodgepole pine forests in the study area were found in dry montane and subalpine areas between 425 and 3,650 m a.s.l.

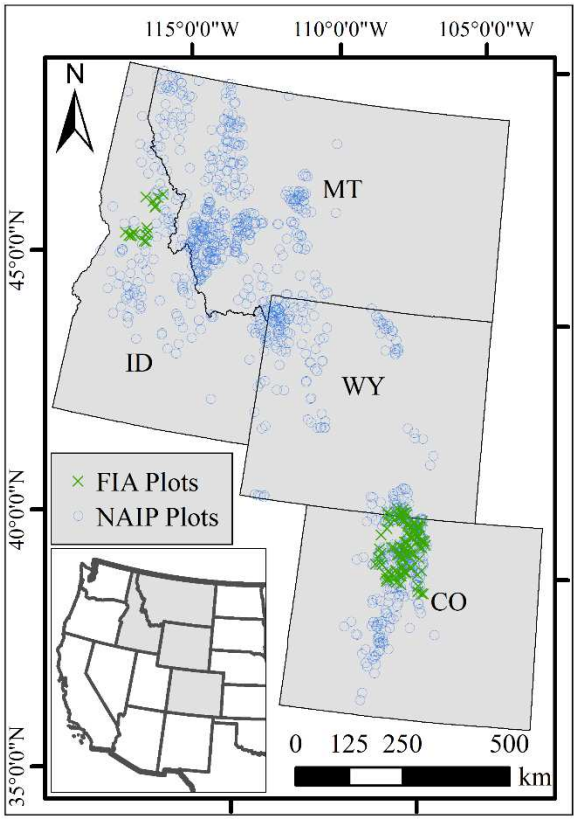

Figure 2.1: The study area encompassed lodgepole pine forests across Colorado (CO), Idaho (ID), Montana (MT), and Wyoming (WY). This map shows the points distributed across lodgepole pine forests that were ocularly sampled with National Agriculture Imagery Program (NAIP) to train mortality severity models. Forest Inventory and Analysis plots (FIA; approximate locations shown) were used to evaluate the mortality severity model and Aerial Detection Surveys.

Table 2.1. Summary of area, elevation, temperature, and precipitation of the lodgepole pine forests (*Pinus contorta*; PICO) of each state in this study (PRISM, 2004).

State	Area (ha)	Lowest elevation (m)	Highest elevation (m)	Mean annual temp (^{O}C)	Mean annual precip (mm)
Colorado	67,901	1,612	3,650	2.4	645.5
Wyoming	50,771	1,522	3,357	2.1	701.5
Montana	94,216	587	3,163	2.9	808.7
Idaho	35,754	425	3,185	3.3	985.3

Digital Sampling

I randomly generated 997 sampling locations distributed within lodgepole pine forests to use for model training. A 30 x 30 m boundary with a 100-point grid was placed at each plot location, matching the pixel size of Landsat imagery. Ocular estimation of four cover classes was conducted at each plot from National Agriculture Imagery Program (NAIP) imagery at 1 m resolution from 2012 (WY) and 2013 (CO, MT, ID). National Agriculture Imagery Program and Landsat imagery have geolocational accuracies that are well suited for paired image interpretation and analysis (Long and Lawrence, 2016; Woodward et al., 2018). Using Google Earth Engine (Gorelick et al., 2017), I mosaiced NAIP quarter quad tiles and created a graphical user interface to record ocular estimates of percent cover for four classes at each plot: live tree canopy, dead tree canopy, shadow, and other (i.e. bareground, urban, water, etc.). Two trained image interpreters calibrated their estimates on calibration plots before sampling the training plots.

Imagery Acquisition and Processing

All image collection and preprocessing were performed in Google Earth Engine. I imported reflectance and thermal imagery from USGS Landsat 5 Collection 1 Tier 1 TOA Reflectance, USGS Landsat 5 Surface Reflectance Tier 1 collection, USGS Landsat 8 Collection 1 Tier 1 TOA Reflectance, USGS Landsat 8 Surface Reflectance Tier 1 collection and synthetic aperture radar imagery from European Space Agency Copernicus Sentinel-1A. The analysis spanned multiple scenes and time periods, so I used surface reflectance and land surface temperature for the most consistency in spectral values despite different atmospheric conditions between images (Young et al., 2017). Top-of-atmosphere (TOA) reflectance was used to derive tasseled cap indices (Baig et al., 2014; Crist, 1985).

I explored different combinations of years and length of season within years to represent pre- and post-outbreak conditions using Google Earth Engine. I optimized model performance among permutations where image availability, image clarity and sensor consistency could be evaluated. This included considering images from 1999-2001 for pre-outbreak years and 2011-2013 for post-outbreak years and exploring months within years ranging from June to October. Using preliminary results from these permutations, I selected the conditions for the final model.

Landsat images were filtered to the years 2001 and 2013 to represent pre- and post-outbreak conditions, respectively. Images acquired between June 1 - October 31 of each year were considered to capture the peak of the growing season and leaf-on conditions of deciduous trees. I used a median composite of the growing season to represent each year. A mask was applied to all Landsat images to remove clouds, cloud shadows, snow and ice using the qa band for each image. Once the images were masked, I selected the median pixel of the remaining imagery to represent each collection. These were then used to calculate indices that included Normalized Difference Vegetation Index (NDVI), Normalized Difference Moisture Index (NDMI), Normalized Burn Ratio (NBR), and tasseled cap greenness, wetness, brightness and angle. I also calculated the difference between these indices from 2001 and 2013. The derived indices (NDVI, NDMI, tasseled cap), the near infrared (NIR), shortwave infrared 1 (SWIR1), shortwave infrared 2 (SWIR2) and thermal bands from 2013 in addition to the differences indices were considered for modeling (Table A2.2). These indices and differenced indices were selected because of their inclusion in other studies to detect bark beetle caused tree mortality (e.g., Bode et al., 2018; Vorster et al., 2017; Woodward et al., 2018). Finally, I used vertical transmit-vertical receive polarisation (VV) backscatter signal from European Space Agency's

(ESA) Sentinel-1 radar data that provides a measure of features on the earth surface based on the active signals that are returned back to the sensor.

I also considered alternative methods for deriving Landsat variables. These included informative variables and harmonized (i.e., fitted) spectral predictors from LandTrendr products (Kennedy et al., 2018, 2010; Vogeler et al., 2018). These relatively new methods to preprocess Landsat spectral data for time series analyses perform well and address some of the radiometric complications with these types of analyses (Vogeler et al., 2018; Woodward et al., 2018). However, these products did not perform as well as the median composites predictor variables described above when model performance was evaluated among the approaches and, therefore, I did not use these for final dead canopy area models (hereafter referred to as mortality severity products).

Aerial Detection Survey Processing

The Aerial Detection Survey (ADS) data for 2001 to 2013 were obtained from the USDA Forest Service Data Portal. Aerial survey data were used to attribute information about the cause and timing of tree mortality to the modeled mortality severity products and as a comparison to the extent and severity shown in the modeled products. Aerial surveys are flown each year and observers in airplanes delineate polygons of areas impacted mainly by insect and disease. For each polygon of forest impacted by insect and/or disease, I used the following attributes: area, damage causal agents (DCA), damage type, forest type, host tree species and measure of mortality (dead trees per acre [TPA]). These polygons may have up to three damage causal agents, damage type, forest type, host tree species and measures of mortality. Since not all forested areas are flown each year, I calculated the percent of the study area covered by annual aerial surveys (Figure 2.2).

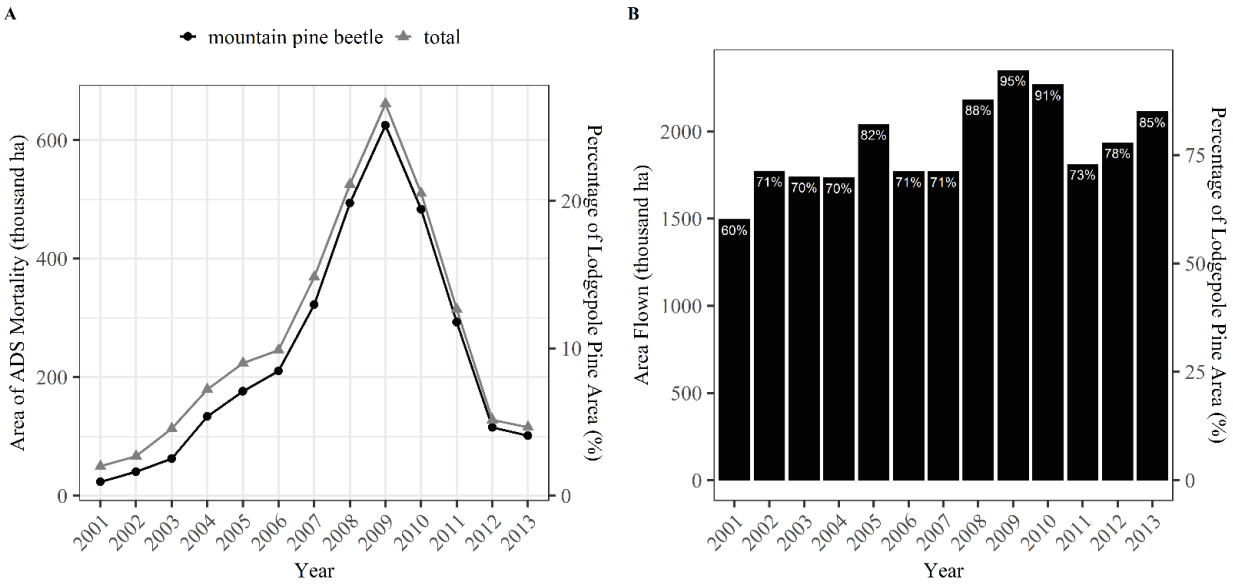

Figure 2.2. (A) Area and percent of lodgepole pine mask impacted by insect or disease in Colorado, Wyoming, Montana, and Idaho, as indicated by Aerial Detection Survey (ADS) data. Calculated using the pixel count of the area attribute in the ADS data, which includes polygons that had NoData values as damage causal agents. (B) Area and percent of lodgepole pine in the study area flown by ADS from 2001 to 2013.

I converted ADS polygon data to rasters for compatibility with modeled mortality severity products and to allow for summarization of ADS data across years for each pixel (e.g., Meddens et al., 2012; Meigs et al., 2015; Meigs et al., 2011). The ADS rasters were created at 30 m grain size to align with modeled mortality severity. All ADS data manipulation and processing was done in R statistical software (R Core Team, 2018). I first converted the polygons to raster format and then clipped them to the lodgepole pine study area. Attributes of interest were summarized and extracted as rasters from the stack to determine the timing and causes of modeled mortality severity and information summarizing mortality dynamics. These attributes included highest dead TPA value, DCA for the year with the highest dead TPA, first year of mortality, last year of mortality, most severe year of mortality, number of years with mortality, most common DCA across all years, and cumulative mortality. The only ADS damage type used to create these rasters was current year mortality and previously undocumented mortality.

Mortality is defined by ADS as, “Standing dead trees that have died since the last survey” (Forest Health Monitoring Program, 1999). Note that the year I report is the year of detection, which is typically one year later than the year of infestation.

Mapping and Evaluating Dead Canopy Cover

I used random forests to model dead canopy cover using digital sampling training plots and remotely-sensed predictor variables. Random forest models are commonly used in remote sensing analyses of forest characteristics because of their high performance, resistance to overfitting, and ability to handle non-parametric data (Belgiu and Drăgu, 2016; Breiman, 2001). Variable Selection Using Random Forest (VSURF) was first used to select predictor variables suitable for prediction (Genuer et al., 2015). Then, for each pair of variables correlated >= |0.7|, I removed the variable with lower variable importance from a random forest run with the prediction variables selected by VSURF. I ran a random forest model for this refined list of predictor variables in R with 500 trees and two variables considered at each split (Liaw and Wiener, 2002).

Model performance was evaluated using a proportion of variance explained (R^2), root mean squared error (RMSE), scatter plots of predicted vs. observed, comparisons of field measurements to model predictions, and through visual evaluation of model predictions over aerial imagery. Out-of-bag error metrics generated from randomly subsetting training data and predictor variables during the model fitting process are robust measures of model performance (Breiman, 2001). I evaluated model performance using out-of-bag measures of the RMSE and the R^2.

I also evaluated the mortality severity predictions and ADS cumulative mortality through comparisons with standing dead basal area at U.S. Forest Service Forest Inventory and Analysis

(FIA) field plots from an area in northern Colorado and a sliver of southern Wyoming defined by the extent of Worldwide Reference System 2 path 34, row 32 (hereafter referred to as Colorado plots) and the Idaho portion of path 42, row 28 (Figure 2.1). Exact plot locations were obtained through a non-disclosure agreement with FIA. I only used plots that fell within the lodgepole pine forest extent and that were sampled between 2012 and 2015 since mortality in lodgepole pine forests had slowed substantially by 2012. This resulted in 99 Colorado plots and 17 Idaho plots.

In addition, I randomly generated 2,000 samples within the lodgepole pine extent across each state (total of 8,000 samples) to evaluate trends across the study area. These samples were used to compare modeled mortality severity to ADS cumulative mortality, duration of impact, and first, most severe, and last year of impact. The samples were restricted to the overlap between where ADS surveys existed and the modeled lodgepole mortality extent so that comparisons could be made between the two products and because I was using attributes from both ADS and modeled mortality severity. I compared mean modeled mortality with these 8,000 points between states using an ANOVA, and evaluated significant differences between states using a Tukey's range test (McDonald, 2014). A threshold was needed to categorize the continuous mortality map into areas of presence or absence of tree mortality to allow comparison to the extent of mortality shown by ADS. I calculated the threshold as the y-intercept from a linear model of the relationship between predicted and observed values at the training points. This threshold value (7.5) represents the average minimum detectable tree mortality from my approach (Wulder et al., 2010). I also tested thresholds of 5 and 10 percent dead canopy cover to explore sensitivity of agreement between the model predictions and ADS to threshold selection.

When ADS surveys are conducted, tree mortality <¼ TPA is considered background mortality and is typically not recorded.

Results

Comparison between modeled mortality severity and Aerial Detection Surveys

Mortality severity predictions captured heterogeneity in tree mortality patterns at a finer scale than ADS surveys (Figure 2.3). The final random forests model performed reasonably well in modelling mortality severity across the expansive four-state region (R^2 = 44.5, RMSE = 13.6 %; Figure 2.4; Figure A2.4). Visual evaluation of the model predictions over aerial imagery showed that the model captured landscape mortality trends (Figure 2.3). The final mortality severity model included six predictor variables (Figure A2.2). The normalized difference moisture index, which represents a difference between pre- and post-outbreak imagery, was the strongest predictor variable.

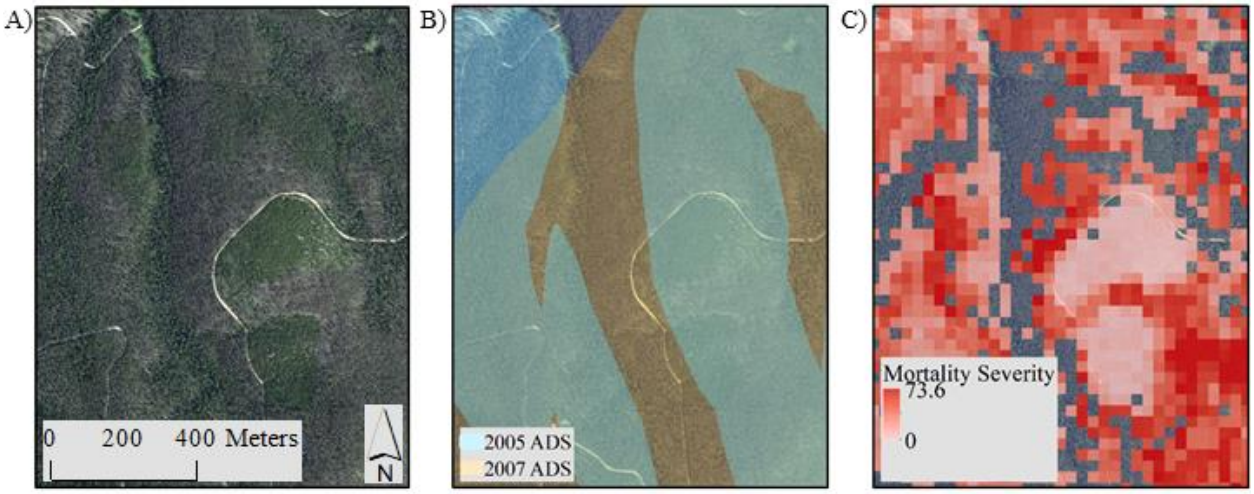

Figure 2.3. Comparison of the same area in (A) aerial imagery, (B) mortality detected by 2005 and 2007 Aerial Detection Surveys (ADS), and (C) mortality severity predictions. Grey areas in the aerial imagery are standing dead trees, and green areas are forests with little mortality. The grey gaps in model predictions in panel C are areas outside of the LANDFIRE derived lodgepole pine forest type mask.

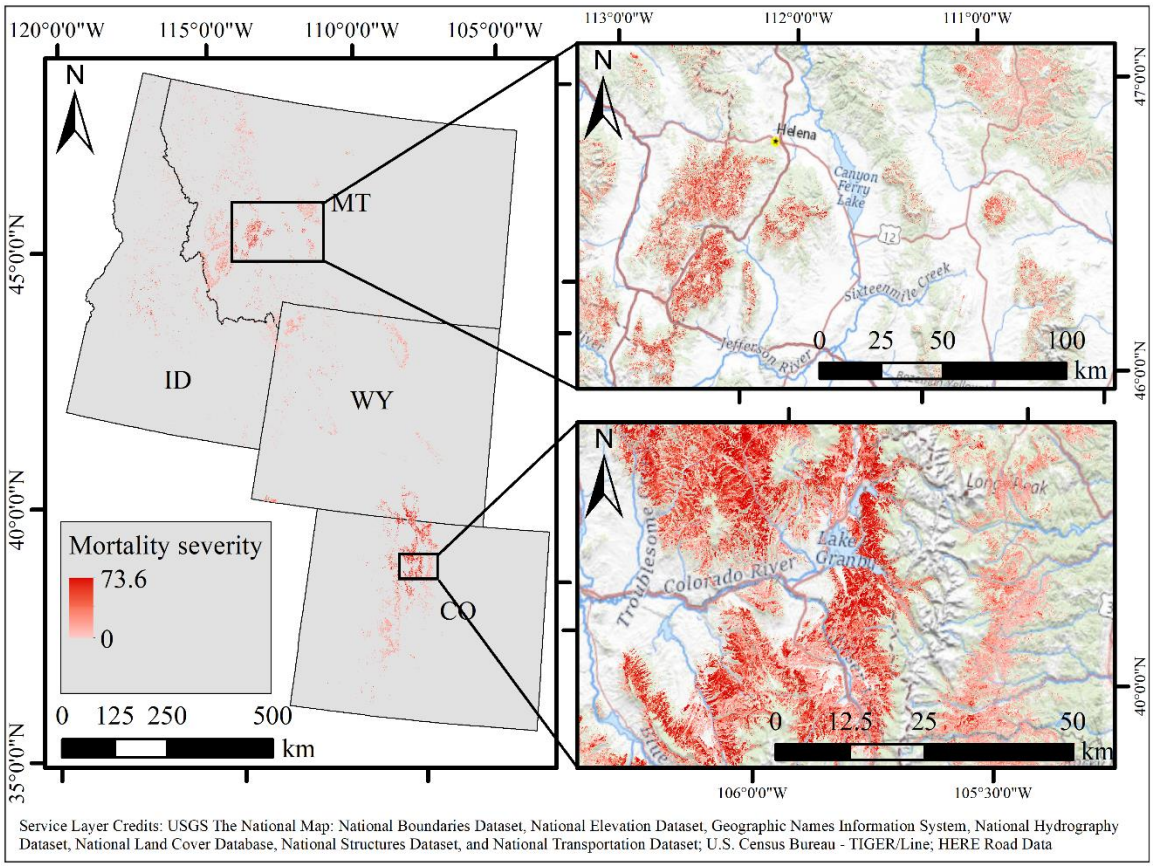

Figure 2.4. Modeled mortality severity across the study area and for geographic subsets in Colorado and Montana (right side). Colorado (CO), Idaho (ID), Montana (MT), and Wyoming (WY)

Modeled mortality severity and ADS cumulative dead TPA were significantly, but weakly correlated (Figure A2.3). When compared to dead basal area in FIA plots, the mortality severity model predictions were more correlated ($R^2 = 0.32$, $p < .0001$) than ADS cumulative mortality ($R^2 = 0.03$, $p = 0.04$; Figure 2.5). The mortality severity model, which mapped percent dead canopy, reasonably represents dead basal area, a field-based measurement that is also highly correlated with dead biomass. Higher mortality severity predictions have larger errors than low mortality predictions.

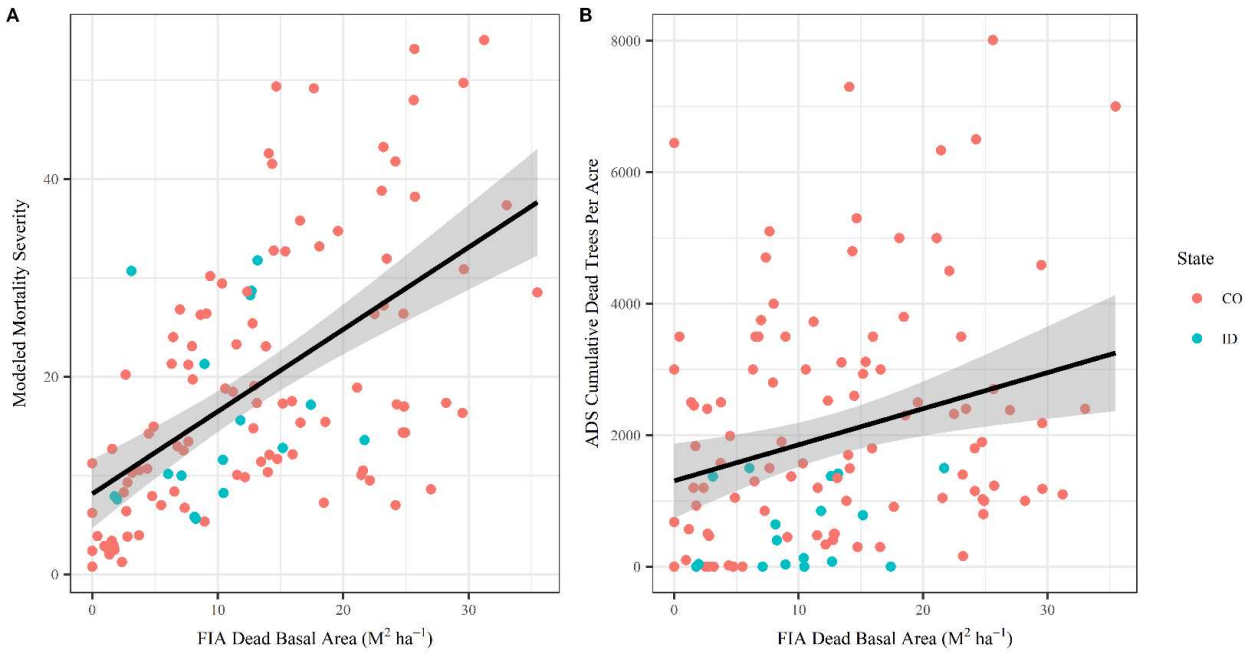

Figure 2.5. Dead basal area measured in FIA plots in Colorado and Idaho compared to (A) modeled mortality severity and (B) Aerial Detection Survey (ADS) cumulative mortality. The black lines show a linear model with the 95% confidence interval.

Comparison to FIA data shows differences in ADS severity observations between Colorado and Idaho. For similar dead basal area values, Colorado ADS data record higher cumulative mortality values than Idaho (Figure 2.5). All Idaho values are less than 2,000 dead TPA compared to Colorado values that reach 8,000. Dead basal area measured at these FIA plots does show lower mortality in Idaho, but to a much lesser degree than ADS (Figure A2.1). Both field-measured FIA dead basal area and modeled mortality at the FIA plot locations show an overlapping distribution of mortality in Colorado relative to Idaho, with Colorado having slightly higher and more variable mortality. In contrast, the distribution of ADS cumulative dead TPA is substantially lower in Idaho than in Colorado (Figure A2.1).

Both modeled mortality severity and ADS data indicated that Colorado and Montana had the most lodgepole pine forest impacted by recent mountain pine beetle outbreaks, followed by Wyoming and Idaho (Figure 2.6). Using the calculated threshold of 7.5 on the mortality severity

model, 1.61 million ha was mapped as impacted by mortality. This changed to 1.84 million ha when a threshold of 5 was applied, and 1.52 million ha for a threshold of 10. Of the 1.61 million ha of lodgepole pine forests flagged as impacted by either ADS or thresholded model predictions, modeled mortality severity predictions and ADS data were in agreement over about half of this area (855,883 ha). Roughly a quarter of this area was unique to modeled mortality severity predictions (370,650 ha) and a quarter unique to ADS (383,796 ha, Figure 2.6). Modeled mortality severity was highest in areas where ADS and the thresholded model overlapped (mean = 21.6%, standard deviation [sd] = 12.7%), followed by mortality areas shown to have mortality according to the thresholded model, but not ADS (mean = 13.4%, sd = 7.3%). Areas where only ADS indicated mortality had the lowest mean mortality severity (mean = 4.5%, sd = 1.8%).

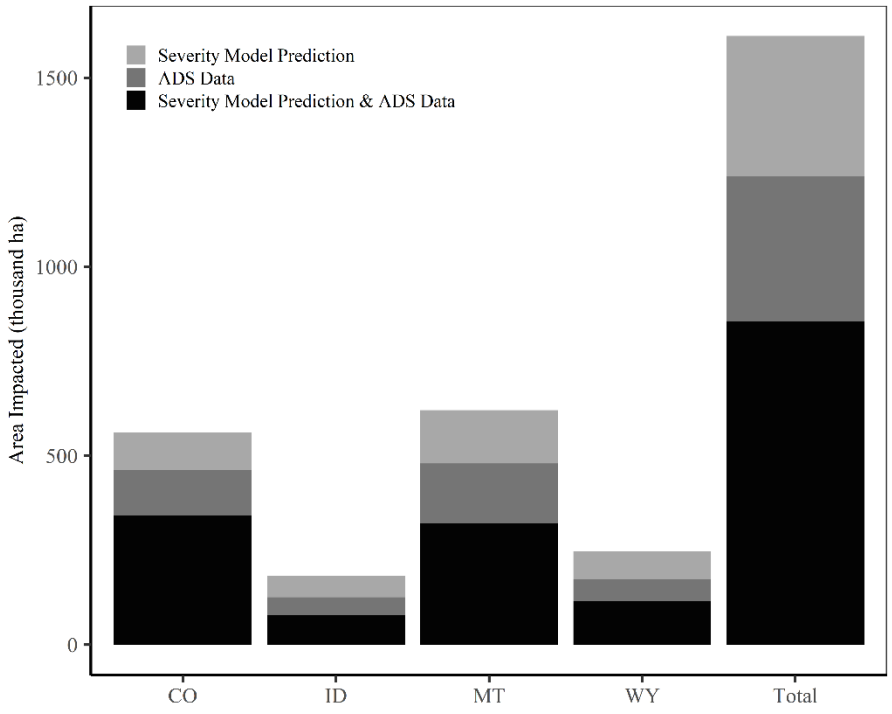

Figure 2.6. (A) Comparison between mortality severity predictions and Aerial Detection Surveys (ADS) cumulative dead TPA at 8,000 points randomly generated across the study area. (B) Agreement and disagreement in the area impacted according to mortality severity predictions and ADS, shown for each state: Colorado (CO), Idaho (ID), Montana (MT), and Wyoming (WY).

Outbreak Dynamics

Information about the timing and cause of mortality from ADS was paired with modeled mortality severity where they overlapped to better understand lodgepole pine mortality dynamics, as this information cannot be captured by using the modeled severity alone. The tree mortality in the study area was predominantly caused by mountain pine beetle outbreaks peaking between 2007 and 2011 (Figure 2.2). Newly-impacted area (e.g., first year of ADS tree mortality detected for each pixel) increased until 2009, after which few areas were newly impacted (Figure 2.7). Pixels first impacted later in the outbreaks (e.g., after 2008) were less severely impacted than areas impacted early in the study period and during the peak of the outbreaks. Stands only impacted early in the outbreak (represented by stands with a last year of mortality before 2006), were few and experienced relatively low mortality. The most severe year of mortality (e.g., the year with the highest ADS dead TPA for each pixel) covered more area starting in 2006, and then sharply declined in 2012, the same year that the last year of mortality declined.

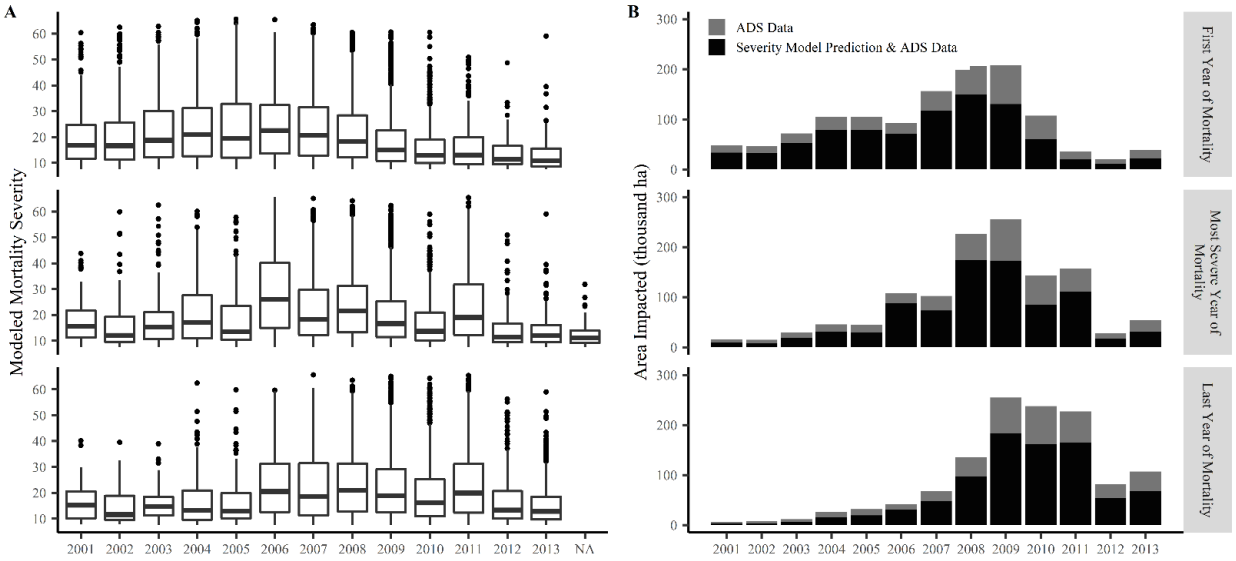

Figure 2.7. (A) Modeled mortality severity between 2001 and 2013 in the first, most severe, and last year of mortality using 8,000 random points distributed across the four-state study area. (B) Area impacted each year that was a pixel's first, most severe, or last year of mortality. Black

represents areas where model predictions overlap with ADS polygons, and grey represents ADS polygons where models did not predict mortality greater than 7.5%. Areas where model predictions show mortality greater than 7.5%, but where ADS polygons are absent are not shown because I do not have information about the year of mortality from ADS for these areas.

Mean mortality between states was variable ($F[3, 7{,}996] = 209.6$, $p = <0.0001$). Post hoc testing showed that all states had statistically significant differences in mortality ($p < 0.0001$) except Colorado and Wyoming ($p = 0.97$). The Colorado and Wyoming lodgepole pine forests experienced higher severity lodgepole pine mortality than Idaho and Montana (Figure 2.8).

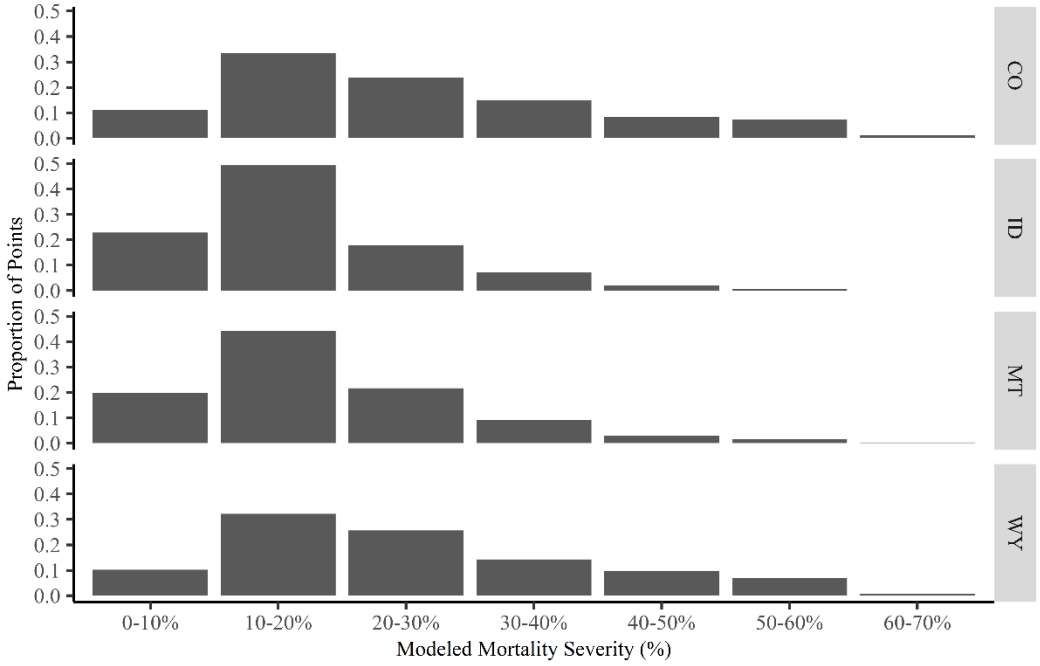

Figure 2.8. Histograms of modeled mortality severity for each state at 8,000 randomly distributed points across the study area. (CO = Colorado, ID = Idaho, MT = Montana, WY = Wyoming)

Low severity mortality (10-20% dead canopy) was the most common in all states, and area declined as severity increased. Mortality greater than 40% was particularly rare in Idaho and Montana (Figure 2.8). The models show the most mortality area (canopy area of dead trees) in Colorado (107,626 ha) and Montana (94,846 ha). Wyoming had roughly half the mortality area (46,042 ha) of Colorado and Montana, but more than Idaho (28,339 ha) because it had slightly

more impacted lodgepole pine forest, and because the severity was higher in Wyoming than Idaho.

When aggregating data across all four states, mortality severity increased with the number of years mortality was observed for a given location by ADS (Figure 2.9A). There was a similar amount of area impacted for one, two, or three years, which then successively declined as the duration increased past four years (Figure 2.9B). Few areas had active mortality for more than six years. Additionally, agreement between ADS and modeled mortality severity improved as duration, and presumably severity, increased.

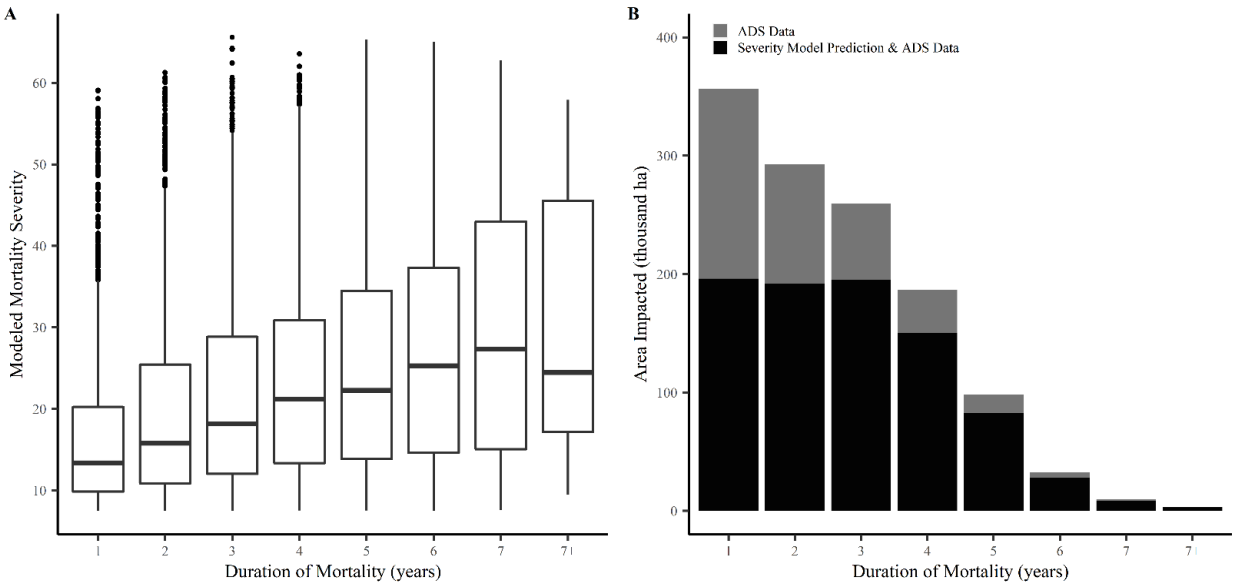

Figure 2.9. (A) Box plots of modeled mortality severity grouped by duration (years) bins of the 8,000 points randomly generated across the study area. (B) The relationship between area impacted by tree mortality and duration of mortality detected by Aerial Detection Surveys (ADS) or both ADS and thresholded modeled mortality severity.

These relationships between duration and mortality severity differed for some states (Figure A2.6). Increasing mortality severity with duration holds for all states except Idaho. This may be influenced by the fact that little area in Idaho was impacted for more than three years.

Lodgepole pine forests were most commonly impacted for one year in Idaho and Montana, and for three years in Colorado.

Discussion

In this study, I mapped tree mortality in lodgepole pine forests from insects and disease across Colorado, Idaho, Montana, and Wyoming. The methodology relies on free and publically-available data sources that are continually collected (e.g., Landsat, NAIP, and FIA), thus lending itself well to efficient applications across large areas in other regions with similar satellite image availability. The maps of mortality severity capture cumulative mortality from 2001 to 2013, showing both area impacted and mortality area at 30 m^2 spatial resolution. Satellite-derived estimates of tree mortality capture the extent and severity of tree mortality at a finer spatial resolution than aerial detection surveys, are more consistent across large areas, and can have better spatial coverage. When compared to independent FIA field data, the maps were better correlated with mortality severity than aerial detection surveys. However, aerial detection surveys provide additional information about the timing, type (e.g., defoliation or mortality), causal insect or disease, and host tree species. I combined these complementary data sources to characterize bark beetle dynamics in lodgepole pine forests.

Mountain pine beetles were the primary cause of insect and disease caused tree mortality between 2001 and 2013 (Figure 2.2; Berner et al., 2017; Meddens et al., 2012). These outbreaks resulted in 276,854 ha of mortality area, most of which was low severity (10-20% mortality; Figure 2.8; Meddens et al., 2012). Meddens et al. (2012) estimated that mortality area of lodgepole pine from mountain pine beetles across the entire western U.S. ranged between 160,541 ha and 2,858,860 ha, with greater confidence in the higher estimate. While it is difficult to make a direct comparison to this study because I mapped a subset of the states they covered,

and I had different methods for determining the extent of lodgepole pine, my estimate of mortality area (276,854 ha) exceeds the low estimate, supporting the claim by Meddens et al. (2012) that the low estimate is unrealistically low.

Expansion of the mountain pine beetles to new areas during the early and late stages of the outbreaks was much less than during peak years (Figure 2.7). Additionally, it was rare for stands to only be impacted early in the outbreaks. Stands were commonly impacted for up to five years. Thus, stands impacted early in the outbreak can be expected to continue experiencing mortality if suitable host trees are present. Meddens and Hicke (2014) found temporal characterization of bark beetle outbreaks to be scale-sensitive, and also report most pixels were impacted for five or less years in northern Colorado. I found that the longer stands were impacted, the higher the mortality severity tended to be (Figure 2.9). Meigs et al. (2011) also reported a positive relationship between duration and mortality severity in Oregon's eastern Cascade Range. These long duration and high mortality severity stands are likely highly susceptible to bark beetles because they have abundant, large pine trees, and thus can support bark beetle populations for a longer duration than low susceptibility stands. Additionally, with many host trees, these stands have the potential to be severely impacted, while a stand with only a few host trees will have low mortality severity as measured by dead canopy area even if all hosts are killed.

The outbreak expanded to new areas most rapidly between 2007 and 2009 (Figure 2.7). The area impacted for the first time in each year represents the degree to which outbreaks were spreading (Figure 2.7). Over the four state region, there was a sharp drop in the areas the beetle was spreading after 2010. At the state scale, bark beetles slowed their spread earlier in Wyoming (2009) and Colorado (2010), than in Montana and Idaho (both 2011). The two states with the

greatest mortality area, Montana and Colorado, exhibited different outbreak dynamics. Colorado's outbreak was consistently sustained over more years, while Montana had a more pronounced peak in bark beetle activity (Figure 2.7).

This study emphasizes that outbreak patterns should be analyzed at multiple scales. Outbreak dynamics at the four-state scale do not always reflect dynamics at the state level, and the patterns in states with less mortality area (i.e., Idaho) can be washed out by patterns in more severely impacted states (i.e., Colorado and Montana). This study analyzed coarse scale patterns, and different patterns may emerge at finer scales. The occurrence of these outbreaks across this region suggests large-scale climatic drivers such as drought and elevated temperatures triggered and maintained these outbreaks (Chapman et al., 2012; Creeden et al., 2014). Yet, fine scale variation in forest structure, composition, and management history shape local mortality severity patterns (Raffa et al., 2008; Vorster et al., 2017). Bark beetles are the dominant cause of tree mortality in Colorado and Wyoming, whereas fire and harvest contribute more of the tree mortality in Idaho and Montana (Berner et al., 2017). While I removed burned areas from this analysis, I did not remove areas where forest management occurred because I am not aware of data across this region that reliably delineates forest management.

The fact that beetle pressure was still high in 2011 (as evidenced by the large amount of area that suffered its most severe year of mortality in Figure 2.7), yet the area impacted for the first time was low, indicates that mountain pine beetles had likely diminished their supply of host trees, leading to their population decline. These low-severity stands first impacted late in the outbreak are likely poor stands for mountain pine beetles (Nelson et al., 2014). The beetles intensified their impacts within the stands they were already in towards the end of the outbreaks, as opposed to expansion to new areas as they did earlier in the outbreaks (Figure 2.7). This

observation of extensification followed by intensification was also reported by Meddens and Hicke (2014) and Bode et al. (2018) in northern Colorado.

Mortality severity was lower early in the outbreaks, and forest recovery and snagfall has had longer to occur in areas impacted early in the outbreaks. These factors give us reduced confidence in the accuracy of the mortality severity predictions in these early-outbreak areas. It is also possible that I underestimated mortality in areas that recover quickly, such as productive sites with rich understory or areas with abundant advanced regeneration (Meigs et al., 2011). A time series approach to mapping bark beetle mortality (e.g., Meigs et al., 2015) could help with these issues. However, the models I constructed using LandTrendr disturbance metrics performed relatively poorly (R^2 = 36.0, RMSE = 14.6 %). Spectrally harmonized images, such as the LandTrendr-fitted images I tested, can reduce noise in spectral values over time. When I used these LandTrendr-fitted images from two points in time (pre and post outbreak), models performed nearly as well (R^2 = 43.0, RMSE = 14.0 %) as the final model. Further research is needed to determine whether harmonizing images across time improves detection of forest insect and disease impacts, or if it removes the signal of these minor spectral changes.

This methodology could also be improved with the use of field data to train models rather than points collected through ocular sampling of aerial imagery. Interpreting NAIP imagery is time efficient and low-cost, but can pose challenges, with some locations having better image clarity than others. Field plots would capture tree mortality more accurately, but are more time-consuming and expensive to collect and are harder to distribute across the landscape and across ownerships. The FIA plot network would be an ideal dataset, since it is already being collected across forested areas in the U.S. With this approach, a different mortality metric than dead canopy area would have to be modeled, such as dead basal area or number of dead trees.

Aerial detection survey data are a valuable resource for monitoring insect and disease impacts, providing an unparalleled historical record of forest insect and disease mortality. However, such an ambitious monitoring program has significant limitations that should be considered when interpreting these findings. Surveys are conducted by different individuals across states and Forest Service regions, leading to issues such as inconsistent estimates of dead trees per acre. This was evident in the comparison of aerial detection surveys to FIA plots—Colorado aerial detection surveys had higher cumulative dead trees per acre values compared to Idaho aerial detection surveys for plot locations with similar dead basal area (Figure 2.5; Figure A2.1). Since ADS observers survey the same regions each year, ADS accuracy and bias varies geographically. Other factors can contribute to biased differences between ADS observations and field observations such as the type of insect or disease, damage type, severity and forest type. These factors may help explain why some studies have found ADS to underestimate mortality severity (Backsen and Howell, 2013; Meddens et al., 2012; Meigs et al., 2011), while others have found ADS to overestimate (Coleman et al., 2018). Caution is advised when comparing ADS dead TPA values across multiple states or U.S. Forest Service regions. Remote sensing modeling approaches to mapping mortality severity are better suited for comparisons of mortality severity across large extents since they provide consistent mortality severity estimates.

I compared ADS, remotely sensed, and field measurements of tree mortality to help define uncertainty surrounding ADS severity and extent. One issue with these comparisons is that ADS polygons are not intended to represent a specific point like remote sensing pixels or field plots. They are intended to provide data to inform forest insect and disease trends and to flag forest conditions to be investigated more closely at the local scale. However, ADS data are being applied at smaller scales for management and research and thus need to be evaluated at

these scales. Like another comparison of forest insect and disease detection between Landsat-based detection, ADS, and field data, I found remote sensing insect and disease detection to be better correlated with field measurements than ADS was with field measurements (Meigs et al., 2011). Meigs et al. (2011) report higher correlations between field measurements and ADS cumulative dead TPA (adjusted $R^2 = 0.37$) than I did in this study ($R^2 = 0.03$). While correlated, Meigs et al. (2011) found dead tree counts were an order of magnitude higher in plot measurements. One reason for the lower correlation in this study may be that I measured mortality severity in field plots in terms of dead basal area, while Meigs et al. (2011) used dead tree count, which is the same metric as ADS. Another possible factor contributing to the lower correlation between FIA and ADS is that while Meigs et al. (2011) mapped mortality in a single state and U.S. Forest Service region, I mapped mortality across four states and three Forest Service regions. Observer differences across such a large area could reduce correlations between ADS and field observations.

In comparisons of the mortality extent between ADS and my maps, I found agreement in roughly half of the area impacted, and these areas had more severe tree mortality than areas only shown by one source (Figure A2.5). A quarter of the total area impacted was solely detected by ADS, and the mortality model solely detected another quarter of the total area impacted (Figure 2.6). A number of factors are likely contributing to the large area only detected by one of the data sources. One factor is scale—ADS maps mortality at a coarser scale, and the polygons likely overestimate the area impacted by mortality since the polygons cover heterogeneous mortality patterns (Meigs et al., 2015). These polygons span areas with and without mortality and even non-forested areas, while the remote sensing products are detecting mortality in 30 m x 30 m pixels (Backsen and Howell, 2013; Meigs et al., 2015). The areas detected solely by the model

could represent areas that were not flown by ADS surveys (Figure 2.2), impacted forests that were not captured in ADS surveys, or modeled false positives. These areas generally represented forests with lower severity tree mortality (Figure A2.5). Low severity mortality is the most difficult to detect with satellite spectral remote sensing, and has the highest potential for commision and omission errors (Cohen et al., 2018; Goodwin et al., 2008; White et al., 2007).

In the areas shown to have mortality by my models, but not by ADS, I analyzed the predicted mortality severity and the FIA plots to determine if these are true or false positives for the models. Pixels indicated to have mortality by the morality models but not by ADS had a mean modeled severity of 13.4%. In comparisons of mortality severity predictions to FIA field measurements, predictions above 13% consistently correctly identified plots as having mortality (Figure 2.5). Additionally, the comparison of FIA dead basal area to ADS cumulative dead TPA showed that ADS is prone to false negatives—plot locations where ADS does not capture mortality measured by FIA (Figure 2.5). Therefore, much of the area predicted to have mortality by the thresholded model, but not by ADS, likely represents areas with true mortality. Aerial detection surveys are likely overestimating mortality extent within the polygons, and are not capturing other areas on the landscape with mortality, particularly low-severity mortality (Bode et al., 2018). My best estimate of mortality impacted lodgepole pine forest area is the sum of the overlapping areas and the model-only areas (1.23 million ha). Thus, the remote sensing method presented in this study seems to better capture both the extent and severity of forest mortality than ADS. These findings suggest that approaches relying on ADS to define the extent of mortality may not capture a substantial amount of impacted forest.

Conclusion

Tree mortality severity is a major determinant of bark beetle's ecological impact—the alterations to forest structure and species composition initiated by these disturbances (Abella and Fornwalt, 2014; Collins et al., 2011) are expected to work in concert with climate change to accelerate forest change (Foster et al., 2018). Consistent representations of the extent and severity of bark beetle outbreaks across large extents is needed. This study addressed this need by mapping mortality severity in lodgepole pine forests across Colorado, Idaho, Montana, and Wyoming. I combined the strengths of satellite remote sensing (detecting canopy change, or mortality severity) with the strengths of existing Aerial Detection Surveys (identifying mortality causal agent and timing) to characterize lodgepole pine forest mortality, with a focus on mountain pine beetles—the dominant causal agent in the 2000s. This method is efficient, as it relies on existing aerial forest health surveys and free satellite imagery, along with aerial image interpretation substituted for field assessments. Remote sensing based estimates can provide a better estimate of both the area impacted and the mortality area, thus more accurately reflecting impacts of disease and insects, and providing a more accurate basis for management planning and for evaluating the insect and disease impacts on ecosystem processes. This approach offers promise for large-area disturbance monitoring.

CHAPTER 3 — QUANTIFYING STANDING DEAD FOREST BIOMASS FROM BARK BEETLE OUTBREAKS AND EVALUATING BIOENERGY PRODUCTION SCENARIOS IN THE SOUTHERN ROCKY MOUNTAINS, USA

Introduction

Widespread tree mortality caused by native bark beetles across western North America has significantly impacted the forest carbon cycle (Hicke et al., 2013; Kurz et al., 2008). These outbreaks transfer carbon from live to dead trees, where the carbon is slowly released to the atmosphere as the dead trees decompose. Growth rates of surviving vegetation typically increase, facilitating the forest's return to serving as a carbon sink within several years to several decades (Hansen, 2013; Raymond et al., 2015). National carbon inventories, like those mandated by the United Nations Framework Convention on Climate Change (UNFCCC, 1992), track and report these forest carbon sources and sinks. Deadwood is one important forest carbon pool (Goodale et al., 2002) that can also benefit biodiversity (Harmon et al., 1986) and forest resilience (Marzano et al., 2013). Methods for improved deadwood estimation are being actively developed (Domke et al., 2011; Woodall et al., 2019) and are improving our understanding of the forest carbon cycle (e.g., Woodall et al., 2012).

Ecosystem models of forest carbon trajectories following bark beetle outbreaks rely on estimates of dead tree biomass (Ghimire et al., 2015), which can be difficult to quantify with remote sensing. Previous work has combined information about bark beetle outbreak severity, extent and timing with biomass estimates to create spatially-explicit dead biomass estimates. Estimates of bark beetle-killed carbon and biomass across the western U.S. forests range from 5 to 15 Tg C yr-1 (2002 – 2009; Ghimire et al., 2015), 2 to 24 Tg C yr-1 (1997 – 2010; Hicke et al., 2013), and 14.6 ± 7.0 Tg C yr^{-1} (2003 – 2012; Berner et al., 2017). Much of the uncertainty in

beetle-killed carbon estimates results from the lack of detailed information about bark beetle outbreak extent and severity (Ghimire et al., 2015). Aerial detection surveys are often the primary data source for insect and disease caused tree mortality used in these dead carbon estimates. Remote sensing analyses more accurately capture the extent and severity of bark beetle outbreaks than ADS (Vorster et al., in prep), and remote sensing captures cumulative, rather than annual mortality. Cumulative mortality severity has been mapped for multiple bark beetle species (Long and Lawrence, 2016; Woodward et al., 2018), annually (Bode et al., 2018), and across large extents (Vorster et al., in prep). Using these maps of cumulative mortality severity paired with biomass data is a promising method for mapping dead biomass. Disturbance mapping using Landsat time series algorithms such as LandTrendr have also been used as the basis for mapping forest insect-killed carbon, basal area, and biomass (e.g., Bright et al., 2014; Hudak et al., 2013; Meigs et al., 2015; Pflugmacher et al., 2012).

Uncertainty in bark beetle-killed carbon and biomass estimates also originates from underlying biomass maps. Biomass has been estimated from existing national biomass maps (Blackard et al., 2008; Hicke et al., 2013), an average of biomass maps (Berner et al., 2017), or by the county average aboveground tree biomass from Forest Inventory and Analysis plots (FIA; Ghimire et al., 2015). Berner et al. (2017) found that national biomass maps significantly disagreed, particularly at the pixel scale, and that addressing this disagreement resulted in improved dead carbon estimates. The use of biomass maps calibrated for smaller regions is a promising avenue for improving spatially explicit dead biomass estimates.

Beetle-affected stands can be left unutilized or salvage logged for timber, bioenergy, and bioproducts. With the tremendous quantities of beetle-killed biomass now spread across forests in the western U.S., utilization of beetle-killed biomass and low-value feedstocks such as slash

and small-diameter material has received interest as a feedstock for bioenergy and bioproducts (Campbell et al., 2018). This is an appealing prospect because this material is often left on site or is treated as a waste product that is burned on site for disposal. It is also a bioenergy feedstock that does not compete with food production. However, the ecological impacts of salvage harvesting (Fornwalt et al., 2018; Johansson et al., 2016; Riffell et al., 2011) and the climate impacts of forest bioenergy (Field et al., 2018; Zanchi et al., 2012) must also be considered. Additional uncertainty surrounds the economic viability of bioenergy from beetle-killed trees, although some bioenergy products may be viable (Campbell et al., 2018). Biomass maps can be used to assess feedstock quantity, location, condition, and accessibility to evaluate bioenergy economic scenarios and inform facility siting (Hogland et al., 2018).

Northern Colorado and southern Wyoming were some of the most severely bark beetle impacted areas in the western U.S. (Berner et al., 2017). The first objective in this study was to test new methods for mapping aboveground standing dead biomass. I calculated dead biomass at field plots, accounting for structural loss and density reduction in standing dead trees. I then paired this field data with mortality severity data, aboveground biomass, climate, and geomorphometric layers to map aboveground standing dead biomass at a moderate resolution (30 m x 30 m). The second objective was to evaluate the distribution of live and dead biomass in this bark beetle-impacted landscape. I analyzed plot and landscape-scale biomass patterns by species and forest type. Lastly, the third objective was to use live, dead, and total biomass maps to quantify potentially accessible biomass for hypothetical bioenergy production scenarios and facility locations.

Methods

Study Area

This study encompassed 1.52 million ha of forest in northern Colorado and southern Wyoming defined by the extent of the Worldwide Reference System 2 path 34, row 32 (Figure 3.1). Elevations span from 1,553 m to 4,135 m above sea level, with mean temperature and precipitation ranging from 13 °C to 52 °C and 31 cm to 180 cm, respectively. Six forest types, as classified and mapped by the U.S. National Vegetation Classification and LANDFIRE (2017), account for 84% of the forested area (listed from most to least area): lodgepole pine forest and woodland; spruce-fir forest and woodland; aspen-mixed conifer forest and woodland; ponderosa pine forest, woodland and savanna; aspen forest, woodland, and parkland; Douglas-fir-ponderosa pine-lodgepole pine forest and woodland; and Douglas-fir forest and woodland. Forest types vary with moisture availability and growing conditions correlated with elevation and aspect. Ponderosa pine montane forests occupy lower elevations, transitioning to mixed conifer forests as elevation increases, to lodgepole pine forests, and to spruce-fir forests at high elevations (Huckaby et al., 2003).

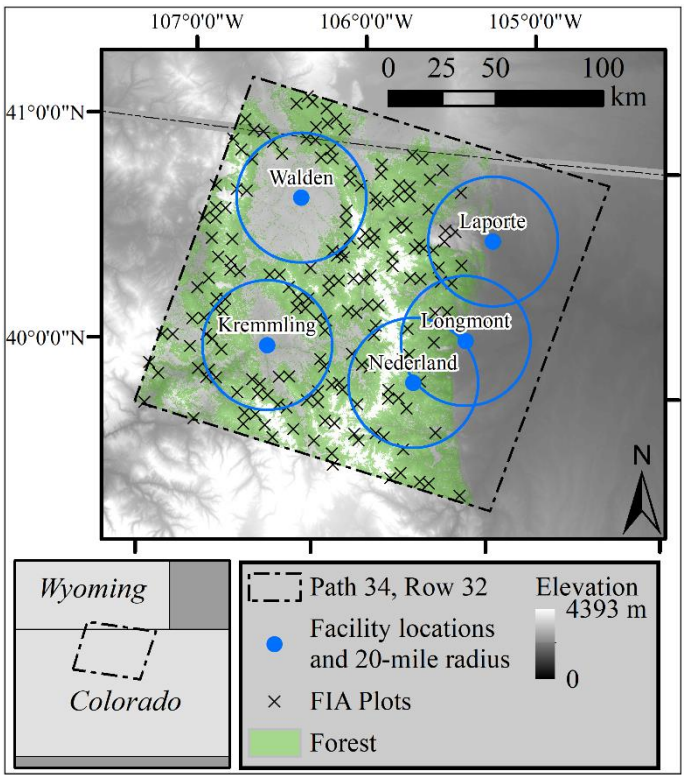

Figure 3.1. Map of the study area showing the forest extent used in this study, hypothetical bioenergy and/or bioproduct facility locations with a 20-mile buffer used to evaluate potentially accessible biomass, the approximate locations of Forest Inventory and Analysis (FIA) plots, and the boundary of Worldwide Reference System 2 path 34, row 32.

Drought, warmer temperatures, and an abundance of host pine trees facilitated severe mountain pine beetle outbreaks in the study area (Chapman et al., 2012; Creeden et al., 2014). These outbreaks started in the early 2000's, peaked from 2006 to 2009, and then began declining in 2010 (Walter and Platt, 2013). By 2013, mountain pine beetle activity had returned to low levels, with bark beetles impacting little new area, but continuing to cause some tree mortality within the stands already impacted (Bode et al., 2018). While mountain pine beetles can utilize all pine species in the study region, lodgepole pine experienced much higher severity impacts than ponderosa pine. Spruce beetle (*Dendroctonus rufipennis* Kirby) outbreaks also associated with drought caused substantial spruce mortality from 1997 – 2007 on the Routt National Forest and 2004 – 2010 on the Roosevelt National Forest (Hart et al., 2014).

I defined the forest extent within the study area as pixels with ten percent canopy cover or more in 2008 as mapped by LANDFIRE Existing Vegetation Cover (Bode et al., 2018; LANDFIRE, 2008). I excluded burned areas (Eidenshink et al., 2007) and clearcut harvests (Woodward et al., 2017) from the study area that occurred between 2001 and 2015. The total standing aboveground biomass layer represents the landscape as of 2001, while the plots I used were measured between 2012 and 2015. The 2001 total biomass layer would not represent biomass accurately in these areas that were subsequently disturbed by fire or harvest.

Field Plot Data

The U.S. Forest Service FIA program monitors U.S. forest resources with a network of permanent plots distributed across forestlands of all ownerships (Tinkham et al., 2018). There is approximately one plot for every 2,428 ha (6,000 acres). Exact plot locations suitable for correlation with remotely sensed imagery were accessed through a non-disclosure agreement with FIA. To capture the impacts of the recent bark beetle outbreaks and to coincide with the 2015 tree mortality map used for modeling, I only used FIA plots sampled after the peak of the recent mountain pine beetle outbreaks (2012 – 2015). These plots were measured soon enough after the majority of tree mortality to reduce the amount of snagfall. I utilized 181 plots: 45 sampled in 2012, 45 sampled in 2013, 50 sampled in 2014, and 41 sampled in 2015. I calculated biomass for both mature trees (> 12.70 cm DBH) measured in four 7.3-m radius subplots and saplings (trees greater than 2.54 cm DBH, but less than 12.70 cm) measured in four 2.1 m radius microplots centered within the subplots. Only live saplings are measured, so I only included standing dead biomass of mature trees. Heterogeneous plots spanning multiple forest or land cover types (conditions) can have diverse spectral signatures, so I only used single-condition FIA plots defined as those that fall entirely within a single land cover (Ohmann et al., 2014).

I calculated dead biomass at each FIA plot by first calculating biomass of each live tree using allometric biomass equations that predict live tree biomass from DBH (Jenkins et al., 2003). These equations were selected because they more accurately predicted tree biomass than the FIA-CRM in this study area (Vorster et al., 2020; Woodall et al., 2011). Locally-developed allometric biomass equations are also available for this study area (Vorster et al., 2020), however these only apply to three species, while Jenkins et al. (2003) equations can be applied to all species in the study area. The Jenkins et al. (2003) equations were also used as the basis for the total (live and dead) standing aboveground biomass maps used in this study.

Dead trees lose biomass as they decompose through structural loss and density reduction. Failing to account for these biomass losses of standing dead trees leads to substantial over-estimation of biomass (Domke et al., 2011). I reduced biomass for each tree using the framework developed by Domke et al., (2011). This approach modifies aboveground biomass for standing dead trees by subtracting structural and density changes from the live tree biomass calculated by allometric biomass equations. Both the structural loss adjustment factor and the density reduction factor vary with the decay class. Forest Inventory and Analysis crews qualitatively assign a decay class to each tree ranging from 1 (little decay) to 5 (highly decayed; O'Connell et al., 2015). I first applied structural loss adjustment factors (Table 2 of Domke et al., 2011) to each biomass component calculated from the Jenkins et al. (2003) equations. This factor estimates the proportion of original biomass retained for each biomass component. A structural loss adjustment factor is not presented for foliage since these factors were designed for allometric biomass equations that don't calculate foliage biomass, so I subtracted the entire foliage component from the live tree estimates (Chung et al., 2017). I next applied density reduction factors from Appendix D of Harmon et al. (2011), which reports density reduction factors for

standing dead trees by tree species and decay class. Density reduction factors are not presented for decay class five, so I used the same density reduction factor for decay classes four and five (Domke et al., 2011). Equations from Jenkins et al., (2003) do not calculate component biomass for woodland species (*Juniperus osteosperma, Juniperus scopulorum, and Quercus gambelii*), so I applied only the density reduction factor to these trees. There were only 33 woodland trees in the FIA plots I used.

Analyses

I mapped dead biomass at a 30 m x 30 m spatial resolution by pairing FIA plot data with total biomass, tree mortality, climate, topography, and geomorphometric variables (Table A3.1). Total (live and dead) standing aboveground biomass and tree mortality are important predictor variables for mapping dead biomass. The total biomass layer represents biomass as of 2001 for this study area, as calculated by Jenkins et al.'s (2003) allometric equations (Vorster et al., 2020). The mortality layer depicts mortality as of 2015, at the tail end of the severe bark beetle outbreaks that occurred in the study area, showing percent mortality for each pixel (Bode et al., 2018). Tree species composition and biomass, and thus dead biomass, correlate with climate, topography, and geomorphometry (Evans and Cushman, 2009; Swetnam et al., 2017). I downscaled 1961 – 1990 climate normals to align with the 30 m x 30 m resolution of other predictor variables (Wang et al., 2016). Topographic and geomorphometric variables derived from the National Elevation Dataset (Gesch et al., 2002; Gesch, 2007) were calculated using Spatial Analyst (Environmental Systems Research Institute, 2017) and the Geomorphometry and Gradient Metrics Toolboxes (Evans et al., 2014). A list of all 42 predictor variables considered in the dead biomass models can be found in Table A3.1.

I used a random forest regression model to relate dead biomass at FIA plots to the predictor variable layers (Belgiu and Drăgu, 2016; Bright et al., 2014). Random forest is a decision tree based algorithm commonly used to map biomass because it is comparatively accurate, efficient, can handle many predictor variables, and is robust to noise, outliers, and overfitting (Breiman, 2001). The final model had 1,000 trees and considered three predictor variables at each split. I narrowed down the 42 predictor variables to a refined set of predictor variables suitable for modeling using a data-driven variable selection routine, Variable Selection Using Random Forest (VSURF; Genuer et al., 2015). VSURF selected eight "prediction" variables. I then removed the variable with the lower variable importance for any pair of these predictor variables correlated by 0.7 or more (Dormann et al., 2013).

Models were evaluated using pseudo R^2, root mean square error (RMSE), RMSE percentage of the mean, bias, and bias as a percentage of the mean. Out-of-bag pseudo R^2 and RMSE were calculated, which are robust methods of calculating evaluation metrics where predictions are tested against the withheld data as each tree is built (Breiman, 2001). Pseudo R^2 indicates the proportion of variability in the observed data explained by the model and RMSE measures the magnitude of differences between predictions and observations. Bias measures the tendency for models to over or under-predict. Note that these error metrics only reflect the errors in the dead biomass mapping model prediction, but fail to capture other sources of error, such as error from tree measurement and allometric errors.

I mapped standing live aboveground biomass by subtracting dead biomass from the total biomass layer. Since I only quantified standing dead biomass, any biomass that fell since 2001 ended up in the live biomass pool. This likely leads to over-estimation of live tree biomass. I next summarized dead, live, total, and the proportion of dead to total biomass by forest type

using LANDFIRE Existing Vegetation type 2014 version 1.4.0 (LANDFIRE, 2017). I show results for the six dominant forest types that made up 84% of the forested area.

Feedstock supply

I approximated dead, live, and total standing forest aboveground biomass accessible to forest management for five hypothetical bioenergy and/or bioproduct facility sites. These sites were selected because they are sites where biomass utilization facilities exist, or have existed in the past. The sites are all in Colorado: Laporte, Longmont, Nederland, Kremmling, and Walden. The goal of this analysis was to evaluate the maximum potential feedstock supply and the feedstock mix between live and dead biomass within 20 miles of hypothetical sites. I defined accessible areas within a 20 mile radius around each site to limit the transportation distance to the facility. I do not consider road distance in this analysis. I then further refined the accessible areas using a map of clearcut harvest events that occurred across the study area between 1984 and 2015 to define accessibility parameters (Woodward et al., 2017). I characterized the 95th percentile slope and distance from roads for this layer and used these parameters to identify areas accessible to timber harvest. Accessible slopes and distances from roads are dependent on local equipment and forestry practices—this approach of using historical harvests to characterize accessibility attempts to account for this. Forests on slopes below 16.6% and within 800 m of roads were considered to be accessible to timber harvesting equipment. Lastly, I removed forests from consideration designated as National Parks or wilderness areas, since their management makes it unlikely to be a commercial biomass source. This definition of accessibility makes many simplifying assumptions. The estimates of biomass within this accessible area represent a maximum biomass. Not all sites would be suitable for forest management, only a portion of the biomass within a treatment would be harvested, and not even all of the harvested biomass would

be utilized for bioenergy or bioproducts. I also do not consider patch size, riparian zones, or numerous other factors influencing forestry best practices.

I next compared this maximum potentially accessible biomass to 20-year feedstock demand of four example bioenergy production scenarios. These production scenarios from Campbell et al. (2018) represent existing or planned technologies in the Rocky Mountain region and have been proposed as alternatives for utilizing beetle-killed biomass. In the biofuel scenario, wood chips are pyrolyzed to produce 1.8 million gallons of near "drop-in" liquid biofuel and 17,700 Mg biochar annually. The pellet scenario involves converting wood chips to 56,500 Mg of pellets for retail and 620 Mg of biochar annually. In the heat scenario, 22,400 million Btu of thermal energy is produced through combustion of wood chips at a distributed-scale, highly-automated thermal power plant. This scenario could heat large buildings or building complexes (i.e., schools). The power scenario produces 89,100 MWh of electricity through combustion of wood chips, which is sent to the electric grid. The annual feedstock demand was calculated by multiplying the feedstock processing capacity (Mg h^{-1}) by the annual operating time (h) from Table 1 of Campbell et al. (2018). This annual feedstock demand was multiplied by 20 to estimate the biomass required for 20 years of operation. I also report this 20-year demand as a percentage of the potentially accessible biomass for each site to understand near-term feedstock demand relative to the current biomass at these locations.

Results

Of the 9,502 trees measured in the FIA plots, 3,024 (32.8%) of the trees were dead. Lodgepole pine was by far the most common dead tree measured (n = 2,104 dead lodgepole pine), followed by subalpine fir (n = 326), Engelmann spruce (n = 239), and quaking aspen (n = 198). Lodgepole pine was the most impacted species by standing aboveground biomass as well.

For lodgepole pine, the most abundant species in the plot data, dead biomass composed 65% of the total biomass stock (Figure 3.2). For all other species, live biomass far exceeded dead biomass (Figure 3.2). Engelmann spruce and subalpine fir, two other subalpine species, were the second and third most abundant species, respectively and also had the second (24%) and third (20%) highest proportions of dead to total biomass, respectively. 35% of all biomass in the FIA plots was dead.

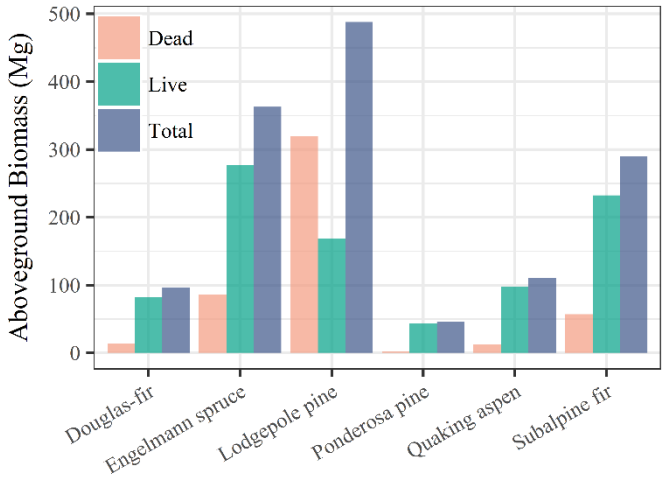

Figure 3.2. Dead, live, and total standing aboveground biomass measured in the Forest Inventory and Analysis (FIA) plots for the six most abundant species.

Most dead trees were classified as being in the lower (i.e., less decayed) decay classes—99% of the dead trees measured had a decay code of three or less, with 78% having a decay code of two or less. A decay class of two represents the following condition, “There are few limbs and no fine branches; the top may be broken; a variable amount of bark remains; sapwood is sloughing with advanced decay; heartwood is sound at base but beginning to decay in the outer part of the upper bole” (O’Connell et al., 2015). While decay class was concentrated in the lower decay classes for all species, lodgepole pine tended to be less decayed than other species, and quaking aspen was more decayed (Figure 3.3).

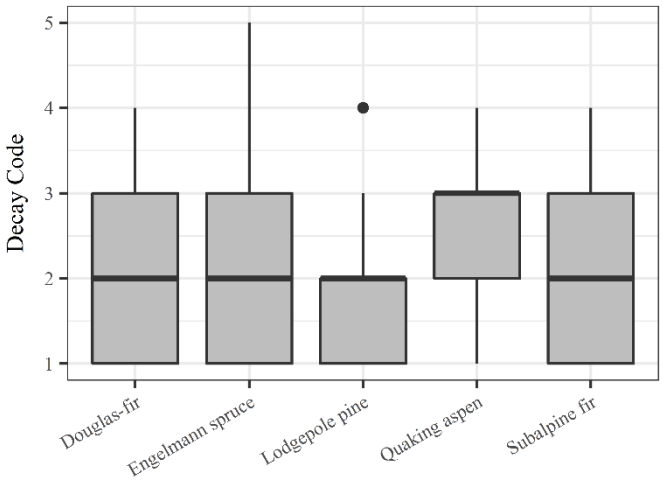

Figure 3.3. Boxplots comparing standing dead tree decay class codes for the most abundant species in this study.

Plots had an average of 131 Mg ha^{-1} (min = 3 Mg ha^{-1}, max = 381 Mg ha^{-1}) of total (live and dead) standing aboveground biomass and an average of 41 Mg ha^{-1} (min = 0 Mg ha^{-1}, max = 228 Mg ha^{-1}) of standing dead biomass (Figure 3.4). On average, 32.1% of standing aboveground biomass in plots was dead (min = 0%, max = 100%).

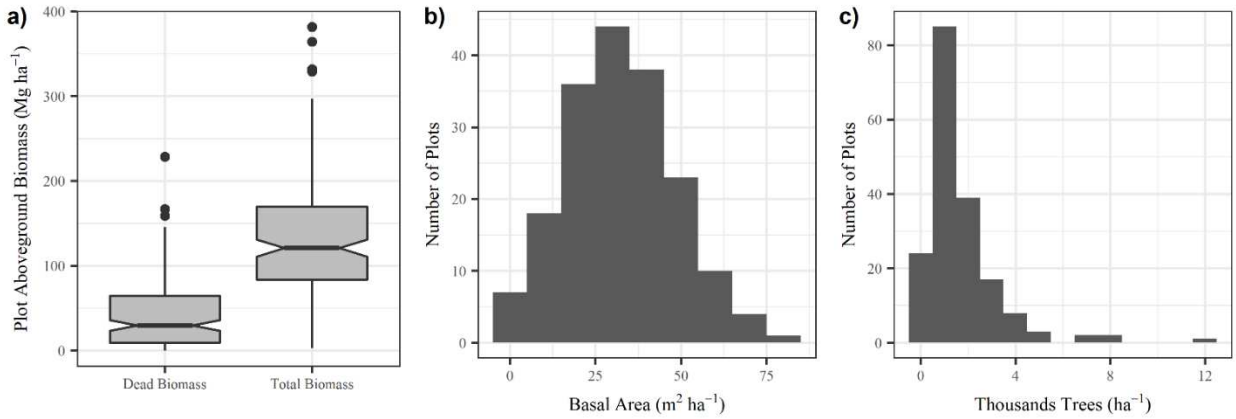

Figure 3.4. a) Comparison of total (live and dead) and dead standing aboveground biomass at the Forest Inventory and Analysis (FIA) plots. Histograms of (b) basal area and (c) trees ha^{-1} at the same FIA plots.

The random forest model predicted standing dead aboveground biomass with out-of-bag pseudo R^2 = 0.47, RMSE = 28.8 Mg ha^{-1}, % RMSE = 69.5%, bias = 1.08 Mg ha^{-1}, and a % bias =

2.6%. Total aboveground biomass and 2015 mortality layers were the top predictor variables (Figure A3.1), followed by frost-free period, northness, elevation, heat load index, and roughness (27 x 27). The relationship between observed and predicted dead biomass shows decent model performance, particularly for plots up to about 100 Mg ha^{-1} (Figure 3.5). The model predictions saturate at about 100 Mg ha^{-1}, leading to an underprediction of dead biomass in the high dead biomass plots. However, the positive bias indicates that the model tends to slightly overpredict biomass on the whole.

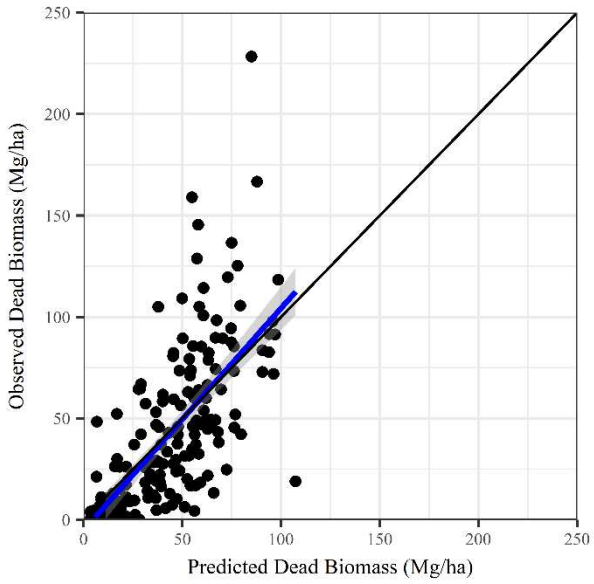

Figure 3.5. Regression of observed and predicted aboveground standing dead plot biomass for the random forest model. $y = 1.094\ x - 5.09$

This random forest model was applied across the landscape to map standing dead aboveground biomass, which was then subtracted from the total biomass map to estimate standing live aboveground biomass (Figure 3.6). The maps indicated 54.8 Tg of the 194.5 Tg of standing aboveground biomass was dead, and that the remaining 139.6 Tg was living.

Converting to carbon using a 0.5 carbon concentration, there was 27.4 Tg dead, 69.8 Tg live, and 97.2 Tg of total standing aboveground carbon (AGC).

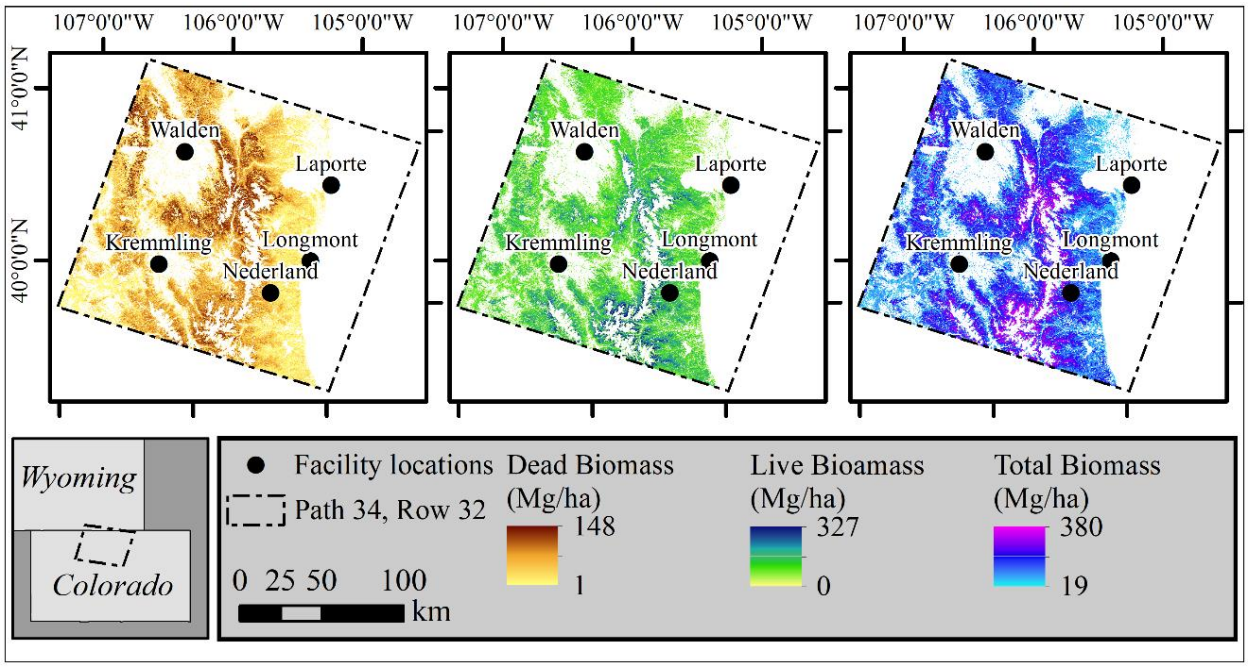

Figure 3.6. Maps of dead, live, and total standing aboveground biomass.

Lodgepole pine and spruce-fir forests covered the largest area. These two forest types also have the greatest mean and summed dead, live and total standing aboveground biomass (Figure 3.7). Additionally, the greatest proportion of total biomass is dead in these forest types. The other four dominant forest types in this area covered similar area. Aspen and aspen-mixed conifer forests were 20% or more dead, on average, and contained slightly more dead, live, and total biomass than Douglas-fir-ponderosa pine-lodgepole pine mixed forests and ponderosa pine forests.

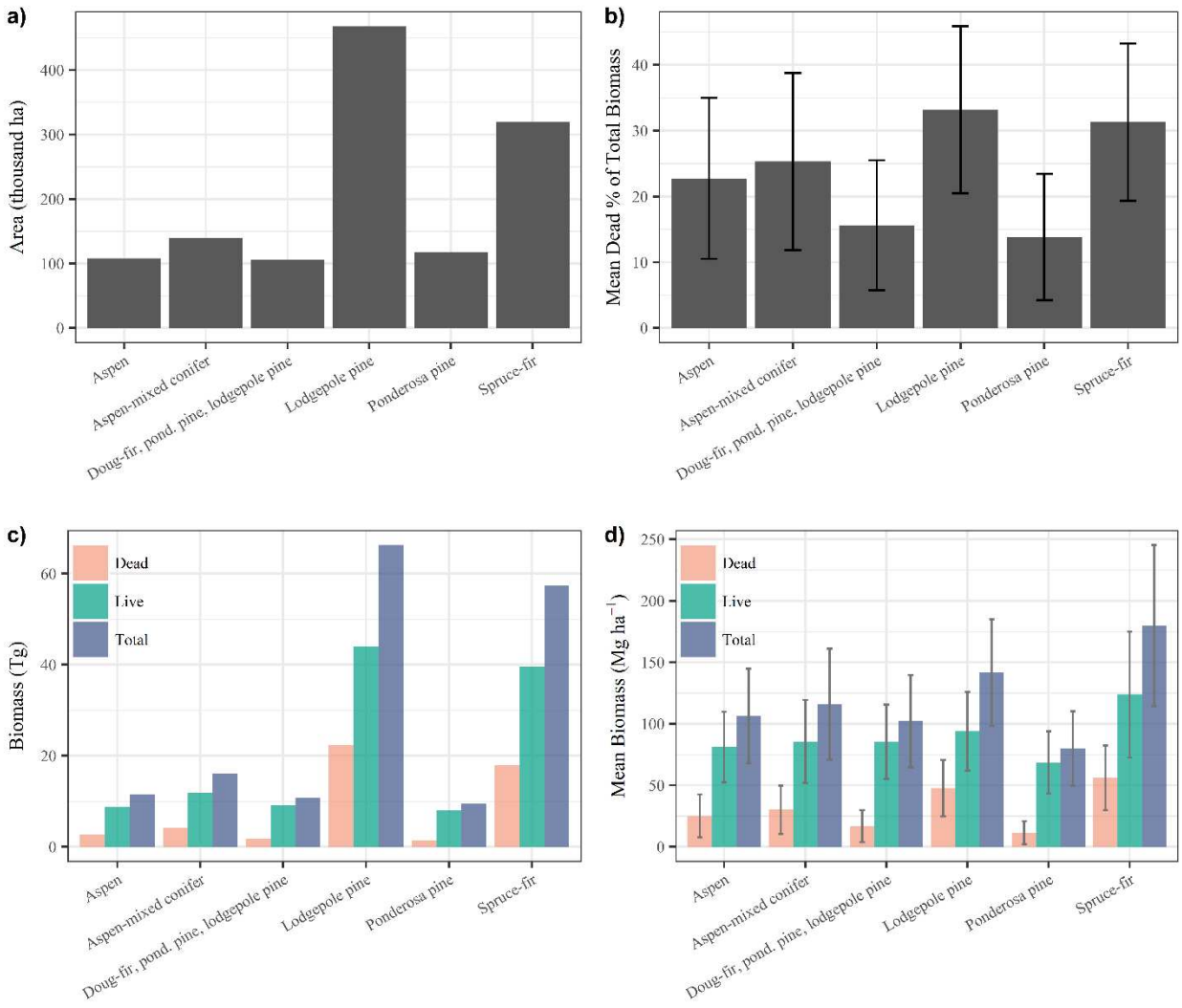

Figure 3.7. (a) The area of each of the most common forest types in the study area as shown by LANDFIRE 2014 version 1.4.0. Panes b – d summarize biomass of pixels by these forest types: (b) the mean dead percentage of total biomass (with standard deviations), (c) aboveground biomass, and (d) mean biomass (with standard deviations).

Limiting biomass maps to areas potentially accessible for timber harvest reduced the forest area from 1.52 million ha to 644,476 ha. Nederland potentially has access to the most total standing aboveground biomass (11.7 Tg), while Laporte had five times less accessible biomass (2.3 Tg; Figure 3.8). Live biomass exceeds dead biomass at all sites. Walden had the highest proportion of dead to total biomass at 33.3%. The distributed-scale heat scenario had very low annual feedstock requirements and would require 0.4% - 1.8% of potentially accessible biomass

over 20 years of operations, depending on the facility location (Table 3.1). The power generation scenario required the most feedstock, accounting for 13.5% - 69.3% of the potentially accessible biomass (Table 3.1).

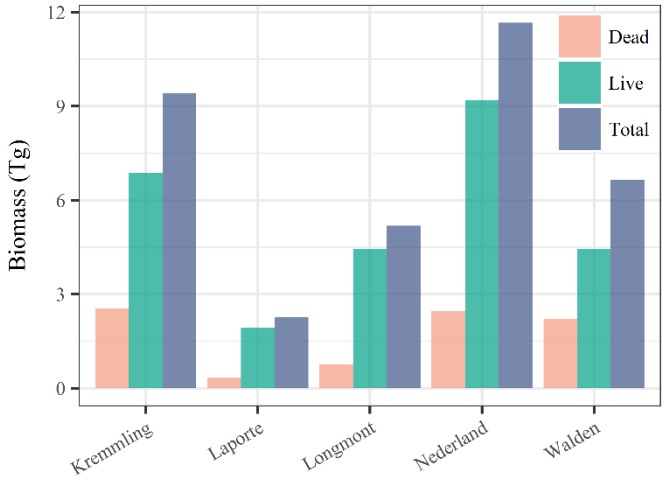

Figure 3.8 Dead, live, and total standing aboveground biomass that is potentially accessible around hypothetical bioenergy facility sites.

Table 3.1 Approximate annual and 20-year feedstock requirement and the percentage of the current potentially accessible biomass to supply each bioenergy production scenario for 20 years.

			Percentage of Potentially Accessible Biomass Required for 20 Years				
Production Scenario	Annual Feedstock (Mg)	20 year Feedstock (Tg)	Kremmling	Laporte	Longmont	Nederland	Walden
Biofuel	65,700	1.31	14.0	57.8	25.3	11.3	19.7
Pellet	67,014	1.34	14.3	58.9	25.9	11.5	20.1
Heat	2,102	0.04	0.4	1.8	0.8	0.4	0.6
Power	78,840	1.58	16.8	69.3	30.4	13.5	23.7

Discussion

I evaluated allocation of forest carbon into dead, live and total standing aboveground biomass stocks across one of the most severely bark beetle impacted landscapes in the western U.S. Standing dead biomass was a major carbon stock—nearly a third of the trees and 35.2% of the biomass measured in the FIA plots were dead. At the plot scale, a mean of 32.1% of the total

plot biomass was dead. Estimates made using the dead biomass maps produced in this study indicate that 28.2% of biomass was dead across the entire 1.52 million ha study area. Berner et al. (2017) estimated 14.6 ± 7.0 Tg AGC yr^{-1} from bark beetles across the western U.S. from 2003 – 2012, for a total of roughly 146 Tg AGC across this time period. My estimate of 27.4 Tg C in standing AGC across northern Colorado and southern Wyoming is 19% of this total beetle-killed carbon across the western U.S. While bark beetles have caused widespread mortality across this study area, I do not attribute the cause or timing of mortality. Some of the standing dead biomass could be remnants from past bark beetle outbreaks (Pelz and Smith, 2012) and other causes of tree mortality.

Plot data indicate that lodgepole pine had far more dead biomass than any other species. Lodgepole pine had more dead than live biomass in the FIA plots. This is a legacy of the historically-severe mountain pine beetle outbreaks that severely impacted this area in the 2000's before beginning to decline around 2010. Spruce bark beetle outbreaks also occurred during the 2000's in this study area, but had less of an impact on biomass stocks than the mountain pine beetle. The plot data show much less standing dead Engelmann spruce than lodgepole pine, but the LANDFIRE summarization of the maps show biomass quantities in spruce-fir forests rivaling lodgepole pine forests. It is possible that the high dead biomass quantities in the spruce-fir forests are attributable to dead lodgepole pine mixed in these forests in addition to moderate mortality in both Engelmann spruce and subalpine fir.

Bark beetles have dramatically impacted these subalpine forests by transferring carbon from standing live to dead trees. These dead trees can be expected to remain standing for years to decades. An analysis within the study area predicts half the snags may fall within 15 – 20 years of mortality, and perhaps sooner at lower elevations (Rhoades et al., 2020). These subalpine

forests also have the highest biomass density in the study area, and beetles preferentially infest large trees within these forests. However, these forests and their carbon stocks are resilient to bark beetle outbreaks, and forest carbon in these areas can be expected to recover to pre-outbreak levels within several years to several decades (Hansen, 2013; Raymond et al., 2015). It will take longer, however, for these forests to catch up to the undisturbed carbon trajectory. Carbon recovery rates can be expected to vary with outbreak severity, advanced regeneration, species composition, and pre-disturbance carbon levels (Hicke et al., 2012; Raymond et al., 2015). The development of these stands, and how these bark beetle caused changes interact with future disturbances, such as fire, drought, and climate change, need to be considered to quantify the full impact of these outbreaks on the forest carbon cycle.

Results show the lower elevation forest types (e.g., ponderosa pine and mixed conifer) have much less total and dead biomass than the subalpine forests. I did not include areas burned between 2001 and 2015 and the associated dead biomass. So, the small quantities of dead biomass that I report in these lower elevation forest types should not be taken as an indication of more stable forest carbon in these forest types. Fires occur more frequently in these lower elevation forests, which has a greater impact on forest carbon than bark beetles (Hicke et al., 2013).

Quantification of dead biomass resulting from bark beetle outbreaks contributes to a better understanding of forest disturbance on the carbon cycle and can inform forest management planning. The impacts of bark beetles on hydrological and ecological processes correlate with the severity of bark beetle mortality (Diskin et al., 2011; Hansen et al., 2015; Pugh and Small, 2012; Rhoades et al., 2016). Dead biomass, as a metric of the severity of tree mortality, may better reflect hydrological and ecological impacts than metrics such as dead trees per acre. Methods to

calculate biomass loss in standing dead trees are actively being refined (e.g., Domke et al., 2011; Harmon et al., 2011; Russell et al., 2015; Woodall et al., 2012). While biomass quantities can be, and commonly are, converted to carbon by applying a 0.5 carbon concentration conversion, carbon concentrations of dead trees vary by general taxa (angiosperms vs. gymnosperms) and decay class. Carbon concentration of gymnosperms increases from 49.3% to 53.5% as decomposition progresses (Harmon et al., 2013).

Accounting for structural loss and density reduction as trees decay helped to avoid over-estimation of individual tree standing dead biomass. The structural loss adjustment factors and density reduction factors I used were designed for use with the FIA-CRM (Heath et al., 2009; Woodall et al., 2011) for calculating individual tree biomass, but I use them here with the Jenkins et al. (2003) allometric biomass equations. The FIA-CRM has similar component biomass definitions, and even utilizes Jenkins et al. (2003) in the method. Additionally, Jenkins et al. (2003) is more accurate than FIA-CRM in the study area (Vorster et al., 2020). One difference between these approaches is that FIA-CRM makes volume and then biomass deductions for rough, rotten, and missing cull but Jenkins et al. (2003) does not. Since deductions are already made with FIA-CRM, the structural loss adjustment factors do not account for structural loss of the bole (Domke et al., 2011). The FIA-CRM is sometimes unsuitable because it requires more tree measurements than are present in many forest inventories and can significantly under-estimate biomass (Vorster et al., 2020). Structural loss adjustment factors designed for use with the majority of allometric biomass equations that only require tree diameter and/or height are needed to further reduce uncertainty in standing dead tree biomass estimates. Using terrestrial lidar to quantify dead tree biomass and structural loss may aid in these efforts (Putman et al., 2018; Stovall et al., 2017).

The FIA plot network is invaluable for forest biomass and carbon quantification efforts because it is continuously collected, publicly available, spans forest types, and includes detailed tree-specific measurements. Measurements such as the decay class and rot are particularly valuable for estimating standing dead tree biomass. One challenge of mapping dead biomass is balancing obtaining enough plots to train a robust model with the need for temporal alignment between forest inventory data and mortality and biomass maps. I utilized four years of FIA data to obtain enough samples to train the standing dead biomass models. The more years of FIA data used, the greater the risk is of plot measurements not capturing mortality captured by the mortality maps. This is more problematic during periods of greater disturbance activity when forests are changing rapidly. It can be easier to align plot data with forest mortality maps for disturbances that end abruptly since you can map dead biomass immediately after the disturbance without missing subsequent impacts. Bark beetle activity, however, can slowly decline over many years after outbreaks peak. Efforts to quantify dead biomass resulting from these longer duration disturbances should aim to capture the impacts of the most intense years. Waiting until bark beetles have returned to endemic levels may mean waiting until many years after the peak, when dead trees have fallen and forests are recovering, making it harder to detect forest mortality with remote sensing. Maps that capture cumulative tree mortality (e.g., Bode et al., 2018), rather than annual estimates of new mortality (e.g., ADS), may be better suited for mapping standing dead tree biomass since they reflect the full disturbance impact rather than just the most recent tree mortality. Furthermore, relying on Landsat-derived tree mortality maps over ADS better represents the extent and severity of tree mortality, thus better representing the location and quantities of dead biomass (Bode et al., 2018; Vorster et al., in prep).

Mapping dead biomass has been a challenging task for remote sensing, and advancements are needed (Russell et al., 2015). Pflugmacher et al. (2012) tested Landsat time series and lidar for mapping downed wood and standing dead biomass, and found Landsat time series to outperform lidar. They achieved RMSE = 31 Mg ha^{-1} and % RMSE = 89%, compared to RMSE = 28.8 Mg ha^{-1} and % RMSE = 69.5% in this study. Kim et al. (2009) used lidar to map live and dead standing tree biomass, achieving RMSE = 42 Mg ha^{-1} and % RMSE= 63% for standing dead tree biomass models. The approach demonstrated in this study provides complementary methodology and similarly promising results. I mapped standing dead tree biomass across a wide range of dead biomass densities and forest types at 30 m x 30 m resolution. Tree mortality and total biomass layers were the most important contributors, and these layers are already available (e.g., Blackard et al., 2008) or are becoming more available across large extents (e.g., Vorster et al., in prep). However, disagreement between national biomass maps is significant at the pixel scale, and can impact the accuracy of dead biomass maps (Berner et al., 2017). These biomass maps will continue to improve with missions like Global Ecosystem Dynamics Investigation (GEDI; Dubayah et al., 2020) and BIOMASS (Quegan et al., 2019). The total biomass map used in this study was derived from multispectral imagery, and thus saturated, or underpredicted biomass in closed-canopy, high biomass forests (Vorster et al., 2020). The saturation of this study's high standing dead biomass values would likely be ameliorated with improved total biomass predictor variables.

I approximated potentially accessible dead, live, and total aboveground biomass for five potential sites and four bioenergy and bioproduct scenarios. High-biomass areas such as Kremmling and Nederland could support all bioenergy production scenarios with less than 17% of potentially accessible biomass stocks over 20 years of production. Lower-elevation sites such

as Laporte and Longmont would utilize 69.3% and 30.4% of potentially accessible biomass, respectively, for the highest feedstock demand production scenario (power generation) over a 20 year span. Thus, these high feedstock demand bioenergy production scenarios are unlikely to be feasible on low elevation sites in this region. The lower-elevation sites (e.g., Laporte and Longmont) had access to much less biomass than higher-elevation sites because they only have forest access to the west (Figure 3.1) and because lower elevation forests have lower biomass densities. This reduced access to biomass would have to be considered alongside tradeoffs that may accompany being located near the Front Range population centers, such as the labor and product markets. These sites may have access to additional biomass in burned areas, but I do not included burned areas in this analysis. Standing dead biomass contributed up to 33.3% of potential feedstock, serving as a significant biomass component for sites utilizing biomass from subalpine forests. The quantity of accessible standing dead biomass will decline over the coming years and decades as these dead trees fall.

Efforts to quantify climate impacts of utilizing beetle-killed material for bioenergy and bioproducts are underway (Field et al., 2018). The dead, live, and total biomass maps produced in this study can assist in these efforts by informing biomass densities, transportation distances, and even spatially-explicit estimates of post-harvest forest carbon deficits. Future work should refine criteria for accessibility and feedstock transportation distances, evaluate a range of production scales, and consider taking an optimization approach to locating facility sites.

Conclusion

Bark beetles have had a significant impact on northern Colorado and southern Wyoming forest biomass stocks, transferring approximately 55 Tg of biomass from live to standing dead stocks. Since this study area was one of the most severely bark beetle-impacted areas in the

western U.S., this represents a severe case of bark beetle impacts on forest carbon. The novel method for mapping dead biomass presented in this study has the potential to be widely applied and frequently updated, as it utilizes continuously collected forest inventory data and biomass and tree mortality maps that are becoming more accurate and widespread. This approach is promising for improving our understanding of the impact of forest disturbances on carbon cycles in a rapid fashion. This method was developed in an area that experienced high severity tree mortality caused by bark beetles, which preferentially kill large host trees. As such, the suitability of this method should be tested in other areas experiencing lower severity disturbance, or experiencing disturbances that also kill understory trees, like western spruce budworm. Finally, I demonstrated the integration of the dead biomass mapping method with readily-available geospatial information to evaluate accessible biomass for bioenergy production. While scenarios presented are site-specific, future assessments utilizing a similar framework can provide valuable information to forest managers and policymakers considering the viability of these options for forest resource utilization in new areas.

CHAPTER 4 — IMPACTS OF POST BARK BEETLE OUTBREAK SALVAGE LOGGING AND CLIMATE CHANGE ON FOREST CARBON, FUEL LOADS, AND SUSCEPTIBILITY TO FUTURE BARK BEETLE OUTBREAKS

Introduction

Disturbance frequency and severity is expected to increase with the changing climate in western U.S. forests (Bentz et al., 2010; Westerling et al., 2011), leading to increased and potentially novel interactions between disturbances. Interacting disturbances can cause nonlinear ecosystem responses, state changes, and can expose hidden ecosystem dynamics (Buma, 2015). It is unclear how these changes to disturbance regimes and disturbance interactions will impact forest carbon stocks (Williams et al., 2016). Research is needed to better understand how interacting disturbances may produce synergistic effects or intensify or temper ecosystem effects (Turner, 2010).

Mountain pine beetles are bark beetles native to western North America that cycle between periods of endemic low density populations that have minor effects and large epidemic populations that cause widespread pine tree mortality (Raffa et al., 2008). The beetles use pheromone signals to coordinate mass attacks against pine tree hosts. At lower beetle populations, healthy host trees can defend themselves against attack. However, beetles can overwhelm even healthy host trees at high population densities, killing trees with the water-transport blocking blue stain fungi that it introduces to the tree (Hubbard et al., 2013).

Driven by warmer temperatures, drought, and an abundance of suitable hosts, mountain pine beetle outbreaks erupted throughout western North America in the late 1990s with populations peaking in northern Colorado between 2006 and 2009 (Walter and Platt, 2013). Mountain pine beetles can affect a variety of pine species, but lodgepole pine is the beetle's

preferred host. Shore and Safranyik (1992) developed a risk rating system for lodgepole pine with two components: the susceptibility index and the beetle pressure index. The susceptibility index rates a stand based on four variables: the percentage of susceptible stand basal area, the age of the stand, stand density, and location factor. The index reflects the preference of bark beetles for stands with an abundance of large, old lodgepole pine. The beetle pressure index represents the beetle population density as a function of the size and proximity of the population. Carbon stocks in lodgepole pine stands are generally resilient to mountain pine beetle impacts, due in large part to the increased growth rates of surviving vegetation. These stands return to fixing more carbon than they are releasing through decomposition within several decades or less (Hansen, 2013; Raymond et al., 2015). The rate of carbon recovery depends on the severity of the mortality, the size distribution of surviving trees, advanced regeneration, species composition, and pre-disturbance carbon stocks (Hansen, 2013; Hansen et al., 2015; Hicke et al., 2012; Pfeifer et al., 2011).

Salvage logging of beetle-impacted stands is conducted to meet a range of objectives ranging from safety to fuels reduction and economic objectives. Beetle-killed biomass is being utilized for timber products, bioenergy, and additional bioenergy and bioproduct scenarios are being considered (Campbell et al., 2018). Beetle-killed snags can be recovered for many years after an outbreak. Snagfall rates are variable across the landscape, but it is estimated that half the snags in lodgepole pine forests may fall within 12 – 20 years (Rhoades et al., 2020). While the short-term impacts of harvesting beetle-killed wood are important (e.g., Fornwalt et al., 2018), disturbances also leave lasting legacies through impacts on species composition, forest structure, and biogeochemical cycling. Legacies from harvesting will influence resistance and resilience to future disturbances. Salvage logging reduced biomass stocks for at least 50 years in the Greater

Yellowstone Ecosystem (Donato et al., 2013). In some areas, subalpine fir is expected to become more abundant in untreated stands, while lodgepole pine is predicted to remain the dominant species in harvested stands (Collins et al., 2011). Fire behavior, and consequently the impacts of fire on carbon storage, will vary between treated and untreated stands because subalpine fir in untreated stands will serve as ladder fuels and surface fuel loads will increase over time as snags fall (Collins et al., 2012). Additionally, the differing species composition between harvested and untreated stands will alter resistance to future bark beetle outbreaks.

Studies evaluating recovery in salvage logged and untreated stands often do not incorporate climate change impacts. This may be for good reason, as climate change will impact forests in complex and unexpected ways that are difficult to capture in modeling exercises. However, scenarios that consider climate change should be explored. Climate change is expected to result in increased temperatures and drought frequency in northern Colorado (Temperli et al., 2015). This will impact forest carbon storage by changing growth rates as well as disturbance frequency and severity. Fires, for example, are expected to be more severe and frequent (Westerling et al., 2011). The effect of changing climatic conditions on mountain pine beetles in Colorado subalpine forests is uncertain, with some studies suggesting climatic conditions to become more suitable (Bentz et al., 2010), and others predicting a decline in climatically-suitable habitat (Evangelista et al., 2011).

The Forest Vegetation Simulator (FVS) is a growth-and-yield model developed and maintained by the US Forest Service (Crookston and Dixon, 2005) that is commonly used to evaluate forest management actions (Caldwell et al., 2013; DeRose and Long, 2009; Donato et al., 2013; Raymond et al., 2015). Regional component models predict the growth and mortality of each tree in a stand. Model extensions can be used to simulate climate change (Crookston et

al., 2010) and disturbances such as fire (Rebain et al., 2010). Climate-FVS modifies FVS to simulate climate change effects by adjusting mortality, regeneration, site index, and growth rates. Climate-FVS uses viability scores that measure the likelihood of climate at a specific location and time overlapping with conditions from species' current ranges (Crookston, 2014). Climate-FVS models regeneration, introducing the most suitable species for predicted climatic conditions. It is assumed that all species are available to establish at each site (e.g., seed distribution is not modeled) and that species' current ranges will reflect future climatic suitability.

The objective of this study was to simulate the stand-level impacts of climate change and harvesting bark beetle-impacted stands on forest carbon, fuels, and susceptibility to future mountain pine beetle outbreaks. I compared clearcut and untreated bark beetle-impacted stands with and without climate change using FVS. The analysis was conducted on lodgepole pine-dominated FIA plots in northern Colorado and southern Wyoming.

Methods

Study Area

This study was conducted across the lodgepole pine forests of northern Colorado and southern Wyoming. I used FIA plots falling within a bounding box around Arapaho and Roosevelt National Forests and Medicine Bow-Routt National Forests. The study area includes lands with a variety of ownerships and management goals: National Forests, Rocky Mountain National Park, state land and private land. The lodgepole pine stands used in this study ranged from 2,490 m to 3,374 m above sea level. Mean annual temperature as measured in 1990 ranged from -1.1 °C to 4.7 °C (mean = 1.5 °C) and mean annual precipitation ranged from 372 mm to 622 mm (mean = 485 mm). By 2090, Climate-FVS shows that under the Ensemble 6.0 climate

scenario, the range of mean annual temperature rises to 2.9 °C to 8.6 °C (mean = 5.4 °C) and precipitation increases to a range of 410 mm to 682 mm (mean = 534 mm). The most commonly co-occurring species with lodgepole pine in the study area are quaking aspen, subalpine fir, and Engelmann spruce.

Plot Data

I used 47 FIA plots sampled between 2012 and 2017 to initialize the FVS model simulations. These plots were all composed of ≥90% lodgepole pine basal area relative to total basal area and had basal area ≥ 20 m^2 ha^{-1}. I selected plots sampled between 2012 and 2017 so the measurements captured post-outbreak stand conditions, and were measured close enough to the bark beetle outbreaks for many of the snags to still be standing. Seven of the plots were sampled in 2012, nine in 2013, six in 2014, 15 in 2015, seven in 2016, and three in 2017. These FIA plots were used to capture variation in forest structure, mountain pine beetle outbreak severity, site productivity, and disturbance legacies.

Forest Vegetation Simulator

I used the FVS Central Rockies Variant (FVS-CRV) along with the Fire and Fuels Extension (FFE) and Climate-FVS to simulate growth in the 47 FIA plots for 100 years from 2012 – 2112. Four scenarios were considered: (1) untreated, (2) harvested, (3) climate change and harvested, and (4) climate change without treatment. Neither climate change nor a treatment were simulated in the untreated scenario. A clearcut was scheduled at the beginning of the simulation for the two harvested scenarios. All live and dead standing trees above 12.7 cm (5 in) diameter were removed. It is common in this region for salvage logging to leave very few standing live or dead mature trees to avoid windthrow of residual live trees (Collins et al., 2012). I simulated lop-and-scatter slash management where non-merchantable biomass is left spread

across the site. Donato et al. (2013) found the impacts of salvage harvesting on biomass and fuels to be similar for lop-and-scatter and whole tree harvest, so I did not evaluate both slash management techniques.

I implemented the default FVS model in the untreated and harvested scenarios without climate change, but specified regeneration based on FIA plot data. I specified conditional regeneration in both the harvested and untreated scenarios that introduced a pulse of seedlings to the stand when the stocking fell below the default of 65%. This seedling pulse consisted of 431 lodgepole pine seedlings $acre^{-1}$, 20 aspen suckers/root sprouts $acre^{-1}$, 30 Engelmann spruce seedlings $acre^{-1}$, and 30 subalpine fir seedlings $acre^{-1}$. For the harvest simulation, I planted 1,054 lodgepole pine seedlings $acre^{-1}$, 49 aspen suckers/root sprouts $acre^{-1}$, 70 Engelmann spruce seedlings $acre^{-1}$, and 70 subalpine fir seedlings $acre^{-1}$ after harvest. These seedling species and counts reflect observations from 559 lodgepole pine FIA plots in Colorado and Wyoming for mature (conditional regeneration) and regenerating stands (for post-harvest planting) (Bagdon et al., n.d.). Aspen sprouting was turned off for the harvested and untreated scenarios because when sprouting is on, I have observed that aspen growth can unrealistically dominate stand growth in FVS.

The climate change scenario was run with default Climate-FVS parameters, including the autoestablishment model (Crookston, 2014; Crookston et al., 2010). Defaults for the autoestablishment model were used. The autoestablishment model plants the four species with the highest viability score, regardless of their previous presence or proximity to a site. Seedling numbers are calculated using stocking rates and viability scores. I used the Ensemble 6.0 climate scenario, which is an ensemble of 17 models from the Intergovernmental Panel on Climate Change's Fifth Assessment Report for representative concentration pathway (RCP) 6.0

(Crookston, 2014; Fekety et al., 2020; IPCC, 2014). Emissions peak around 2080 in RCP 6.0, and would be expected to result in 2.2 °C of warming between 2081 and 2100.

The FFE was used to track forest carbon and metrics that reflect the potential impact of fire. I used Jenkins et al. (2003) allometric biomass equations to calculate carbon, although the FFE approach is still used for dead trees, forest floor, down dead wood, and shrub/herb pools (Rebain et al., 2010). Jenkins et al.'s (2003) equations were used rather than Vorster et al. (2020) allometric equations because the Vorster et al. (2020) equations only apply to three species. I tracked total stand carbon, which includes aboveground live and dead trees, down dead wood, live and dead roots, litter and duff, and shrubs and herbaceous vegetation.

I also tracked four metrics reflecting potential impacts of fire: canopy base height, crown bulk density, torching index, and crowning index. Torching index is the "20-ft wind speed required to cause torching of some trees under severe conditions" and the crowning index is the "20-ft wind speed required to cause an active crown fire under severe conditions" (Rebain et al., 2010). Crowning and torching indices are functions of surface fuels, fuel and foliar moisture, canopy base height, canopy bulk density, slope, and canopy wind dynamics (Scott and Reinhardt, 2001). Lower torching and crowning indices indicate that severe fire effects resulting from torching and crowning crown fires are more likely to occur in the event of a fire. Canopy base height indicates the height of canopy fuels off the ground, and thus how fire might transition from surface to the canopy. Canopy bulk density is a canopy fuel characteristic that estimates the density of canopy fuels, and thus how likely it is for fire to move through the canopy.

The mountain pine beetle susceptibility index is calculated as an estimate of susceptibility to mountain pine beetles should an outbreak occur (Shore and Safranyik, 1992). This index is

described in the Introduction. I was only able to include the percentage of susceptible pine basal area and the density factor when calculating the index because the formula for calculating the location factor was developed for British Columbia and does not apply to this study area. I was also unable to incorporate the age factor because I did not have age information for each tree. The location and age factors are simply multipliers between 0 and 1 that re-scale the susceptibility index. The susceptibility index can still be calculated as the product of the percentage of susceptible pine basal area and the density factor.

In summary, I tracked the following metrics for each stand and simulation: species composition and other stand structure metrics, carbon stocks, fire indices, canopy fuel characteristics, and mountain pine beetle susceptibility. The 95% confidence intervals for the mean response from across the 47 plots are shown, and non-overlapping confidence intervals are interpreted as significant differences between simulations.

Results

Stand Structure and Composition

Lodgepole pine maintained dominance over the 100-year projections in both scenarios that did not incorporate climate change (Figure 4.1). Engelmann spruce and subalpine fir were most abundant in the harvest scenario. Under climate change scenarios, lodgepole pine basal area and trees per acre declined quickly to none by the end of the 100-year projection, regardless of whether the stand was clearcut. In the climate change untreated scenario, lodgepole pine basal area increases similarly to the untreated FVS default until 2022 before rapidly declining. Of the four species shown in Figure 4.1 that are currently common in these forest types, only aspen abundance increased in both climate change scenarios, although only to modest densities. A diversity of other species had established by the end of the climate change projections: *Juniperus*

monosperma, Juniperus osteosperma, Juniperus scopulorum, Larix occidentalis, Pinus edulis, Pinus flexilis, Pinus ponderosa, Picea pungens, Populus deltoides, and *Quercus gambelii*.

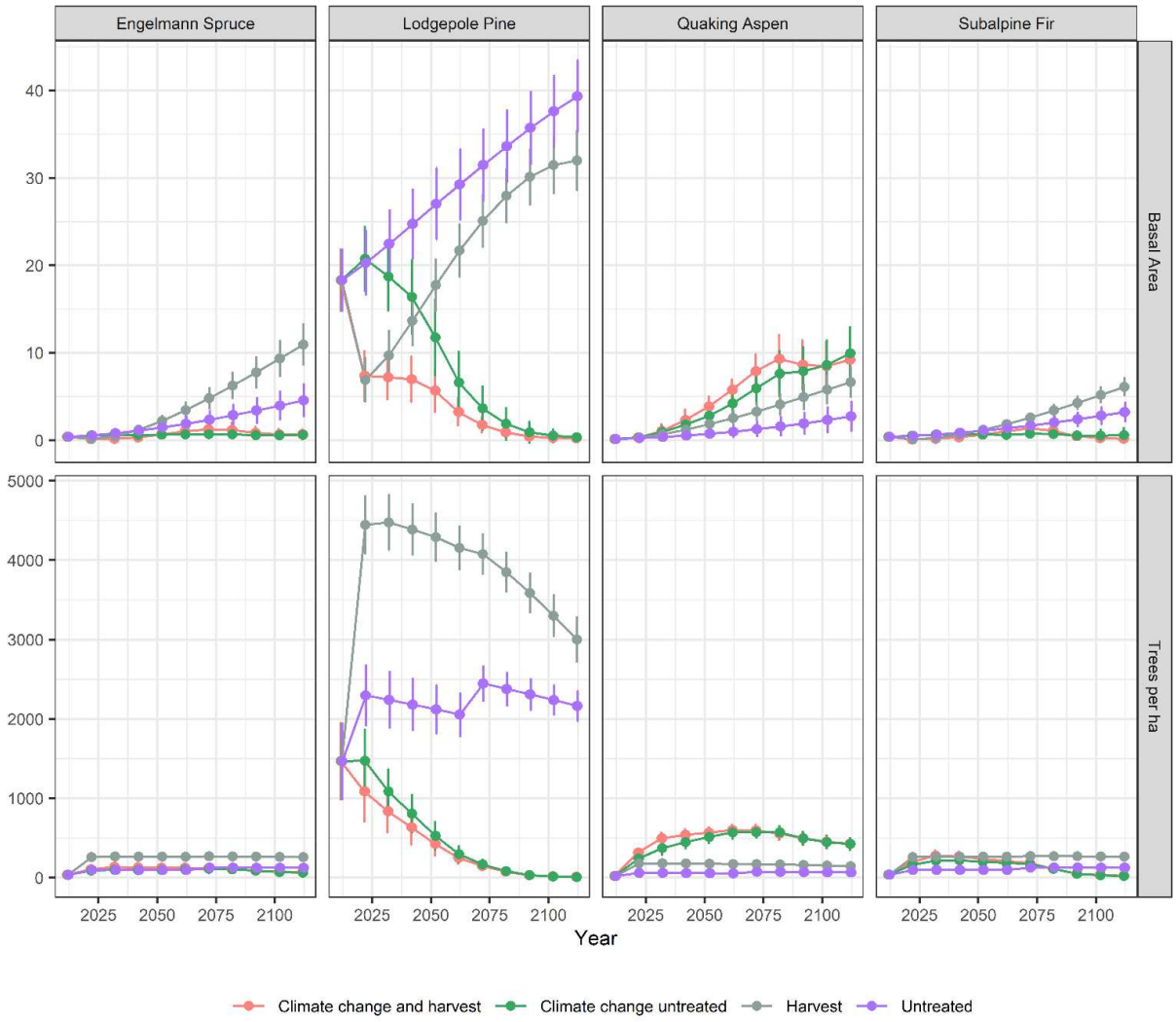

Figure 4.1. Average basal area ($m^2\ ha^{-1}$) and trees ha^{-1} with 95% confidence intervals for the 47 stands simulated in this study.

Climate change scenarios had similar basal areas to each other by the end of the 100-year projections. This basal area was less than half of the basal area achieved by scenarios without climate change (Figure 4.2). While climate change scenarios had far fewer trees, their trees were of a similar average diameter to the harvested default scenario.

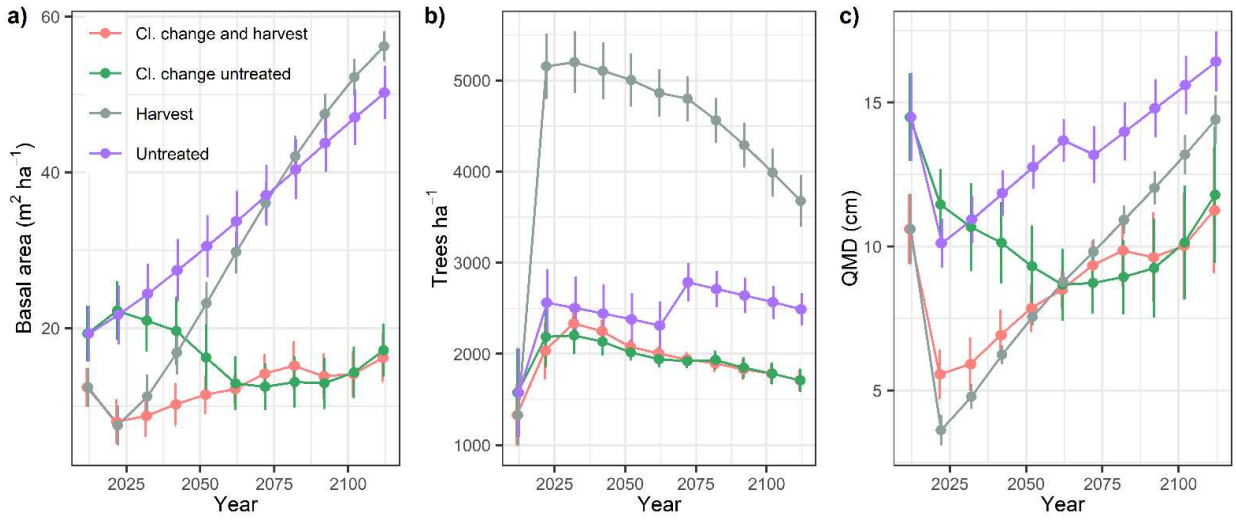

Figure 4.2. Mean (±95% confidence interval) basal area, tree density, and quadratic mean diameter (QMD) for the four simulations considered in this study.

Harvests showed similar impacts on forest carbon with and without climate change (Figure 4.3). In both cases, the harvested stands trailed their untreated counterparts in total stand carbon for 80 years before eventually catching up. Standing dead carbon accumulated in climate change scenarios as the changing climate stressed and killed trees. After fifty years into the simulations, the climate change scenarios lagged significantly in total aboveground live carbon compared to stands without climate change impacts. Ultimately, climate change was more impactful on total stand carbon by the end of the projections than harvesting (Figure 4.3).

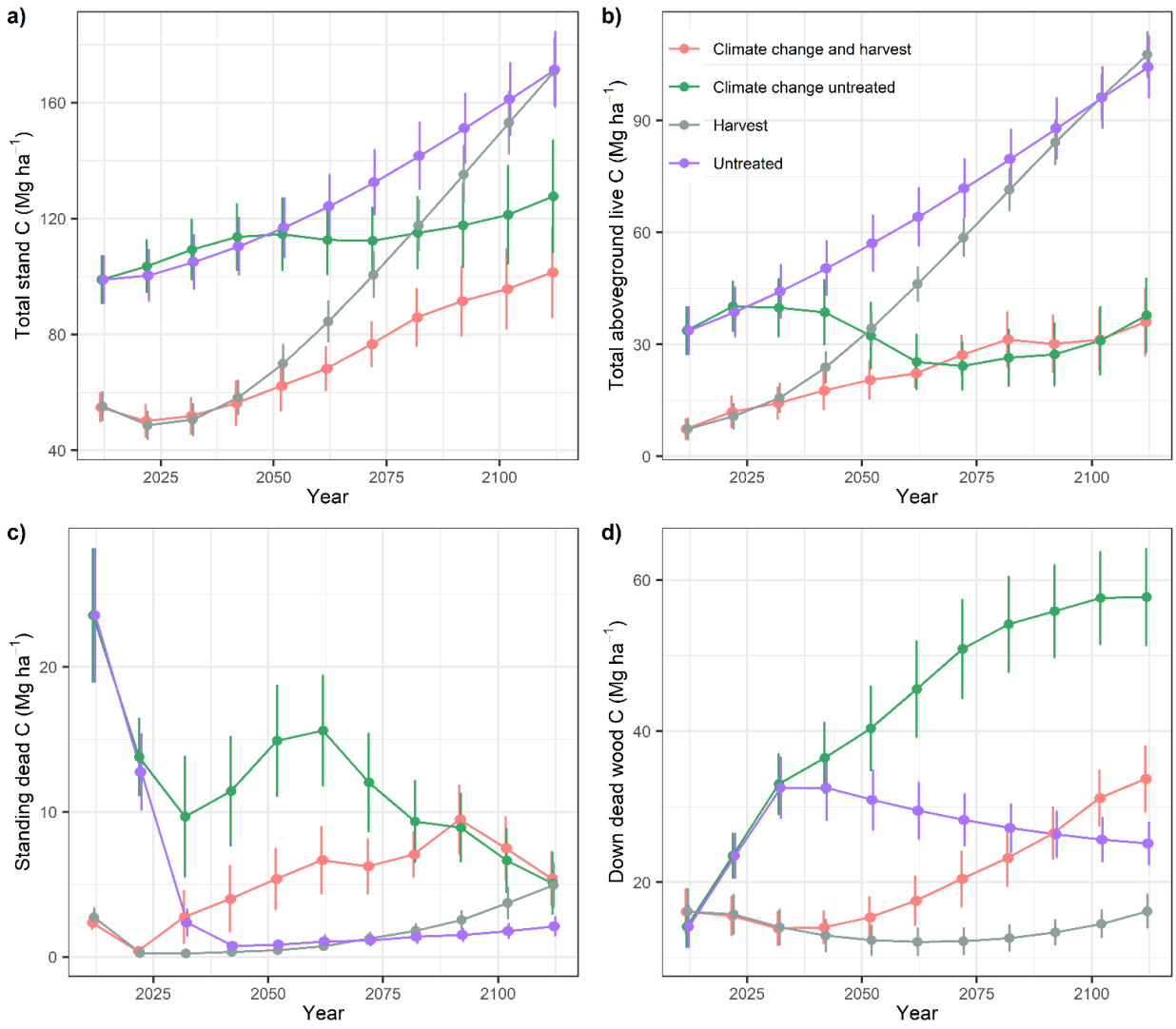

Figure 4.3. Mean (±95% confidence interval) forest carbon stocks.

Disturbance Susceptibility

All scenarios showed a decline in mountain pine beetle susceptibility (Figure 4.4). The mountain pine beetle susceptibility index declined sharply after harvest because the harvest removed all host trees. The susceptibility index slowly remained low for the treated scenario relative to untreated for the 100-year projection due to high stand density, greater species diversity, and lower quadratic mean diameter in the treatment. Climate change reduced mountain pine beetle susceptibility compared to the untreated default scenario, but raised it slightly

compared to the harvest scenario. Other pine host species, such as ponderosa pine and limber pine, established in the climate change scenarios.

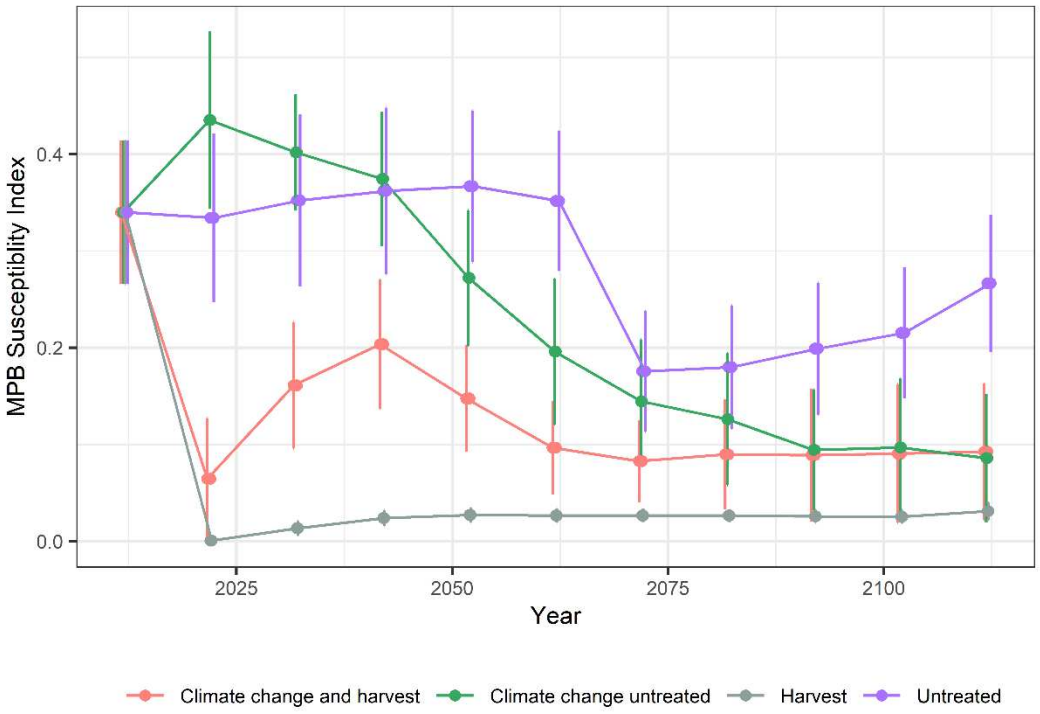

Figure 4.4. The average (±95% confidence interval) mountain pine beetle (MPB) susceptibility index for each simulation (Shore and Safranyik, 1992).

Both the default and climate change harvest scenarios were initially more susceptible to torching but less susceptible to crowning relative to untreated default and climate change scenarios. The default harvested and untreated stands had the greatest susceptibility to crown fire, as indicated by a greater canopy bulk density after about 30 years (Figure 4.5). The two climate change scenarios converged in their canopy fuel characteristics by 30 years, having relatively low canopy bulk densities and canopy base heights.

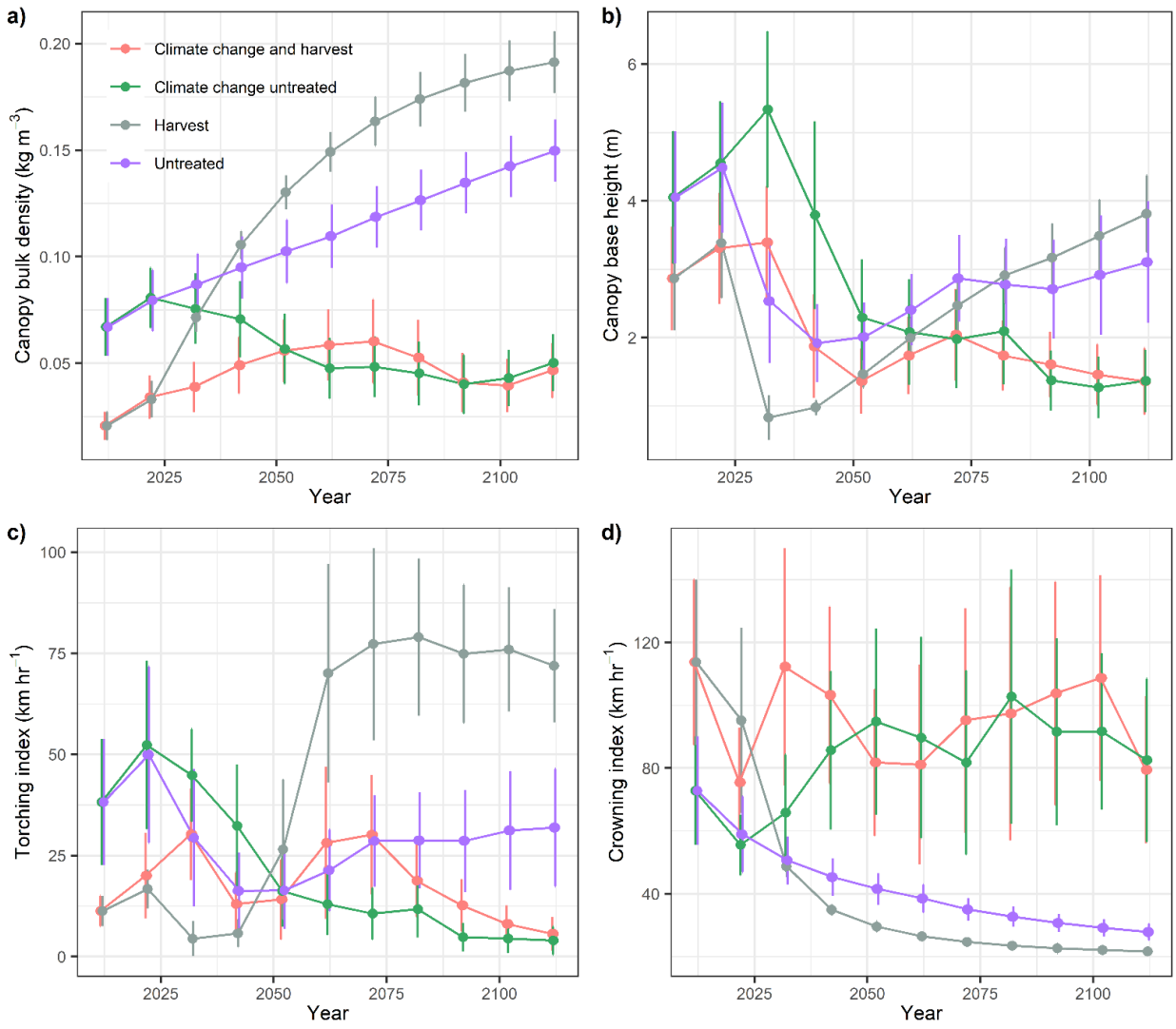

Figure 4.5. (a) Canopy bulk density, (b) canopy base height, (c) torching index, and (d) crowning index for the Forest Vegetation Simulator projections. Means (±95% confidence interval) of the 47 simulated stands are shown.

Discussion

The impacts of climate change on forest carbon, as projected by Climate-FVS, were dramatic and exceeded the effects of salvage harvesting alone after roughly 50 years. Climate change significantly reduced total stand carbon at the end of the 100-year projection. The climatic suitability for lodgepole pine decreased from the start of the simulation period, with noticeable impacts on the carbon cycle by 2042. As climatic suitability declines, the dead carbon

pool can be expected to increase at the expense of live carbon pools (Figure 4.3). Total aboveground live carbon stocks were similarly low in both treated and untreated climate change scenarios by 50 years, and had roughly a third of the total aboveground live carbon of scenarios that did not incorporate climate change by 100 years. Species currently associated with lower elevations (i.e., ponderosa pine and Gambel oak) are projected by Climate-FVS to be better adapted for the subalpine sites in this study than current species.

While this is just one model built on many assumptions, these results are attention-grabbing. Climate change has the potential to change forest structure and composition in this region, and to greatly reduce forest carbon stocks. The rate at which the current species become unsuitable highlights the need for climate-adaptive forest management (Janowiak et al., 2014) and for continued research to anticipate climate change effects on forests. Bark beetle outbreaks can select for trees more genetically resistant to future bark beetle outbreaks (Six et al., 2018). These impacts are not captured in model simulations. Where conditions are suitable and windthrow risk is deemed acceptable, retention of live trees during salvage harvest should be considered. These live trees may be better adapted for future conditions than the trees that were killed by bark beetles (Six et al., 2018). Additionally, retaining healthy live trees can increase carbon stocks relative to clearcuts (Mathys et al., 2013).

Salvage logging reduces short term fire risk (Collins et al., 2012), and here I show that mountain pine beetle susceptibility also declines with harvest. This result is not surprising, given the preference of bark beetles for large host trees and aligns with observations of reduced mortality severity in historical forest treatments completed ~20-50 years before bark beetle outbreaks (Vorster et al., 2017). It was surprising that susceptibility to mountain pine beetles in untreated stands only increased modestly before declining over the course of the 100-year

projection. I expect that the susceptibility would begin increasing in default (no climate change) scenarios if these simulations were extended beyond 100 years as the lodgepole pine host trees grow. One of the main factors leading to reduced mountain pine beetle susceptibility in climate change scenarios is the greater species diversity and abundance of non-pine trees. The harvested default scenario gained more Engelmann spruce and subalpine fir than the untreated default, contradicting findings from other studies that have found greater abundance of subalpine fir in untreated stands (Collins et al., 2012). This, combined with the high density of trees in the untreated default kept susceptibility to mountain pine beetles low. The regeneration pulse that I plant after harvest is based on summarized FIA data, while Collins et al., (2012) measured regeneration in salvage harvested plots to initialize their FVS simulations. The FVS is sensitive to regeneration (Bagdon et al., n.d.). Thus, this reduced susceptibility of salvage harvested stands needs further exploration. Future analyses should model a variety of species compositions and seedling counts to better capture the range of stand development trajectories. Case studies in the literature and FIA plots could provide this range of regeneration observations to project in FVS.

These differences in susceptibility to future disturbances have implications for forest carbon sequestration and for the climate impacts of forest products. For example, the different susceptibilities to mountain pine beetle suggests that while the carbon stocks in the harvested stands are less than the untreated alternative for the first 80 years, the carbon is perhaps less likely to be lost in future bark beetle outbreaks. Accounting for the impacts of multiple disturbances is complicated, though, because other disturbances, such as fire in this study, have opposing and temporally-dependent trends in susceptibility between the different scenarios. Nonetheless, Climate-FVS is a great tool to help consider the stability of carbon stocks when comparing carbon outcomes of management alternatives.

Climate change exacerbated the most recent mountain pine beetle outbreaks. However, my results suggest that climate change may have an indirect dampening effect on mountain pine beetle outbreaks in this area in the long run by decreasing suitability for their preferred host trees. This phenomena has also been projected for Engelmann spruce and spruce beetles (Temperli et al., 2015). While the projections show substantially decreased susceptibility to severe fire in the climate change scenario, this is not likely to be the case. As new vegetation communities develop on this site, their fuel characteristics will shape fire susceptibility.

Conclusion

This study uses the FVS to compare salvage logged and untreated stands, finding salvage-logged sites to recover to untreated total stand carbon stocks after 80 years. Salvage-logged sites had lower susceptibility to mountain pine beetles. Impacts of salvage logging on fuel canopy characteristics were mixed depending on the timeframe being considered. Canopy fuel characteristics changed more rapidly than mountain pine beetle susceptibility. Less than 20% of the landscape is expected to be salvage-harvested, so these changes to disturbance susceptibility may be minor at the landscape scale (Collins et al., 2012). Future work should evaluate if heterogeneity resulting from a patchwork of salvaged and untreated areas reduces susceptibility to bark beetle outbreaks at the landscape scale. Climate change impacts on stand structure, forest carbon, and disturbance susceptibility were dramatic, suggesting that climate change may outsize post-outbreak forest management effects. While great uncertainty surrounds climate change projections on forest regeneration, mortality, and growth, these models are useful for exploring forest processes that occur over long time frames and larges spatial extents that are otherwise difficult to evaluate with other ecological methods. The approach employed in this study cannot account for spatial dynamics, and does not adequately represent the variability in forest

development. Future work should evaluate a range of developmental trajectories and should consider spatial disturbance interactions.

CONCLUSION

In this dissertation, I estimated forest biomass from individual tree to landscape scales, quantified the impacts of bark beetles on this biomass, and projected how forest management may shape both biomass stocks and susceptibility to future forest disturbances. I leveraged remote sensing, advances in cloud computing, and existing data source to advance the accuracy, rigor, and spatial scale of forest biomass and disturbance assessments. This information was used to improve understanding of the ecological processes underlying and resulting from forest disturbance.

I demonstrated the foundational role of allometric biomass equations in the accuracy of biomass estimates, and that these equations should be carefully evaluated before application. Tree growth form varies with species, genetics, and growing conditions. Equations developed to make predictions across large regions or countries may not capture local growth forms. Thus, allometric equations must be evaluated with trees from the area where they are being applied to truly understand their errors. This step can reduce errors in final biomass estimates drastically—informed allometric equation selection reduced landscape biomass errors by 70%. This evaluation revealed that allometric equations used for national carbon inventories (Environmental Protection Agency, 2018) have substantial negative bias in the study area. Failure to consider the contributions of these allometric errors to landscape biomass estimates results in drastic under-reporting of uncertainty. However, obtaining independent data to represent local tree form is challenging. These data are expensive to obtain and rare. Efforts to gather and share existing destructive sampling data (Radtke et al., 2015) can alleviate this problem. I also worked on a collaborative project to advance methods for non-destructively

sampling individual tree biomass (Stovall et al., 2017). This technology has the potential to make individual tree data more available, leading to improved allometric biomass equations and more widespread local evaluation of allometric equations.

The fact that allometric uncertainty is rarely accounted for means that error of forest biomass estimates is frequently and substantially under-estimated. As a result, the general perception is that we can confidently estimate forest carbon stocks. This confidence guides investment in forest carbon markets to mitigate climate change. Yet, once allometric uncertainty was accounted for, I found uncertainty to be as high as 164.5% of the mean and only as low as 94.4%. These high levels of uncertainty in forest biomass estimates is surprising, and underscores the importance of refining methods for quantifying forest biomass.

In Chapter 2, I found that efficient remote sensing methods can better quantify the extent and severity of tree mortality than the existing standard datasets. These remote sensing methods can quantify forest mortality at a finer spatial resolution, with greater coverage, and with consistency across large extents (i.e., multiple states in this case). Aerial detection surveys, the existing method widely used to quantify insect impacts, complement remote sensing methods by identifying the year of impact and the causal insect or disease. The fusion of these products led to insights about bark beetle population dynamics. Mapping mortality severity at finer scales can help to quantify the ecosystem impacts of bark beetle outbreaks—as the effects of bark beetles on hydrologic and ecosystem processes scale with mortality severity. I have been working with others to apply these mortality severity maps to understand the effects of bark beetles on streamflow in headwaters.

This approach to mapping tree mortality also advances our ability to map dead biomass, which is a task that has challenged the remote sensing field. Chapter 3 demonstrated how pairing

mortality severity maps with biomass maps and field data can be used to quantify dead, live, and total forest biomass. Nearly 30% of total biomass was transferred to standing dead biomass in the study area following severe bark beetle outbreaks. The standing dead carbon pool is clearly significant, thus methods designed to specifically quantify dead carbon are critical for carbon inventories. I also used these maps around potential bioenergy facilities to assess the quantity and condition of potentially accessible biomass relative to 20-year demand of four bioenergy production scenarios.

In the last chapter, I modeled the impacts of forest management and climate change on bark beetle-impacted lodgepole pine forests. Salvage logging had lasting impacts on forest carbon, and also influenced susceptibility to future fire and bark beetle outbreaks. However, climate change had a greater effect on forest carbon and disturbance susceptibility. Climate change impacts on forest processes will continue to be pervasive, and thus cannot be excluded from forest projections. However, these impacts are unpredictable and poorly understood. Simulating climate change effects on forests, and how climate change should be considered in forest management is a particularly important topic for continued research.

Forests face many threats from land use change, invasive species, climate change, and associated severe, frequent, and novel disturbance patterns. Simultaneously, forests are increasingly essential for their contributions to hydrological function, biodiversity, carbon storage, food production, and fiber. The field of forest ecology has important contributions to make in this predicament by informing forest management, guiding policy, and engaging the public. This dissertation shows how remote sensing technologies, field data, and simulation models can advance understanding about interactions between biotic disturbances, climate change, and forest management. This research addresses pressing questions such as the carbon

footprint and feasibility of forest bioenergy in forests with substantial tree mortality, the connections between forest disturbance and hydrology, and how to accurately and efficiently monitor the role of forests and disturbances in forest carbon sequestration.

REFERENCES

Abella, S.R., Fornwalt, P.J., 2014. Ten years of vegetation assembly after a North American mega fire. Glob. Chang. Biol. 21, 789–802. doi:10.1111/gcb.12722

Anderson, J.E., Romme, W.H., 1991. Initial Floristics in Lodgepole Pine (Pinus contorta) Forests Following the 1988 Yellowstone Fires. Int. J. Wildl. Fire 1, 119–124. doi:10.1071/WF9910119

Baccini, A., Goetz, S.J., Walker, W.S., Laporte, N.T., Sun, M., Sulla-Menashe, D., Hackler, J., Beck, P.S.A., Dubayah, R., Friedl, M.A., Samanta, S., Houghton, R.A., 2012. Estimated carbon dioxide emissions from tropical deforestation improved by carbon-density maps. Nat. Clim. Chang. 2, 182–185. doi:10.1038/nclimate1354

Backsen, J.C., Howell, B., 2013. Comparing Aerial Detection and Photo Interpretation for Conducting Forest Health Surveys. West. J. Appl. For. 28, 3–8.

Bagdon, B., Field, J., Vorster, A.G., Trung, N., Paustian, K., n.d. An accessible, data-driven approach for robust calibration of the Forest Vegetation Simulator. Prep.

Bagdon, B.A., Nguyen, T.H., Vorster, A.G., Paustian, K., Field, J.L., n.d. A model evaluation framework applied to the Forest Vegetation Simulator (FVS) in Colorado and Wyoming lodgepole pine forests. Rev.

Baig, M.H.A., Zhang, L., Shuai, T., Tong, Q., 2014. Derivation of a tasselled cap transformation based on Landsat 8 at-satellite reflectance. Remote Sens. Lett. 5, 423–431. doi:10.1080/2150704X.2014.915434

Baker, D.J., Richards, G., Grainger, A., Gonzalez, P., Brown, S., DeFries, R., Held, A., Kellndorfer, J., Ndunda, P., Ojima, D., Skrovseth, P.E., Souza, C., Stolle, F., 2010.

Achieving forest carbon information with higher certainty: A five-part plan. Environ. Sci. Policy 13, 249–260. doi:10.1016/j.envsci.2010.03.004

Baskerville, G.L., 1972. Use of Logarithmic Regression in the Estimation of Plant Biomass. Can. J. For. Res. 2, 49–53.

Belgiu, M., Drăgu, L., 2016. Random forest in remote sensing: A review of applications and future directions. ISPRS J. Photogramm. Remote Sens. 114, 24–31. doi:10.1016/j.isprsjprs.2016.01.011

Bentz, B.J., Régnière, J., Fettig, C.J., Hansen, E.M., Hayes, J.L., Hicke, J. a., Kelsey, R.G., Negrón, J.F., Seybold, S.J., 2010. Climate Change and Bark Beetles of the Western United States and Canada: Direct and Indirect Effects. Bioscience 60, 602–613. doi:10.1525/bio.2010.60.8.6

Berg, E.E., Henry, J.D., Fastie, C.L., Volder, A.D. De, Matsuoka, S.M., 2006. Spruce beetle outbreaks on the Kenai Peninsula, Alaska, and Kluane National Park and Reserve, Yukon Territory: Relationship to summer temperatures and regional differences in disturbance regimes. For. Ecol. Manage. 227, 219–232. doi:10.1016/j.foreco.2006.02.038

Berner, L.T., Law, B.E., Meddens, A.J., Hicke, J.A., 2017. Tree mortality from fires, bark beetles, and timber harvest during a hot and dry decade in the western United States (2003-2012). Environ. Res. Lett. 12, 13. doi:10.1088/1748-9326/aa6f94

Blackard, J.A., Finco, M. V., Helmer, E.H., Holden, G.R., Hoppus, M.L., Jacobs, D.M., Lister, A.J., Moisen, G.G., Nelson, M.D., Riemann, R., Ruefenacht, B., Salajanu, D., Weyermann, D.L., Winterberger, K.C., Brandeis, T.J., Czaplewski, R.L., McRoberts, R.E., Patterson, P.L., Tymcio, R.P., 2008. Mapping U.S. forest biomass using nationwide forest inventory data and moderate resolution information. Remote Sens. Environ. 112, 1658–1677.

doi:10.1016/j.rse.2007.08.021

Blaszczynski, J.S., 1997. Landform Characterization with Geographic Information Systems. Photogramm. Eng. Remote Sens. 63, 183–191.

Bode, E.T., Lawrence, R.L., Powell, S.L., Savage, S.L., Trowbridge, A.M., 2018. Time-series approach for mapping mountain pine beetle infestation extent and severity in the U.S. Central Rocky Mountains. J. Appl. Remote Sens. 12. doi:10.1117/1.JRS.12.046030

Boisvenue, C., Smiley, B.P., White, J.C., Kurz, W.A., Wulder, M.A., 2016. Integration of Landsat time series and field plots for forest productivity estimates in decision support models. For. Ecol. Manage. 376, 284–297. doi:10.1016/j.foreco.2016.06.022

Breiman, L., 2001. Random forests. Mach. Learn. 45, 5–32. doi:10.1023/A:1010933404324

Bright, B.C., Hudak, A.T., Kennedy, R.E., Meddens, A.J.H., 2014. Landsat time series and lidar as predictors of live and dead basal area across five bark beetle-affected forests. IEEE J. Sel. Top. Appl. Earth Obs. Remote Sens. 7, 3440–3452. doi:10.1109/JSTARS.2014.2346955

Buma, B., 2015. Disturbance interactions: characterization, prediction, and the potential for cascading effects. Ecosphere 6, 1–15. doi:10.1890/ES15-00058.1

Caldwell, M.K., Hawbaker, T.J., Briggs, J.S., Cigan, P.W., Stitt, S., 2013. Simulated impacts of mountain pine beetle and wildfire disturbances on forest vegetation composition and carbon stocks in the Southern Rocky Mountains. Biogeosciences 10, 8203–8222. doi:10.5194/bg-10-8203-2013

Campbell, R., Anderson, N., Daugaard, D., Naughton, H., 2018. Technoeconomic and Policy Drivers of Project Performance for Bioenergy Alternatives Using Biomass from Beetle-Killed Trees. Energies 11, 293. doi:10.3390/en11020293

Carroll, A.L., Taylor, S.W., Régnière, J., Safranyik, L., 2003. Effects of Climate Change on

Range Expansion by the Mountain Pine Beetle in British Columbia, Mountain Pine Beetle Symposium: Challenges and Solutions. Kelowna, British Columbia.

Carvalho, J.P., Parresol, B.R., 2003. Additivity in tree biomass components of Pyrenean oak (Quercus pyrenaica Willd.). For. Ecol. Manage. 179, 269–276. doi:10.1016/S0378-1127(02)00549-2

Chander, G., Markham, B.L., Helder, D.L., 2009. Summary of current radiometric calibration coefficients for Landsat MSS, TM, ETM+, and EO-1 ALI sensors. Remote Sens. Environ. 113, 893–903. doi:10.1016/j.rse.2009.01.007

Chapman, T.B., Veblen, T.T., Schoennagel, T., 2012. Spatiotemporal patterns of mountain pine beetle activity in the southern Rocky Mountains. Ecology 93, 2175–2185. doi:10.1890/11-1055.1

Chave, J., Condit, R., Aguilar, S., Hernandez, A., Lao, S., Perez, R., 2004. Error propagation and scaling for tropical forest biomass estimates. Philos. Trans. R. Soc. B Biol. Sci. 359, 409–420. doi:10.1098/rstb.2003.1425

Chen, Q., Vaglio Laurin, G., Valentini, R., 2015. Uncertainty of remotely sensed aboveground biomass over an African tropical forest: Propagating errors from trees to plots to pixels. Remote Sens. Environ. 160, 134–143. doi:10.1016/j.rse.2015.01.009

Chojnacky, D.C., Heath, L.S., Jenkins, J.C., 2014. Updated generalized biomass equations for North American tree species. Forestry 87, 129–151. doi:10.1093/forestry/cpt053

Chung, W., Evangelista, P., Anderson, N., Vorster, A., Han, H., Poudel, K., Sturtevant, R., 2017. Estimating Aboveground Tree Biomass for Beetle-Killed Lodgepole Pine in the Rocky Mountains of Northern Colorado. For. Sci. 63, 413–419. doi:10.5849/FS.2016-065

Cohen, W.B., Yang, Z., Healey, S.P., Kennedy, R.E., Gorelick, N., 2018. A LandTrendr

multispectral ensemble for forest disturbance detection. Remote Sens. Environ. 205, 131–140. doi:10.1016/j.rse.2017.11.015

Coleman, T.W., Graves, A.D., Heath, Z., Flowers, R.W., Hanavan, R.P., Cluck, D.R., Ryerson, D., 2018. Accuracy of aerial detection surveys for mapping insect and disease disturbances in the United States. For. Ecol. Manage. 430, 321–336. doi:10.1016/j.foreco.2018.08.020

Collins, B.J., Rhoades, C.C., Battaglia, M.A., Hubbard, R.M., 2012. The effects of bark beetle outbreaks on forest development, fuel loads and potential fire behavior in salvage logged and untreated lodgepole pine forests. For. Ecol. Manage. 284, 260–268. doi:10.1016/j.foreco.2012.07.027

Collins, B.J., Rhoades, C.C., Hubbard, R.M., Battaglia, M.A., 2011. Tree regeneration and future stand development after bark beetle infestation and harvesting in Colorado lodgepole pine stands. For. Ecol. Manage. 261, 2168–2175. doi:10.1016/j.foreco.2011.03.016

Collins, B.J., Rhoades, C.C., Underhill, J., Hubbard, R.M., 2010. Post-harvest seedling recruitment following mountain pine beetle infestation of Colorado lodgepole pine stands: a comparison using historic survey records. Can. J. For. Res. 40, 2452–2456. doi:10.1139/X10-172

Creeden, E.P., Hicke, J.A., Buotte, P.C., 2014. Climate, weather, and recent mountain pine beetle outbreaks in the western United States. For. Ecol. Manage. 312, 239–251. doi:10.1016/j.foreco.2013.09.051

Crist, E.P., 1985. A TM Tasseled Cap equivalent transformation for reflectance factor data. Remote Sens. Environ. 17, 301–306. doi:10.1016/0034-4257(85)90102-6

Crookston, N.L., 2014. Climate-FVS Version 2: Content, Users Guide, Applications, and Behavior. Fort Collins, CO.

Crookston, N.L., Dixon, G.E., 2005. The forest vegetation simulator: A review of its structure, content, and applications. Comput. Electron. Agric. 49, 60–80. doi:10.1016/j.compag.2005.02.003

Crookston, N.L., Rehfeldt, G.E., Dixon, G.E., Weiskittel, A.R., 2010. Addressing climate change in the forest vegetation simulator to assess impacts on landscape forest dynamics. For. Ecol. Manage. 260, 1198–1211. doi:10.1016/j.foreco.2010.07.013

Cudmore, T.J., Bjo, N., Carroll, A.L., Lindgren, B.S., 2010. Climate change and range expansion of an aggressive bark beetle: evidence of higher beetle reproduction in naive host tree populations. J. Appl. Ecol. 47, 1036–1043. doi:10.1111/j.1365-2664.2010.01848.x

Daba, D.E., Soromessa, T., 2019. The accuracy of species-specific allometric equations for estimating aboveground biomass in tropical moist montane forests: case study of Albizia grandibracteata and Trichilia dregeana. Carbon Balance Manag. 14. doi:10.1186/s13021-019-0134-8

DeRose, R.J., Long, J.N., 2009. Wildfire and Spruce Beetle Outbreak: Simulation of Interacting Disturbances in the Central Rocky Mountains. Ecoscience 16, 28–38. doi:10.2980/16-1-3160

Dilling, L., Kelsey, K.C., Fernandez, D.P., Huang, Y.D., Milford, J.B., Neff, J.C., 2016. Managing Carbon on Federal Public Lands: Opportunities and Challenges in Southwestern Colorado. Environ. Manage. doi:10.1007/s00267-016-0714-2

Diskin, M., Rocca, M.E., Nelson, K.N., Aoki, C.F., Romme, W.H., 2011. Forest developmental trajectories in mountain pine beetle disturbed forests of Rocky Mountain National Park, Colorado. Can. J. For. Res. 41, 782–792. doi:10.1139/x10-247

Domke, G.M., Woodall, C.W., Smith, J.E., 2011. Accounting for density reduction and structural

loss in standing dead trees: Implications for forest biomass and carbon stock estimates in the United States. Carbon Balance Manag. 6, 14. doi:10.1186/1750-0680-6-14

Donato, D.C., Simard, M., Romme, W.H., Harvey, B.J., Turner, M.G., 2013. Evaluating post-outbreak management effects on future fuel profiles and stand structure in bark beetle-impacted forests of Greater Yellowstone. For. Ecol. Manage. 303, 160–174. doi:10.1016/j.foreco.2013.04.022

Dormann, C.F., Elith, J., Bacher, S., Buchmann, C., Carl, G., Carré, G., Marquéz, J.R.G., Gruber, B., Lafourcade, B., Leitão, P.J., Münkemüller, T., Mcclean, C., Osborne, P.E., Reineking, B., Schröder, B., Skidmore, A.K., Zurell, D., Lautenbach, S., 2013. Collinearity: A review of methods to deal with it and a simulation study evaluating their performance. Ecography (Cop.). 36, 27–46. doi:10.1111/j.1600-0587.2012.07348.x

Duane, M. V, Cohen, W.B., Campbell, J.L., Hudiburg, T., Turner, D.P., Weyermann, D.L., 2010. Implications of Alternative Field-Sampling Designs on Landsat-Based Mapping of Stand Age and Carbon Stocks in Oregon Forests. For. Sci. 56, 405–416.

Dubayah, R., Bryan, J., Goetz, S., Fatoyinbo, L., Hansen, M., Healey, S., Hofton, M., Hurtt, G., Kellner, J., Luthcke, S., Armston, J., Tang, H., Duncanson, L., Hancock, S., Jantz, P., Marselis, S., Patterson, P.L., Qi, W., Silva, C., 2020. The Global Ecosystem Dynamics Investigation: High-resolution laser ranging of the Earth's forests and topography. Sci. Remote Sens. 1, 100002. doi:10.1016/j.srs.2020.100002

Duncanson, L., Rourke, O., Dubayah, R., 2015. Small Sample Sizes Yield Biased Allometric Equations in Temperate Forests. Sci. Rep. 5. doi:10.1038/srep17153

Duque, A., Saldarriaga, J., Meyer, V., Saatchi, S., 2017. Structure and allometry in tropical forests of Chocó, Colombia. For. Ecol. Manage. 405, 309–318.

doi:10.1016/j.foreco.2017.09.048

Eckert, S., 2012. Improved Forest Biomass and Carbon Estimations Using Texture Measures from WorldView-2 Satellite Data. Remote Sens. 4, 810–829. doi:10.3390/rs4040810

Eidenshink, J.C., Schwind, B., Brewer, K., Zhu, Z.-L., Quayle, B., Howard, S., 2007. A Project for Monitoring Trends in Burn Severity. Fire Ecol. 3, 3–21. doi:10.4996/fireecology.0301003

Environmental Protection Agency, 2018. Inventory of U.S. Greenhouse Gas Emissions and Sinks: 1990-2016. U.S. Environmental Protection Agency, Washington, DC.

Environmental Systems Research Institute, 2017. ArcGIS.

Evangelista, P.H., Kumar, S., Stohlgren, T.J., Young, N.E., 2011. Assessing forest vulnerability and the potential distribution of pine beetles under current and future climate scenarios in the Interior West of the US. For. Ecol. Manage. 262, 307–316. doi:10.1016/j.foreco.2011.03.036

Evans, J.S., Cushman, S.A., 2009. Gradient modeling of conifer species using random forests. Landsc. Ecol. 24, 673–683. doi:10.1007/s10980-009-9341-0

Evans, J.S., Oakleaf, J., Cushman, S.A., Theobald, D., 2014. An ArcGIS Toolbox for Surface Gradient and Geomorphometric Modeling.

Fekety, P.A., Crookston, N.L., Hudak, A.T., Filippelli, S.K., Vogeler, J.C., Falkowski, M.J., 2020. Hundred year projected carbon loads and species compositions for four National Forests in the northwestern USA. Carbon Balance Manag. 15, 1–14. doi:10.1186/s13021-020-00140-9

Feldpausch, T.R., Banin, L., Phillips, O.L., Baker, T.R., Lewis, S.L., Quesada, C.A., Affum-Baffoe, K., Arets, E.J.M.M., Berry, N.J., Bird, M., Brondizio, E.S., De Camargo, P., Chave,

J., Djagbletey, G., Domingues, T.F., Drescher, M., Fearnside, P.M., França, M.B., Fyllas, N.M., Lopez-Gonzalez, G., Hladik, A., Higuchi, N., Hunter, M.O., Iida, Y., Salim, K.A., Kassim, A.R., Keller, M., Kemp, J., King, D.A., Lovett, J.C., Marimon, B.S., Marimon-Junior, B.H., Lenza, E., Marshall, A.R., Metcalfe, D.J., Mitchard, E.T.A., Moran, E.F., Nelson, B.W., Nilus, R., Nogueira, E.M., Palace, M., Patiño, S., Peh, K.S.H., Raventos, M.T., Reitsma, J.M., Saiz, G., Schrodt, F., Sonké, B., Taedoumg, H.E., Tan, S., White, L., Wöll, H., Lloyd, J., 2011. Height-diameter allometry of tropical forest trees. Biogeosciences 8, 1081–1106. doi:10.5194/bg-8-1081-2011

Field, J., Bagdon, B., Nguyen, T., Vorster, A., Paustian, K., 2018. A Framework for Quantifying Climate Outcomes of Beetle-Killed Forest Biomass Utilization, in: LCA XVIII. American Center for Life Cycle Assessment, pp. 15–27.

Forest Health Monitoring Program, 1999. Aerial Survey Standards.

Fornwalt, P.J., Rhoades, C.C., Hubbard, R.M., Harris, R.L., Faist, A.M., Bowman, W.D., 2018. Short-term understory plant community responses to salvage logging in beetle-affected lodgepole pine forests. For. Ecol. Manage. 409, 84–93. doi:10.1016/j.foreco.2017.10.056

Foster, A.C., Shuman, J.K., Shugart, H.H., Negron, J., 2018. Modeling the interactive effects of spruce beetle infestation and climate on subalpine vegetation. Ecosphere 9, 21. doi:10.1002/ecs2.2437

Friedman, J.H., 2001. Greedy Function Approximation : A Gradient Boosting Machine. Ann. Stat. 29, 1189–1232.

Genuer, R., Poggi, J., Tuleau-Malot, C., 2015. VSURF : An R Package for Variable Selection Using Random Forests. R J. 7, 19–33.

Gesch, D., Oimoen, M., Greenlee, S., Nelson, C., Steuck, M., Tyler, D., 2002. The National

Elevation Dataset. Photogramm. Eng. Remote Sens. 68.

Gesch, D.B., 2007. The National Elevation Dataset, in: Maune, D. (Ed.), Digital Elevation Model Technologies and Applications: The DEM User's Manual. American Society for Photogrammetry and Remote Sensing, Bethesda, Maryland, pp. 99–118.

Gessler, P.E., Moore, I.D., Mckenzie, N.J., Ryan, P.J., 1995. Soil-landscape modelling and spatial prediction of soil attributes. Int. J. Geogr. Inf. Syst. 9, 421–432. doi:10.1080/02693799508902047

Ghimire, B., Williams, C.A., Collatz, G.J., Vanderhoof, M., Rogan, J., Kulakowski, D., Masek, J.G., 2015. Large Carbon Release Legacy from Bark Beetle Outbreaks across Western United States. Glob. Chang. Biol. 21, 3087–3101. doi:10.1111/gcb.12933

Gitelson, A.A., Kaufman, Y.J., Merzlyak, M.N., 1996. Use of a Green Channel in Remote Sensing of Global Vegetation from EOS-MODIS. Remote Sens. Environ. 58, 289–298.

Goodale, C.L., Apps, M.J., Birdsey, R.A., Field, C.B., Heath, L.S., Houghton, R.A., Jenkins, J.C., Kohlmaier, G.H., Kurz, W., Liu, X.S., Nabuurs, G., Nilsson, S., Shvidenko, A.Z., 2002. Forest Carbon Sinks in the Northern Hemisphere. Ecol. Appl. 12, 891–899. doi:10.1890/1051-0761(2002)012[0891:FCSITN]2.0.CO;2

Goodwin, N.R., Coops, N.C., Wulder, M.A., Gillanders, S., Schroeder, T.A., Nelson, T., 2008. Estimation of insect infestation dynamics using a temporal sequence of Landsat data. Remote Sens. Environ. 112, 3680–3689. doi:10.1016/j.rse.2008.05.005

Gorelick, N., Hancher, M., Dixon, M., Ilyushchenko, S., Thau, D., Moore, R., 2017. Google Earth Engine: Planetary-scale geospatial analysis for everyone. Remote Sens. Environ. 202, 18–27. doi:10.1016/j.rse.2017.06.031

Graham, V., Laurance, S.G., Grech, A., Venter, O., 2017. Spatially explicit estimates of forest

carbon emissions, mitigation costs and REDD+ opportunities in Indonesia. Environ. Res. Lett. 12, 11. doi:10.1088/1748-9326/aa6656

Guisan, A., Weiss, S.B., Weiss, A.D., 1999. GLM versus CCA spatial modeling of plant species distribution. Plant Ecol. 143, 107–122. doi:10.1023/A:100984151

Hall, R.J., Skakun, R.S., Arsenault, E.J., Case, B.S., 2006. Modeling forest stand structure attributes using Landsat ETM+ data: Application to mapping of aboveground biomass and stand volume. For. Ecol. Manage. 225, 378–390. doi:10.1016/j.foreco.2006.01.014

Hansen, E.M., 2013. Forest Development and Carbon Dynamics After Mountain Pine Beetle Outbreaks. For. Sci. 60, 476–488. doi:10.5849/forsci.13-039

Hansen, E.M., Amacher, M.C., Miegroet, H. Van, Long, J.N., Ryan, M.G., 2015. Carbon Dynamics in Central US Rockies Lodgepole Pine Type After Mountain Pine Beetle Outbreaks. For. Sci. 61, 1–15. doi:10.5849/forsci.14-094

Hardisky, M.A., Klemas, V., Smart, R.M., 1983. The Influence of Soil Salinity, Growth Form, and Leaf Moisture on-the Spectral Radiance of Spartina alterniflora Canopies. Photogramm. Eng. Remote Sens. 49, 77–83.

Harmon, M.E., Fasth, B., Woodall, C.W., Sexton, J., 2013. Carbon concentration of standing and downed woody detritus: Effects of tree taxa, decay class, position, and tissue type. For. Ecol. Manage. 291, 259–267. doi:10.1016/j.foreco.2012.11.046

Harmon, M.E., Franklin, J.F., Swanson, F.J., Sollins, P., Gregory, S.V., Lattin, J.D., Anderson, N.H., Cline, S.P., Aumen, N.G., Sedell, J.R., Lienkaemper, G.W., Cromack Jr., K., Cummins, K.W., 1986. Ecology of Coarse Woody Debris in Temperate Ecosystems. Adv. Ecol. Res. 15, 133–263. doi:10.1016/S0065-2504(08)60121-X

Harmon, M.E., Woodall, C.W., Fasth, B., Sexton, J., Yatkov, M., 2011. Differences between

standing and downed dead tree wood density reduction factors: a comparison across decay classes and tree species, RP NRS-15. ed. Newtown Square, PA.

Hart, S.J., Veblen, T.T., Eisenhart, K.S., Jarvis, D., Kulakowski, D., 2014. Drought induces spruce beetle (Dendroctonus rufipennis) outbreaks across northwestern Colorado. Ecology 95, 930–939. doi:10.1890/13-0230.1

Heath, L.S., Hansen, M.H., Smith, J.E., Smith, W.B., Miles, P.D., 2009. Investigation into Calculating Tree Biomass and Carbon in the FIADB Using a Biomass Expansion Factor Approach, in: McWilliams, W., Moisen, G., Czaplewski, R. (Eds.), 2008 Forest Inventory and Analysis (FIA) Symposium, USDA Forest Service Proceddings - RMRS-P-56. U.S. Department of Agriculture, Forest Service, Rocky Mountain Research Station, Park City, UT.

Hermosilla, T., Wulder, M.A., White, J.C., Coops, N.C., Hobart, G.W., Campbell, L.B., 2016. Mass data processing of time series Landsat imagery: pixels to data products for forest monitoring. Int. J. Digit. Earth 8947. doi:10.1080/17538947.2016.1187673

Hicke, J. a., Allen, C.D., Desai, A.R., Dietze, M.C., Hall, R.J., Hogg, E.H.T., Kashian, D.M., Moore, D., Raffa, K.F., Sturrock, R.N., Vogelmann, J., 2012. Effects of biotic disturbances on forest carbon cycling in the United States and Canada. Glob. Chang. Biol. 18, 7–34. doi:10.1111/j.1365-2486.2011.02543.x

Hicke, J.A., Jenkins, J.C., 2008. Mapping lodgepole pine stand structure susceptibility to mountain pine beetle attack across the western United States. For. Ecol. Manage. 255, 1536–1547. doi:10.1016/j.foreco.2007.11.027

Hicke, J.A., Meddens, A.J.H., Allen, C.D., Kolden, C.A., 2013. Carbon stocks of trees killed by bark beetles and wildfire in the western United States. Environ. Res. Lett. 8, 035032.

doi:10.1088/1748-9326/8/3/035032

Hicke, J.A., Meddens, A.J.H., Kolden, C.A., 2016. Recent Tree Mortality in the Western United States from Bark Beetles and Forest Fires. For. Sci. 62, 141–153. doi:10.5849/forsci.15-086

Hogland, J., Anderson, N., Chung, W., 2018. New Geospatial Approaches for Efficiently Mapping Forest Biomass Logistics at High Resolution over Large Areas. Int. J. Geo-Information 7, 19. doi:10.3390/ijgi7040156

Holtsmark, B., 2012. Harvesting in boreal forests and the biofuel carbon debt. Clim. Change 112, 415–428. doi:10.1007/s10584-011-0222-6

Huang, C., Wylie, B., Yang, L., Homer, C., Zylstra, G., 2002. Derivation of a tasselled cap transformation based on Landsat 7 at-satellite reflectance. Int. J. Remote Sens. 23, 1741–1748. doi:10.1080/01431160110106113

Hubbard, R.M., Rhoades, C.C., Elder, K., Negron, J., 2013. Changes in transpiration and foliage growth in lodgepole pine trees following mountain pine beetle attack and mechanical girdling. For. Ecol. Manage. 289, 312–317. doi:10.1016/j.foreco.2012.09.028

Huckaby, L.S., Kaufmann, M.R., Fornwalt, P.J., Stoker, J.M., Dennis, C., 2003. Identification and Ecology of Old Ponderosa Pine Trees in the Colorado Front Range, RMRS-GTR-1. ed. U.S. Department of Agriculture, Forest Service, Rocky Mountain Research Station, Fort Collins, CO.

Hudak, A.T., Bright, B.C., Kennedy, R.E., 2013. Predicting live and dead basal area from LandTrendr variables in beetle-affected forests. MultiTemp 2013 - 7th Int. Work. Anal. Multi-Temporal Remote Sens. Images "Our Dyn. Environ. Proc. 4–7. doi:10.1109/Multi-Temp.2013.6866024

Hudiburg, T.W., Law, B.E., Wirth, C., Luyssaert, S., 2011. Regional carbon dioxide implications

of forest bioenergy production. Nat. Clim. Chang. 1, 419–423. doi:10.1038/nclimate1264

Huete, A.R., 1988. A Soil-Adjusted Vegetation Index (SAVI). Remote Sens. Environ. 309, 295–309. doi:10.1016/0034-4257(88)90106-X

IPCC, 2014. Climate Change 2014: Synthesis Report. Contribution of Working Groups I, II and III to the Fifth Assessment Report of the Intergovernmental Panel on Climate Change. Geneva, Switzerland.

Ivan, J.S., Seglund, A.E., Truex, R.L., Newkirk, E.S., 2018. Mammalian responses to changed forest conditions resulting from bark beetle outbreaks in the southern Rocky Mountains. Ecosphere 9, 18. doi:10.1002/ecs2.2369

Janowiak, M.K., Swanston, C.W., Nagel, L.M., Brandt, L.A., Butler, P.R., Handler, S.D., Shannon, P.D., Iverson, L.R., Matthews, S.N., Prasad, A., Peters, M.P., 2014. A Practical Approach for Translating Climate Change Adaptation Principles into Forest Management Actions. J. For. 112, 424–433. doi:10.5849/jof.13-094

Jenkins, J.C., Chojnacky, D.C., Heath, L.S., Birdsey, R.A., 2003. National-scale biomass estimators for United States tree species. For. Sci. 49, 12–35. doi:10.1093/forestscience/49.1.12

Ji, L., Wylie, B.K., Nossov, D.R., Peterson, B., Waldrop, M.P., McFarland, J.W., Rover, J., Hollingsworth, T.N., 2012. Estimating aboveground biomass in interior Alaska with Landsat data and field measurements. Int. J. Appl. Earth Obs. Geoinf. 18, 451–461. doi:10.1016/j.jag.2012.03.019

Johansson, V., Felton, A., Ranius, T., 2016. Long-term landscape scale effects of bioenergy extraction on dead wood-dependent species. For. Ecol. Manage. 371, 103–113. doi:10.1016/j.foreco.2015.10.046

Johnson, E.W., Ross, J., 2008. Quantifying error in aerial survey data. Aust. For. 71, 216–222. doi:10.1080/00049158.2008.10675038

Johnson, E.W., Wittwer, D., 2008. Aerial detection surveys in the United States. Aust. For. 71, 212–215. doi:10.1080/00049158.2008.10675037

Johnston, R.S., Bartos, D.L., 1977. Summary of nutrient and biomass data from two aspen sites in western United States, RN-INT-227. ed. U.S. Department of Agriculture, Forest Service, Intermountain Forest and Range Experiment Station, Ogden, UT.

Kaiser, K.E., Mcglynn, B.L., Emanuel, R.E., 2013. Ecohydrology of an outbreak: Mountain pine beetle impacts trees in drier landscape positions first. Ecohydrology 6, 444–454. doi:10.1002/eco.1286

Kashian, D.M., Romme, W.H., Tinker, D.B., Turner, M.G., Ryan, M.G., 2006. Carbon storage on landscapes with stand-replacing fires. Bioscience 56, 598–606. doi:10.1641/0006-3568(2006)56[598:CSOLWS]2.0.CO;2

Kautz, M., Meddens, A.J.H., Hall, R.J., Arneth, A., 2017. Biotic disturbances in Northern Hemisphere forests – a synthesis of recent data, uncertainties and implications for forest monitoring and modelling. Glob. Ecol. Biogeogr. 26, 533–552. doi:10.1111/geb.12558

Kayes, L.J., Tinker, D.B., 2012. Forest structure and regeneration following a mountain pine beetle epidemic in southeastern Wyoming. For. Ecol. Manage. 263, 57–66. doi:10.1016/j.foreco.2011.09.035

Keith, H., Lindenmayer, D., Macintosh, A., Mackey, B., 2015. Under What Circumstances Do Wood Products from Native Forests Benefit Climate Change Mitigation? PLoS One 10, e0139640. doi:10.1371/journal.pone.0139640

Kelsey, K.C., Neff, J.C., 2014. Estimates of aboveground biomass from texture analysis of

landsat imagery. Remote Sens. 6, 6407–6422. doi:10.3390/rs6076407

Kennedy, R.E., Yang, Z., Cohen, W.B., 2010. Detecting trends in forest disturbance and recovery using yearly Landsat time series: 1. LandTrendr — Temporal segmentation algorithms. Remote Sens. Environ. 114, 2897–2910. doi:10.1016/j.rse.2010.07.008

Kennedy, R.E., Yang, Z., Gorelick, N., Cohen, W.B., Healey, S., 2018. Implementation of the LandTrendr Algorithm on Google Earth Engine. Remote Sens. 10. doi:10.3390/rs10050691

Kershaw, J.A.J., Maguire, D.A., 1995. Crown structure in western hemlock, Douglas-fir, and grand fir in western Washington: trends in branch-level mass and leaf area. Can. J. For. Res. 25, 1897–1912.

Kim, Y., Yang, Z., Cohen, W.B., Pflugmacher, D., Lauver, C.L., Vankat, J.L., 2009. Distinguishing between live and dead standing tree biomass on the North Rim of Grand Canyon National Park, USA using small-footprint lidar data. Remote Sens. Environ. 113, 2499–2510. doi:10.1016/j.rse.2009.07.010

Klutsch, J.G., Negrón, J.F., Costello, S.L., Rhoades, C.C., West, D.R., Popp, J., Caissie, R., 2009. Stand characteristics and downed woody debris accumulations associated with a mountain pine beetle (Dendroctonus ponderosae Hopkins) outbreak in Colorado. For. Ecol. Manage. 258, 641–649. doi:10.1016/j.foreco.2009.04.034

Kumar, S., Stohlgren, T.J., Chong, G.W., 2006. Spatial heterogeneity influences native and nonnative plant species richness. Ecology 87, 3186–3199. doi:10.1890/0012-9658(2006)87[3186:SHINAN]2.0.CO;2

Kurz, W.A., Dymond, C.C., Stinson, G., Rampley, G.J., Neilson, E.T., Carroll, A.L., Ebata, T., Safranyik, L., 2008. Mountain pine beetle and forest carbon feedback to climate change. Nature 452, 987–990. doi:10.1038/nature06777

LANDFIRE, 2017. Existing Vegetation Cover Layer 1.4.0. U.S. Department of the Interior, Geological Survey.

LANDFIRE, 2008. Existing Vegetation Cover Layer 1.1.0.

LANDFIRE, 2001. Existing Vegetation Type Layer 1.0.5.

Landis, T.D., Mogren, E.W., 1975. Tree Strata Biomass of Subalpine Spruce-fir Stands in Southwestern Colorado. For. Sci. 21. doi:10.1093/forestscience/21.1.9

Liaw, A., Wiener, M., 2002. Classification and Regression by randomForest. R News 18–22.

Liu, H.Q., Huete, A., 1995. A Feedback Based Modificatoin of the NDVI to Minimize Canopy Background and Atmospheric Noise. IEEE Trans. Geosci. Remote Sens. 33, 457–465. doi:10.1109/TGRS.1995.8746027

Liu, K., Wang, J., Zeng, W., Song, J., 2017. Comparison and Evaluation of Three Methods for Estimating Forest Above Ground Biomass Using TM and GLAS Data. Remote Sens. 9. doi:10.3390/rs9040341

Long, J.A., Lawrence, R.L., 2016. Mapping Percent Tree Mortality Due to Mountain Pine Beetle Damage. For. Sci. 62, 1–11. doi:10.5849/forsci.15-046

López-Serrano, P.M., Corral-Rivas, J.J., Díaz-Varela, R.A., Álvarez-González, J.G., López-Sánchez, C.A., 2016. Evaluation of Radiometric and Atmospheric Correction Algorithms for Aboveground Forest Biomass Estimation Using Landsat 5 TM Data. Remote Sens. 8, 1–19. doi:10.3390/rs8050369

Loudermilk, E.L., Scheller, R.M., Weisberg, P.J., Yang, J., Dilts, T.E., Karam, S.L., Skinner, C., 2013. Carbon dynamics in the future forest: The importance of long-term successional legacy and climate-fire interactions. Glob. Chang. Biol. 19, 3502–3515. doi:10.1111/gcb.12310

Lu, D., 2005. Aboveground biomass estimation using Landsat TM data in the Brazilian Amazon. Int. J. Remote Sens. 26, 2509–2525. doi:10.1080/01431160500142145

Lu, D., Batistella, M., 2005. Exploring TM Image Texture and its Relationships with Biomass Estimation in Rondônia, Brazilian Amazon. Acta Amaz. 35, 249–257. doi:10.1590/S0044-59672005000200015

Mantgem, P.J. van, Stephenson, N.L., Byrne, J.C., Daniels, L.D., Franklin, J.F., Fulé, P.Z., Harmon, M.E., Larson, A.J., Smith, J.M., Taylor, A.H., Veblen, T.T., 2009. Widespread increase of tree mortality rates in the western United States. Science (80-.). 323, 521–524. doi:10.1126/science.1165000

Marzano, R., Garbarino, M., Marcolin, E., Pividori, M., Lingua, E., 2013. Deadwood anisotropic facilitation on seedling establishment after a stand-replacing wildfire in Aosta Valley (NW Italy). Ecol. Eng. 51, 117–122. doi:10.1016/j.ecoleng.2012.12.030

Masek, J.G., Vermote, E.F., Saleous, N.E., Wolfe, R., Hall, F.G., Huemmrich, K.F., Gao, F., Kutler, J., Lim, T., 2006. A Landsat Surface Reflectance Data Set for North America, 1990–2000. IEEE Geosci. Remote Sens. Lett. 3, 68–72. doi:10.1109/LGRS.2005.857030

Mathys, A., Black, T.A., Nesic, Z., Nishio, G., Brown, M., Spittlehouse, D.L., Fredeen, A.L., Bowler, R., Jassal, R.S., Grant, N.J., Burton, P.J., Trofymow, J.A., Meyer, G., 2013. Carbon balance of a partially harvested mixed conifer forest following mountain pine beetle attack and its comparison to a clear-cut. Biogeosciences 10, 5451–5463. doi:10.5194/bg-10-5451-2013

McCune, B., Keon, D., 2002. Equations for potential annual direct incident radiation and heat load. J. Veg. Sci. 13, 603–606. doi:10.1111/j.1654-1103.2002.tb02087.x

McDonald, J.H., 2014. Handbook of Biological Statistics, 3rd ed. Sparky House Publishing,

Baltimore, Maryland.

McFeeters, S.K., 1996. The use of the Normalized Difference Water Index (NDWI) in the delineation of open water features. Int. J. Remote Sens. 17, 1425–1432. doi:10.1080/01431169608948714

Mckinley, D.C., Ryan, M.G., Birdsey, R.A., Giardina, C.P., Harmon, M.E., Heath, L.S., Houghton, R.A., Jackson, R.B., Morrison, J.F., Murray, B.C., Pataki, D.E., Skog, K.E., 2011. A synthesis of current knowledge on forests and carbon storage in the United States. Ecol. Appl. 21, 1902–1924. doi:10.1890/10-0697.1

McRoberts, R.E., Næsset, E., Liknes, G.C., Chen, Q., Walters, B.F., Saatchi, S., Herold, M., 2019. Using a Finer Resolution Biomass Map to Assess the Accuracy of a Regional , Map-Based Estimate of Forest Biomass. Surv. Geophys. doi:10.1007/s10712-019-09507-1

Meddens, A., Hicke, J., Ferguson, C., 2012. Spatiotemporal patterns of observed bark beetle-caused tree mortality in British Columbia and the western United States. Ecol. Appl. 22, 1876–1891. doi:10.1890/11-1785.1

Meddens, A.J.H., Hicke, J.A., 2014. Spatial and temporal patterns of Landsat-based detection of tree mortality caused by a mountain pine beetle outbreak in Colorado, USA. For. Ecol. Manage. 322, 78–88. doi:10.1016/j.foreco.2014.02.037

Meddens, A.J.H., Hicke, J.A., Vierling, L.A., Hudak, A.T., 2013. Evaluating methods to detect bark beetle-caused tree mortality using single-date and multi-date Landsat imagery. Remote Sens. Environ. 132, 49–58. doi:10.1016/j.rse.2013.01.002

Meigs, G.W., Campbell, J.L., Zald, H.S., Bailey, J.D., Shaw, D.C., Kennedy, R.E., 2015. Does wildfire likelihood increase following insect outbreaks in conifer forests? Ecosphere 6, 1–24.

Meigs, G.W., Kennedy, R.E., Cohen, W.B., 2011. A Landsat time series approach to characterize bark beetle and defoliator impacts on tree mortality and surface fuels in conifer forests. Remote Sens. Environ. 115, 3707–3718. doi:10.1016/j.rse.2011.09.009

Meigs, G.W., Kennedy, R.E., Gray, A.N., Gregory, M.J., 2015. Spatiotemporal dynamics of recent mountain pine beetle and western spruce budworm outbreaks across the Pacific Northwest Region, USA. For. Ecol. Manage. 339, 71–86. doi:10.1016/j.foreco.2014.11.030

Miles, P.D., Smith, W.B., 2009. Specific Gravity and Other Properties of Wood and Bark for 156 Tree Species Found in North America, RN-NRS-38. ed. U.S. Department of Agriculture, Forest Service, Northern Research Station, Newtown Square, PA.

Mitchard, E.T.A., Feldpausch, T.R., Brienen, R.J.W., Lopez-Gonzalez, G., Monteagudo, A., Baker, T.R., Lewis, S.L., Lloyd, J., Quesada, C.A., Gloor, M., ter Steege, H., Meir, P., Alvarez, E., Araujo-Murakami, A., Aragão, L.E.O.C., Arroyo, L., Aymard, G., Banki, O., Bonal, D., Brown, S., Brown, F.I., Cerón, C.E., Chama Moscoso, V., Chave, J., Comiskey, J.A., Cornejo, F., Corrales Medina, M., Da Costa, L., Costa, F.R.C., Di Fiore, A., Domingues, T.F., Erwin, T.L., Frederickson, T., Higuchi, N., Honorio Coronado, E.N., Killeen, T.J., Laurance, W.F., Levis, C., Magnusson, W.E., Marimon, B.S., Marimon Junior, B.H., Mendoza Polo, I., Mishra, P., Nascimento, M.T., Neill, D., Núñez Vargas, M.P., Palacios, W.A., Parada, A., Pardo Molina, G., Peña-Claros, M., Pitman, N., Peres, C.A., Poorter, L., Prieto, A., Ramirez-Angulo, H., Restrepo Correa, Z., Roopsind, A., Roucoux, K.H., Rudas, A., Salomão, R.P., Schietti, J., Silveira, M., de Souza, P.F., Steininger, M.K., Stropp, J., Terborgh, J., Thomas, R., Toledo, M., Torres-Lezama, A., Van Andel, T.R., van der Heijden, G.M.F., Vieira, I.C.G., Vieira, S., Vilanova-Torre, E., Vos, V.A., Wang, O., Zartman, C.E., Malhi, Y., Phillips, O.L., 2014. Markedly divergent

estimates of Amazon forest carbon density from ground plots and satellites. Glob. Ecol. Biogeogr. 23, 935–946. doi:10.1111/geb.12168

Montagu, K.D., Düttmer, K., Barton, C.V.M., Cowie, A.L., 2005. Developing general allometric relationships for regional estimates of carbon sequestration—an example using Eucalyptus pilularis from seven contrasting sites. For. Ecol. Manage. 204, 113–127. doi:10.1016/j.foreco.2004.09.003

Moore, I.D., Grayson, R.B., Ladson, A.R., 1991. Digital terrain modelling: a review of hydrological, geomorphological, and biological applications. Hydrol. Process. 5, 3–30. doi:10.1002/hyp.3360050103

Nay, S.M., Bormann, B.T., 2014. Site-Specific Douglas-Fir Biomass Equations from the Siskiyou Mountains, Oregon, Compared with Others from the Pacific Northwest. For. Sci. 60, 1140–1147. doi:10.5849/forsci.13-084

Nelson, K.N., Rocca, M.E., Diskin, M., Aoki, C.F., Romme, W.H., 2014. Predictors of bark beetle activity and scale-dependent spatial heterogeneity change during the course of an outbreak in a subalpine forest. Landsc. Ecol. 29, 97–109. doi:10.1007/s10980-013-9954-1

Nemani, R., Pierce, L., Running, S., Band, L., 1993. Forest ecosystem processes at the watershed scale: sensitivity to remotely-sensed Leaf Area Index estimates. Int. J. Remote Sens. 14, 2519–2534. doi:10.1080/01431169308904290

O'Connell, B.M., LaPoint, E.B., Turner, J.A., Ridley, T., Pugh, S.A., Wilson, A.M., Wadell, K.L., Conkling, B.L., 2015. The Forest Inventory and Analysis Database: Database Description and User Guide for Phase 2.

Ohmann, J.L., Gregory, M.J., Roberts, H.M., 2014. Scale considerations for integrating forest inventory plot data and satellite image data for regional forest mapping. Remote Sens.

Environ. 151, 3–15. doi:10.1016/j.rse.2013.08.048

Parresol, B.R., 2001. Additivity of nonlinear biomass equations. Can. J. For. Res. 31, 865–878. doi:10.1139/x00-202

Patriquin, M.N., Wellstead, A.M., White, W.A., 2007. Beetles, trees, and people: Regional economic impact sensitivity and policy considerations related to the mountain pine beetle infestation in British Columbia, Canada. For. Policy Econ. 9, 938–946. doi:10.1016/j.forpol.2006.08.002

Peichl, M., Arain, M.A., 2007. Allometry and partitioning of above- and belowground tree biomass in an age-sequence of white pine forests. For. Ecol. Manage. 253, 68–80. doi:10.1016/j.foreco.2007.07.003

Pelz, K.A., Smith, F.W., 2012. Thirty year change in lodgepole and lodgepole/mixed conifer forest structure following 1980s mountain pine beetle outbreak in western Colorado, USA. For. Ecol. Manage. 280, 93–102. doi:10.1016/j.foreco.2012.05.032

Perovich, C., Sibold, J.S., 2016. Forest composition change after a mountain pine beetle outbreak, Rocky Mountain National Park, CO, USA. For. Ecol. Manage. 366, 184–192. doi:10.1016/j.foreco.2016.02.010

Pfeifer, E.M., Hicke, J. a., Meddens, A.J.H., 2011. Observations and modeling of aboveground tree carbon stocks and fluxes following a bark beetle outbreak in the western United States. Glob. Chang. Biol. 17, 339–350. doi:10.1111/j.1365-2486.2010.02226.x

Pflugmacher, D., Cohen, W.B., Kennedy, R.E., 2012. Using Landsat-derived disturbance history (1972-2010) to predict current forest structure. Remote Sens. Environ. 122, 146–165. doi:10.1016/j.rse.2011.09.025

Pflugmacher, D., Cohen, W.B., Kennedy, R.E., Yang, Z., 2014. Using Landsat-derived

disturbance and recovery history and lidar to map forest biomass dynamics. Remote Sens. Environ. 151, 124–137. doi:10.1016/j.rse.2013.05.033

Phalla, T., Ota, T., Mizoue, N., Kajisa, T., Yoshida, S., Vuthy, M., Heng, S., 2018. The Importance of Tree Height in Estimating Individual Tree Biomass while Considering Errors in Measurements and Allometric Models. AGRIVITA J. Agric. Sci. 40, 131–140. doi:10.17503/agrivita.v40i1.1730

Phillips, J., Duque, Á., Scott, C., Wayson, C., Galindo, G., Cabrera, E., Chave, J., Peña, M., Álvarez, E., Cárdenas, D., Duivenvoorden, J., Hildebrand, P., Stevenson, P., Ramírez, S., Yepes, A., 2016. Live aboveground carbon stocks in natural forests of Colombia. For. Ecol. Manage. 374, 119–128. doi:10.1016/j.foreco.2016.05.009

Poudel, K.P., Temesgen, H., 2016. Methods for estimating aboveground biomass and its components for Douglas-fir and lodgepole pine trees. Can. J. For. Res. 46, 77–87. doi:10.1139/cjfr-2015-0256

Poudel, K.P., Temesgen, H., Gray, A.N., 2015. Evaluation of sampling strategies to estimate crown biomass. For. Ecosyst. 2. doi:10.1186/s40663-014-0025-0

Powell, S.L., Cohen, W.B., Healey, S.P., Kennedy, R.E., Moisen, G.G., Pierce, K.B., Ohmann, J.L., 2010. Quantification of live aboveground forest biomass dynamics with Landsat time-series and field inventory data: A comparison of empirical modeling approaches. Remote Sens. Environ. 114, 1053–1068. doi:10.1016/j.rse.2009.12.018

PRISM, C.G., 2004. Oregon State University [WWW Document]. URL http://prism.oregonstate.edu

Pugh, E., Small, E., 2012. The impact of pine beetle infestation on snow accumulation and melt in the headwaters of the colorado river. Ecohydrology 5, 467–477. doi:10.1002/eco.239

Putman, E.B., Popescu, S.C., Eriksson, M., Zhou, T., Klockow, P., Vogel, J., Moore, G.W., 2018. Detecting and quantifying standing dead tree structural loss with reconstructed tree models using voxelized terrestrial lidar data. Remote Sens. Environ. 209, 52–65. doi:10.1016/j.rse.2018.02.028

Qi, J., Chehbouni, A., Huete, A.R., Kerr, Y.H., Sorooshian, S., 1994. A Modified Soil Adjusted Vegetation Index. Remote Sens. Environ. 48, 119–126. doi:10.1016/0034-4257(94)90134-1

Quegan, S., Le, T., Chave, J., Dall, J., Exbrayat, J., Ho, D., Minh, T., Lomas, M., Mariotti, M., Alessandro, D., Paillou, P., Papathanassiou, K., Rocca, F., Saatchi, S., Scipal, K., Shugart, H., Smallman, T.L., Soja, M.J., Tebaldini, S., Ulander, L., Villard, L., Williams, M., 2019. The European Space Agency BIOMASS mission: Measuring forest aboveground biomass from space. Remote Sens. Environ. 227, 44–60. doi:10.1016/j.rse.2019.03.032

R Core Team, 2018. R Statistical Software.

Radtke, P.J., Walker, D.M., Weiskittel, A.R., Frank, J., Coulston, J.W., Westfall, J.A., 2015. Legacy tree data: A national database of detailed tree measurements for volume, weight, and physical properties. PNW-GTR-931, in: New Directions in Inventory Techniques & Applications Forest Inventory & Analysis (FIA) Symposium 2015. U.S. Department of Agriculture, Forest Service, Pacific Northwest Reserach Station, pp. 25–30.

Raffa, K.F., Aukema, B.H., Bentz, B.J., Carroll, A.L., Hicke, J.A., Turner, M.G., Romme, W.H., 2008. Cross-scale Drivers of Natural Disturbances Prone to Anthropogenic Amplification: The Dynamics of Bark Beetle Eruptions. Bioscience 58, 501–517. doi:10.1641/B580607

Raile, G.K., 1982. Estimating stump volume, RP-NC-224. ed. U.S. Department of Agriculture, Forest Service, North Central Forest Experiment Station, St. Paul, MN.

Raymond, C.L., Healey, S., Peduzzi, A., Patterson, P., 2015. Representative regional models of

post-disturbance forest carbon accumulation: Integrating inventory data and a growth and yield model. For. Ecol. Manage. 336, 21–34. doi:10.1016/j.foreco.2014.09.038

Rebain, S.A., Reinhardt, E.D., Crookston, N.L., Beukema, S.J., Kurz, W.A., Greenough, J.A., Robinson, D.C.E., Lutes, D.C., 2010. The Fire and Fuels Extension to the Forest Vegetation Simulator: Updated Model Documentation. U.S. Department of Agriculture, Forest Service, Forest Management Service Center, Fort Collins, CO.

Reid, C.P.P., 1974. Effects of clearcutting on nutrient cycling in lodgepole pine forests. Colorado State University, Fort Collins, CO.

Reu, J. De, Bourgeois, J., Bats, M., Zwertvaegher, A., Gelorini, V., Smedt, P. De, Chu, W., Antrop, M., Maeyer, P. De, Finke, P., Meirvenne, M. Van, Verniers, J., Crombé, P., 2013. Application of the topographic position index to heterogeneous landscapes. Geomorphology 186, 39–49. doi:10.1016/j.geomorph.2012.12.015

Rhoades, C.C., Hubbard, R.M., Elder, K., 2016. A Decade of Streamwater Nitrogen and Forest Dynamics after a Mountain Pine Beetle Outbreak at the Fraser Experimental Forest, Colorado. Ecosystems 1–13. doi:10.1007/s10021-016-0027-6

Rhoades, C.C., Hubbard, R.M., Hood, P.R., Starr, B.J., Tinker, D.B., Elder, K., 2020. Snagfall the first decade after severe bark beetle infestation of high-elevation forests in Colorado, USA. Ecol. Appl. 30, 1–13. doi:10.1002/eap.2059

Rhoades, C.C., McCutchan, J.H., Cooper, L. a, Clow, D., Detmer, T.M., Briggs, J.S., Stednick, J.D., Veblen, T.T., Ertz, R.M., Likens, G.E., Lewis, W.M., 2013. Biogeochemistry of beetle-killed forests: explaining a weak nitrate response. Proc. Natl. Acad. Sci. 110, 1756–60. doi:10.1073/pnas.1221029110

Riffell, S., Verschuyl, J., Miller, D., Wigley, T.B., 2011. Biofuel harvests, coarse woody debris,

and biodiversity – A meta-analysis. For. Ecol. Manage. 261, 878–887. doi:10.1016/j.foreco.2010.12.021

Riley, S.J., DeGloria, S.D., Elliot, R., 1999. A Terrain Ruggedness Index That Quantifies Topographic Heterogeneity. Intermt. J. Sci. 5, 23–27.

Rock, B.N., Williams, D.L., Vogelmann, J.E., 1985. Field and airborne spectral characterization of suspected damage in red spruce (Picea rubens) from Vermont, in: Machine Processing of Remotely Sensed Data Symposium. West Lafayette, Indiana, pp. 71–81.

Rouse, J.W., Haas, R.H., Schell, J.A., Deering, D.W., 1974. Monitoring vegetation systems in the Great Plains with ERTS. NASA Spec. Publ. 351, 309–317.

Russell, M.B., Fraver, S., Aakala, T., Gove, J.H., Woodall, C.W., Amato, A.W.D., Ducey, M.J., 2015. Quantifying carbon stores and decomposition in dead wood: A review. For. Ecol. Manage. 350, 107–128. doi:10.1016/j.foreco.2015.04.033

Rutishauser, E., Noor'an, F., Laumonier, Y., Halperin, J., Rufi'ie, Hergoualch, K., Verchot, L., 2013. Generic allometric models including height best estimate forest biomass and carbon stocks in Indonesia. For. Ecol. Manage. 307, 219–225. doi:10.1016/j.foreco.2013.07.013

Sánchez Meador, A., 2007. Legacy Tree Data [WWW Document]. URL Legacytreedata.org (accessed 2.19.19).

SAS Institute Inc, ., 2017. SAS OnDemand.

Schoennagel, T., Veblen, T.T., Negron, J.F., Smith, J.M., 2012. Effects of mountain pine beetle on fuels and expected fire behavior in lodgepole pine forests, Colorado, USA. PLoS One 7. doi:10.1371/journal.pone.0030002

Schulze, E.D., Körner, C., Law, B.E., Haberl, H., Luyssaert, S., 2012. Large-scale bioenergy from additional harvest of forest biomass is neither sustainable nor greenhouse gas neutral.

GCB Bioenergy 4, 611–616. doi:10.1111/j.1757-1707.2012.01169.x

Scott, J.H., Reinhardt, E.D., 2001. Assessing Crown Fire Potential by Linking Models of Surface and Crown Fire Behavior, Research Paper RMRS-RP-29. Fort Collins, CO.

Senf, C., Seidl, R., Hostert, P., 2017. Remote sensing of forest insect disturbances: current state and future directions. Int. J. Appl. Earth Obs. Geoinf. 60, 49–60. doi:10.1016/j.jag.2017.04.004

Shore, T., Safranyik, L., 1992. Susceptibility and risk rating systems for the mountain pine beetle in lodgepole pine stands BC-X-336, 12.

Sidder, A.M., Kumar, S., Laituri, M., Sibold, J.S., 2016. Using spatiotemporal correlative niche models for evaluating the effects of climate change on mountain pine beetle. Ecography (Cop.). 7, 1–22. doi:e01396. 10.1002/ecs2.1396

Six, D.L., Vergobbi, C., Cutter, M., 2018. Are Survivors Different? Genetic-Based Selection of Trees by Mountain Pine Beetle During a Climate Change-Driven Outbreak in a High-Elevation Pine Forest. Front. Plant Sci. 9, 1–11. doi:10.3389/fpls.2018.00993

Smithwick, E.A.H., Harmon, M.E., Domingo, J.B., 2007. Changing temporal patterns of forest carbon stores and net ecosystem carbon balance: The stand to landscape transformation. Landsc. Ecol. 22, 77–94. doi:10.1007/s10980-006-9006-1

Stovall, A.E.L., Anderson-Teixeira, K.J., Shugart, H.H., 2018a. Assessing terrestrial laser scanning for developing non-destructive biomass allometry. For. Ecol. Manage. 427, 217–229. doi:10.1016/j.foreco.2018.06.004

Stovall, A.E.L., Anderson-Teixeira, K.J., Shugart, H.H., 2018b. Terrestrial LiDAR-derived non-destructive woody biomass estimates for 10 hardwood species in Virginia. Data Br. 19, 1560–1569. doi:10.1016/j.dib.2018.06.046

Stovall, A.E.L., Shugart, H.H., 2018. Improved Biomass Calibration and Validation With Terrestrial LiDAR: Implications for Future LiDAR and SAR Missions. IEEE J. Sel. Top. Appl. Earth Obs. Remote Sens. 11, 3527–3537. doi:10.1109/JSTARS.2018.2803110

Stovall, A.E.L., Vorster, A.G., Anderson, R.S., Evangelista, P.H., Shugart, H.H., 2017. Non-destructive aboveground biomass estimation of coniferous trees using terrestrial LiDAR. Remote Sens. Environ. 200, 31–42. doi:10.1016/j.rse.2017.08.013

Swetnam, T.L., Brooks, P.D., Barnard, H.R., Harpold, A.A., Gallo, E.L., 2017. Topographically driven differences in energy and water constrain climatic control on forest carbon sequestration. Ecosphere 8. doi:10.1002/ecs2.1797

Taylor, S.L., Maclean, D.A., 2008. Validation of Spruce Budworm Outbreak History Developed from Aerial Sketch Mapping of Defoliation in New Brunswick. North. J. Appl. For. 25, 139–145. doi:10.1093/njaf/25.3.139

Temesgen, H., Monleon, V., Weiskittel, A., Wilson, D., 2011. Sampling strategies for efficient estimation of tree foliage biomass. For. Sci. 57, 153–163.

Temperli, C., Veblen, T.T., Hart, S.J., Kulakowski, D., Tepley, A.J., 2015. Interactions among spruce beetle disturbance, climate change and forest dynamics captured by a forest landscape model. Ecosphere 6, 1–20.

Ter-mikaelian, M.T., Colombo, S.J., Chen, J., 2015. The Burning Question: Does Forest Bioenergy Reduce Carbon Emissions ? A Review of Common Misconceptions about Forest Carbon Accounting. J. For. 113, 57–68. doi:10.5849/jof.14-016

Ter-Mikaelian, M.T., Korzukhin, M.D., 1997. Biomass equations for sixty-five North American tree species. For. Ecol. Manage. 97, 1–24. doi:10.1016/S0378-1127(97)00019-4

Tinkham, W.T., Mahoney, P.R., Hudak, A.T., Domke, G.M., Falkowski, M.J., Woodall, C.W.,

Smith, A.M.S., 2018. Applications of the United States Forest Inventory and Analysis dataset: a review and future directions. Can. J. For. Res. 48, 1251–1268.

Tossey, G.B., 1982. Biomass Equations of Small Trees of Four Rocky Mountain Species with Reference to Habitat. Colorado State University, Fort Collins, CO.

Turner, M.G., 2010. Disturbance and landscape dynamics in a changing world. Ecology 91, 2833–2849. doi:doi:10.1890/10-0097.1

Turner, M.G., Romme, W.H., Gardner, R.H., 1999. Prefire Heterogeneity, Fire Severity, and Early Postfire Plant Reestablishment in Subalpine Forests of Yellowstone National Park, Wyoming. Int. J. Wi 9, 21–36. doi:10.1071/WF99003

UNFCCC, 1992. United Nations Framework Convention on Climate Change.

van Breugel, M., Ransijn, J., Craven, D., Bongers, F., Hall, J.S., 2011. Estimating carbon stock in secondary forests: Decisions and uncertainties associated with allometric biomass models. For. Ecol. Manage. 262, 1648–1657. doi:10.1016/j.foreco.2011.07.018

Vermote, E., Justice, C., Claverie, M., Franch, B., 2016. Preliminary analysis of the performance of the Landsat 8/OLI land surface reflectance product. Remote Sens. Environ. 185, 46–56. doi:10.1016/j.rse.2016.04.008

Vogeler, J., Braaten, J., Slesak, R., Falkowski, M., 2018. Extracting the full value of the Landsat archive: Inter-sensor harmonization for the mapping of Minnesota forest canopy cover (1973–2015). Remote Sens. Environ. 209, 363–374. doi:10.1016/j.rse.2018.02.046

Vogeler, J.C., Slesak, R.A., Fekety, P.A., Falkowski, M.J., 2020. Characterizing over Four Decades of Forest Disturbance in Minnesota, USA. Forests 11. doi:10.3390/f11030362

Volkova, L., Roxburgh, S.H., Weston, C.J., Benyon, R.G., Sullivan, A.L., Polglase, P.J., 2018. Importance of disturbance history on Net Primary Productivity in the world's most

productive forests and implications for the global carbon cycle. Glob. Chang. Biol. 0–2. doi:10.1111/gcb.14309

Vorster, A.G., Evangelista, P.H., Stohlgren, T.J., Kumar, S., Rhoades, C.C., Hubbard, R.M., Cheng, A.S., Elder, K., 2017. Severity of a mountain pine beetle outbreak across a range of stand conditions in Fraser Experimental Forest, Colorado, United States. For. Ecol. Manage. 389, 116–126. doi:10.1016/j.foreco.2016.12.021

Vorster, A.G., Evangelista, P.H., Stovall, A.E.L., Ex, S., 2020. Variability and uncertainty in forest biomass estimates from the tree to landscape scale: the role of allometric equations. Carbon Balance Manag. 15. doi:10.1186/s13021-020-00143-6

Vorster, A.G., Woodward, B., Young, N., Girma, R., Evangelista, P.H., LaRoe, J., Filippelli, S., n.d. Fusing satellite monitoring with aerial forest health surveys to characterize lodgepole pine forest mortality due to bark beetle outbreaks across the Intermountain West, USA. Prep.

Walter, J.A., Platt, R. V., 2013. Multi-temporal analysis reveals that predictors of mountain pine beetle infestation change during outbreak cycles. For. Ecol. Manage. 302, 308–318. doi:10.1016/j.foreco.2013.03.038

Wang, T., Hamann, A., Spittlehouse, D., Carroll, C., 2016. Locally downscaled and spatially customizable climate data for historical and future periods for North America. PLoS One 11. doi:10.1371/journal.pone.0156720

Weiskittel, A.R., MacFarlane, D.W., Radtke, P.J., Affleck, D.L.R., Temesgen, H., Woodall, C.W., Westfall, J.A., Coulston, J.W., 2015. A Call to Improve Methods for Estimating Tree Biomass for Regional and National Assessments. J. For. 113, 414–424. doi:10.5849/jof.14-091

West, G.B., Brown, J.H., Enquist, B.J., 1999. A general model for the structure and allometry of plant vascular systems. Nature 400, 664–667.

Westerling, A.L., 2016. Increasing western US forest wildfire activity: sensitivity to changes in the timing of spring. Philos. Trans. R. Soc. B Biol. Sci. 371, 20160373. doi:10.1098/rstb.2016.0373

Westerling, A.L., Hidalgo, H.G., Cayan, D.R., Swetnam, T.W., 2006. Warming and earlier spring increase western U.S. forest wildfire activity. Science 313, 940–943. doi:10.1126/science.1128834

Westerling, A.L., Turner, M.G., Smithwick, E.A.H., Romme, W.H., Ryan, M.G., 2011. Continued warming could transform Greater Yellowstone fire regimes by mid-21st century. Proc. Natl. Acad. Sci. 108, 13165–13170. doi:10.1073/pnas.1110199108

White, J.C., Coops, N.C., Hilker, T., Wulder, M.A., Carroll, A.L., 2007. Detecting mountain pine beetle red attack damage with EO-1 Hyperion moisture indices. Int. J. Remote Sens. 28, 2111–2121. doi:10.1080/01431160600944028

Williams, A.P., Allen, C.D., Macalady, A.K., Griffin, D., Woodhouse, C.A., Meko, D.M., Swetnam, T.W., Rauscher, S.A., Seager, R., Grissino-mayer, H.D., Dean, J.S., Cook, E.R., Gangodagamage, C., Cai, M., Mcdowell, N.G., 2013. Temperature as a potent driver of regional forest drought stress and tree mortality. Nat. Clim. Chang. 3, 292–297. doi:10.1038/nclimate1693

Williams, C.A., Gu, H., MacLean, R., Masek, J.G., Collatz, G.J., 2016. Disturbance and the carbon balance of US forests: A quantitative review of impacts from harvests, fires, insects, and droughts. Glob. Planet. Change 143, 66–80. doi:10.1016/j.gloplacha.2016.06.002

Woodall, C.W., Domke, G.M., MacFarlane, D.W., Oswalt, C.M., 2012. Comparing field-and

model-based standing dead tree carbon stock estimates across forests of the US. Forestry 85, 125–133. doi:10.1093/forestry/cpr065

Woodall, C.W., Heath, L.S., Domke, G.M., Nichols, M.C., 2011. Methods and Equations for Estimating Aboveground Volume, Biomass, and Carbon for Trees in the U.S. Forest Inventory, 2010, GTR NRS-88. ed. U.S. Department of Agriculture, Forest Service, Northern Research Station, Newtown Square, PA.

Woodall, C.W., Monleon, V.J., Fraver, S., Russell, M.B., Hat, M.H., Campbell, J.L., Domke, G.M., 2019. The downed and dead wood inventory of forests in the United States. Sci. Data 6, 1–13. doi:10.1038/sdata.2018.303

Woodward, B., Engelstad, P., Vorster, A., Beddow, C., Krail, S., Vashisht, A., Evangelista, P., 2017. Forest harvest dataset for northern Colorado Rocky Mountains (1984–2015) generated from a Landsat time series and existing forest harvest records. Data Br. 15, 724–727. doi:10.1016/j.dib.2017.10.030

Woodward, B.D., Evangelista, P.H., Vorster, A.G., 2018. Mapping progression and severity of a Southern Colorado spruce beetle outbreak using calibrated image composites. Forests 9, 1–14. doi:10.3390/f9060336

Wulder, M.A., Dymond, C.C., White, J.C., Leckie, D.G., Carroll, A.L., 2006. Surveying mountain pine beetle damage of forests: A review of remote sensing opportunities. For. Ecol. Manage. 221, 27–41. doi:10.1016/j.foreco.2005.09.021

Wulder, M.A., White, J.C., Gillis, M.D., Walsworth, N., Hansen, M.C., Potapov, P., 2010. Multiscale satellite and spatial information and analysis framework in support of a large-area forest monitoring and inventory update. Environ. Monit. Assess. 170, 417–433. doi:10.1007/s10661-009-1243-8

Yang, B., Xue, W., Yu, S., Zhou, J., Zhang, W., 2019. Effects of Stand Age on Biomass Allocation and Allometry of Quercus Acutissima in the Central Loess Plateau of China. Forests 10. doi:10.3390/f10010041

Young, N.E., Anderson, R.S., Chignell, S.M., Vorster, A.G., Lawrence, R., Evangelista, P.H., 2017. A survival guide to Landsat preprocessing. Ecology 98, 920–932. doi:10.1002/ecy.1730

Zanchi, G., Pena, N., Bird, N., 2012. Is woody bioenergy carbon neutral? A comparative assessment of emissions from consumption of woody bioenergy and fossil fuel. Bioenergy 4, 761–772. doi:10.1111/j.1757-1707.2011.01149.x

Zevenbergen, L.W., Thorne, C.R., 1987. Quantitative analysis of land surface topography. Earth Surf. Process. Landforms 12, 47–56. doi:10.1002/esp.3290120107

Zhao, F., Guo, Q., Kelly, M., 2012. Allometric equation choice impacts lidar-based forest biomass estimates: A case study from the Sierra National Forest, CA. Agric. For. Meteorol. 165, 64–72. doi:10.1016/j.agrformet.2012.05.019

Zhao, P., Lu, D., Wang, G., Wu, C., Huang, Y., Yu, S., 2016. Examining Spectral Reflectance Saturation in Landsat Imagery and Corresponding Solutions to Improve Forest Aboveground Biomass Estimation. Remote Sens. 8. doi:10.3390/rs8060469

Zolkos, S.G., Goetz, S.J., Dubayah, R., 2013. A meta-analysis of terrestrial aboveground biomass estimation using lidar remote sensing. Remote Sens. Environ. 128, 289–298. doi:10.1016/j.rse.2012.10.017

Zvoleff, A., 2016. glcm: Calculate Textures from Grey-Level Co-Occurrence Matrices (GLCMs).

APPENDIX

Chapter 1 Appendices

Appendix 1.1: Additional information for the methods

Tables and text detailing additional information about methods, such as destructive sampling, component calculation, branch wood and foliage component estimation, predictor variables used for biomass mapping, and a comparison of trees from the various data sources in this study.

Additional details about the methods

Destructive Sampling

I collected size and mass measurements in the field for the bole, bark, crown (defined as the portion of the tree between the first live branch and the 10.2 cm top), and top of the tree (everything above the 10.2 cm top) using digital scales (OHAUS Valor 1000 model V11P6 precision scale, maximum 6 kg, least count 0.001 kg; Tree LVS 700 large scale, maximum 320 kg, least count 0.1 kg). Bole, bark, branch wood, and branch foliage subsamples were collected and oven dried at 105°C (Poudel and Temesgen, 2016) to determine moisture content and component biomass. Disks cut from the top of 1.2 m bole segments served as the bole and bark subsamples. I measured the weight and dimensions of the disk, with and without bark. A 10 cm strip of bark was measured, weighed, and kept for oven-drying. Six live branches—two randomly selected from the lower, middle, and upper third of the crown—were collected from each tree as wood and foliage subsamples. For small trees with fewer than six branches below the 10.2 cm top, I randomly selected four subsample branches from the 15 lowest branches. Only a portion of branch wood was kept for branches >5 kg to expedite oven drying, but all foliage

was retained. Dead branches were also subsampled for moisture content (n = 10 lodgepole pine, n = 12 ponderosa pine, n = 14 Douglas-fir).

Component Biomass Calculation

Bole and bark component biomass were calculated using the disks and 1.2 m bole segments. I calculated the bark mass per unit bole surface area from the disks, and then averaged across all disks for an individual tree. This average for each tree was multiplied by the surface area of each segment and summed to obtain bark wet mass. Bole wood wet mass was calculated by subtracting the bark wet mass from the field-measured four-foot segments. The percentage moisture content from the bark subsamples and disks were applied to obtain bark dry mass and bole wood dry mass, respectively. The disk moisture content was also used to calculate the dry mass of the top main stem.

I developed regression equations for each species to estimate branch foliage and wood mass for each crown branch (Chung et al., 2017; Kershaw and Maguire, 1995; Poudel and Temesgen, 2016; Temesgen et al., 2011). The first step was to predict the length for the two thirds of the crown branches where length was not measured so that length could be considered as a predictor variable when estimating branch foliage and wood mass. I generated a multiple regression equation for each species to predict branch length considering the following predictor variables in linear and log-linear equations: branch diameter, DBH, stem height at base of branch, tree height, relative branch depth (Poudel et al., 2015), crown width at widest axis, and height to first branch. Equations expected to perform well were developed a priori (Table A1.1.1) and were then modified based on model evaluation statistics and reduction of predictor variables correlated by 0.70 or more (Dormann et al., 2013). Equations were selected that performed best based on adjusted R^2 and root mean square error (RMSE) and that met

assumptions of residual normality and homoscedasticity. The same method used to select the branch length equations was used to determine the best equation for branch foliage and branch wood wet mass. I considered the same predictor variables with the addition of branch length. The top models (Table A1.1.2) were used to estimate branch foliage and branch wood wet mass for each branch of each destructively sampled tree. To account for potential downward bias when back-transforming the log transformed model predictions, a correction factor can be applied (Baskerville, 1972). However, this correction factor can also introduce bias, particularly with low sample size equations. So, as suggested by other studies (Jenkins et al., 2003), I reported but did not apply the correction factor (Table A1.1.3).

These estimates of branch wood and foliage mass for each crown branch served as the basis for calculating the branch and foliage component of the whole tree. I generated a ratio of wood to crown wet mass and foliage to crown wet mass for each tree using the sum of branch foliage and wood from the branch-by-branch estimation. These ratios were applied to crown and top branch mass, then the water weights were subtracted using a tree-specific water content for each component. For trees too small to have crown branches, I calculated branch and foliage ratios from the subsampled branches. This approach of using the wood and foliage ratios ensured that the sum of wood and foliage biomass equaled the total crown and top mass measured in the field. Dry top main stem mass and dry dead branch mass were then added to the branch wood component.

Allometric Equation Calculation

While including height as a predictor variable with DBH can increase the accuracy of allometric equations, I used DBH as the only predictor variable in these allometric equations for several reasons. Diameter at breast height is more commonly and accurately measured than tree

height, so using DBH only makes the equations more widely applicable and less prone to measurement error (Phalla et al., 2018). Additionally, the small sample size of destructively sampled trees did not capture the variation in tree height for trees with similar diameters.

Details about FIA-CRM Component Biomass Calculation

Bark volume is estimated as a percentage of bole volume and is converted to bark biomass using specific gravity. Biomass of the entire tree, merchantable bole, and belowground biomass is calculated using equations from Jenkins et al. (2003). Then, equations from Raile (Raile, 1982) are used to calculate stump volume. Top biomass is calculated as the difference between total aboveground biomass and all other components. Lastly, an adjustment factor calculated as the ratio of bole biomass between the regional volume based-estimate and the Jenkins et al. (2003) estimate is applied to adjust the biomass of all tree components. The FIA-CRM equations do not estimate foliage biomass. Sapling (trees < 12.7 cm [5.0 inches] DBH) biomass is calculated as the product of total aboveground biomass, excluding foliage, from Jenkins et al. (2003) and a sapling adjustment factor found in Heath et al. (2009). This same method is used for estimating aboveground biomass of woodland species (i.e., trees where diameter is measured at root collar) that are less than 12.7 cm (5.0 inches). For woodland trees greater than or equal to 12.7 cm (5 inches), biomass is calculated from volume just as it is for tree boles, and component biomass is not calculated.

Predictor Variables for Biomass Mapping

Texture statistics were generated from grey-level co-occurrence matrices using the glcm package in R (Zvoleff, 2016). I made the following texture metrics for ETM+ bands 1, 2, 3, 4, 5, and 7 on a 3x3, 5x5, 7x7, 9x9, and 11x11 window and a (1,1) shift: mean, variance, homogeneity, contrast, dissimilarity, entropy, second moment, and correlation. Some of these

texture measures have shown promise in other studies relating Landsat imagery to forest biomass (Kelsey and Neff, 2014; Lu, 2005; Lu and Batistella, 2005; Zhao et al., 2016). I generated each combination of band, window size, and texture measures because the relationship between texture and forest biomass varies with many factors including vegetation type, imagery, and window size.

I generated additional topographic, geomorphometric, and climatic predictor variables that correlate with tree species and biomass distributions (Evans and Cushman, 2009; Swetnam et al., 2017). Elevation, slope, northness, and eastness were derived from the National Elevation Dataset (Gesch et al., 2002; Gesch, 2007; Kumar et al., 2006). Using the Spatial Analyst (Environmental Systems Research Institute, 2017) and Geomorphometry and Gradient Metrics Toolboxes (Evans et al., 2014), I also generated the compound topographic index, heat load index, curvature, and slope position and roughness on a 3x3, 6x6, 9x9, 12x12, 15x15, 21x21, and 27x27 window size. Climate normals (1961 – 1990) were downscaled to a 30 m x 30 m spatial resolution to match the scale of other rasters (Wang et al., 2016).

Variable Selection Using Random Forest (VSURF)

Variable Selection Using Random Forest (VSURF) was used to select variables for modeling biomass across the landscape (Genuer et al., 2015). VSURF first ranks all variables by the variability in their variable importance score across 50 random forest runs. More important variables have higher variability than less important variables. Variables falling below an importance threshold are removed. An “interpretation” set of variables is next determined from this reduced set of variables by running 25 random forest runs with the top variable and then adding the next-most-important variable one-by-one and rerunning the models. The interpretation variables are those from the simplest model of the models with an out-of-bag error

within one standard deviation of the minimum error. A "prediction" set of variables is selected by adding interpretation variables step-wise, and only keeping variables that reduce the out-of-bag error significantly more than adding a noisy variable. The VSURF procedure resulted in an interpretation set of variables each with a relationship to aboveground biomass and a prediction set with reduced redundancy suitable for prediction.

Modeling Plot-Scale Biomass Differences

At the plot scale, I identified the stand characteristics most correlated with biomass estimate differences between different sets of allometric equations. This was done using a random forest model to predict the plot biomass difference between allometric equations using stand structure and composition predictor variables. The following predictors were considered: number of trees per hectare, basal area, average DBH, and basal area by species of the most common species in the plot data (lodgepole pine, Engelmann spruce, subalpine fir, aspen, Douglas-fir, and ponderosa pine). I also considered the proportion of total basal area for these same species, but removed them from the model due to high correlation with the species absolute basal area values and the sensitivity of variable importance metrics to correlated predictor variables. I calculated variable importance and generated partial dependence plots (Friedman, 2001) to characterize relationships between stand structure and allometric biomass equation differences.

Calculating Dry Mass of Sánchez Meador (2007) Trees

Only green mass was reported for 212 of the 285 Legacy trees used in the study (Sánchez Meador, 2007). For these trees, I converted above-stump green mass to dry mass using moisture contents and component proportions from the destructive sampling. A species-specific, whole-tree water percentage was calculated as the mean of each component's moisture content (Table

A1.2.1) weighted by the percentage of tree biomass in each component (Figure A1.2.1). Foliage mass was included but was not reported as a separate component for these trees sampled by Sánchez Meador (2007), so I calculated foliage using the local equations and subtracted it from the above-stump dry weight to obtain a value comparable to the dry wood and bark mass used for trees from Reid et al. (1974) and Tossey (1982).

Table A1.1.1. A priori equations tested for predicting branch length, foliage, and branch wood for individual branches of each species. Several additional species-specific equations were also tested (not shown).

Branch Length Equations (m)	Branch Wood and Foliage Equations (g)
$\beta_0 + \beta_1 B_{ij} + \beta_2 C_i$	$\beta_0 + \beta_1 B_{ij} + \beta_2 L_{ij}$
$\beta_0 + \beta_1 B_{ij} + \beta_2 C_i + \beta_3 R_{ij}$	$\beta_0 + \beta_1 B_{ij} + \beta_2 L_{ij} + \beta_3 D_i$
$\beta_0 + \beta_1 B_{ij} + \beta_2 R_{ij} + \beta_3 G_i + \beta_4 D_i$	$\beta_0 + \beta_1 B_{ij} + \beta_2 L_{ij} + \beta_3 R_{ij}$
$\beta_0 + \beta_1 B_{ij} + \beta_2 H_i + \beta_3 S_{ij}$	$\beta_0 + \beta_1 B_{ij} + \beta_2 C_i + \beta_3 S_{ij}$
$\beta_0 + \beta_1 B_{ij} + \beta_2 D_i + \beta_3 C_i + \beta_4 S_{ij}$	$\beta_0 + \beta_1 B_{ij} + \beta_2 D_i + \beta_3 R_{ij} + \beta_4 G_i$
$\beta_0 + \beta_1 B_{ij} + \beta_2 D_i + \beta_3 C_i$	$\beta_0 + \beta_1 B_{ij} + \beta_2 L_{ij} + \beta_3 H_i$
$\beta_0 + \beta_1 \ln(B_{ij}) + \beta_2 \ln(C_i)$	$\beta_0 + \beta_1 B_{ij} + \beta_2 S_{ij} + \beta_3 C_i + \beta_4 D_i$
$\beta_0 + \beta_1 \ln(B_{ij}) + \beta_2 \ln(C_i) + \beta_3 \ln(R_{ij})$	$\beta_0 + \beta_1 \ln(B_{ij}) + \beta_2 \ln(L_{ij})$
$\beta_0 + \beta_1 \ln(B_{ij}) + \beta_2 \ln(R_{ij}) + \beta_3 \ln(G_i) + \beta_4 \ln(D_i)$	$\beta_0 + \beta_1 \ln(B_{ij}) + \beta_2 \ln(L_{ij}) + \beta_3 \ln(D_i)$
$\beta_0 + \beta_1 \ln(B_{ij}) + \beta_2 \ln(H_i) + \beta_3 \ln(S_{ij})$	$\beta_0 + \beta_1 \ln(B_{ij}) + \beta_2 \ln(L_{ij}) + \beta_3 \ln(R_{ij})$
$\beta_0 + \beta_1 \ln(B_{ij}) + \beta_2 \ln(D_i) + \beta_3 \ln(C_i) + \beta_4 \ln(S_{ij})$	$\beta_0 + \beta_1 \ln(B_{ij}) + \beta_2 \ln(C_i) + \beta_3 \ln(S_{ij})$
$\beta_0 + \beta_1 \ln(B_{ij}) + \beta_2 \ln(D_i) + \beta_3 \ln(C_i)$	$\beta_0 + \beta_1 \ln(B_{ij}) + \beta_2 \ln(D_i) + \beta_3 \ln(R_{ij}) + \beta_4 \ln(G_i)$
	$\beta_0 + \beta_1 \ln(B_{ij}) + \beta_2 \ln(L_{ij}) + \beta_3 \ln(H_i)$
	$\beta_0 + \beta_1 \ln(B_{ij}) + \beta_2 \ln(D_i) + \beta_3 \ln(S_{ij}) + \beta_4 \ln(C_i)$

j^{th} branch on the i^{th} tree
L= branch length (m); D = tree diameter at breast height (cm); B = branch diameter (cm); C= width of crown at widest axis (m); S = height where branch meets main stem (m); R = relative branch depth; H= tree height (m); G = height to first branch (m)

Table A1.1.2. Model form selected for regression models used to predict branch length, foliage, and branch wood for individual branches.

Species	Component	Formula
Lodgepole Pine	Branch Length	$L_{ij} = \beta_0 + \beta_1 B_{ij} + \beta_2 D_i + \beta_3 C_i$
	Foliage	$\ln(F_{ij}) = \beta_0 + \beta_1 \ln(B_{ij}) + \beta_2 \ln(S_{ij}) + \beta_3 \ln(R_{ij})$
	Wood	$\ln(W_{ij}) = \beta_0 + \beta_1 \ln(B_{ij}) + \beta_2 \ln(L_{ij}) + \beta_3 \ln(H_i)$
Ponderosa Pine	Branch Length	$L_{ij} = \beta_0 + \beta_1 B_{ij} + \beta_2 C_i + \beta_3 S_{ij} + \beta_4 G_i$
	Foliage	$\ln(F_{ij}) = \beta_0 + \beta_1 \ln(B_{ij}) + \beta_2 \ln(D_i) + \beta_3 \ln(R_{ij}) + \beta_4 \ln(G_i)$
	Wood	$\ln(W_{ij}) = \beta_0 + \beta_1 \ln(B_{ij}) + \beta_2 \ln(S_{ij}) + \beta_3 \ln(C_i)$
Douglas-Fir	Branch length	$L_{ij} = \beta_0 + \beta_1 B_{ij} + \beta_2 D_i + \beta_3 G_i$
	Foliage	$\ln(F_{ij}) = \beta_0 + \beta_1 \ln(L_{ij}) + \beta_2 \ln(D_i) + \beta_3 \ln(R_{ij})$
	Wood	$\ln(W_{ij}) = \beta_0 + \beta_1 \ln(L_{ij}) + \beta_2 \ln(D_i)$

j^{th} branch on the i^{th} tree
L= branch length (m), F= foliage mass (g), W= wood mass (g)

D = tree diameter at breast height (cm); B = branch diameter (cm); C= width of crown at widest axis (m); S = height where branch meets main stem (m); R = relative branch depth; H= tree height (m); G = height to first branch (m)

Table A1.1.3. Parameter values and evaluation statistics for the regression models used to predict branch length, foliage and branch wood for individual branches. Numbers in parentheses are standard errors of the parameter values. Corr. Factor = correction factor; PICO = lodgepole pine (*Pinus contorta*); PIPO = ponderosa pine (*P. ponderosa*); PSME = Douglas fir (*Pseudotsuga menziesii)*

Species	Component	n	β_0	β_1	β_2	β_3	β_4	Corr. Factor	Adj, R^2	RMSE *
PICO	Branch Length (m)	289	0.53 (0.085)	0.41 (0.019)	-0.025 (0.004)	0.12 (0.022)		NA	0.63	0.3
	Foliage (g)	102	3.73 (0.111)	1.80 (0.129)	0.30 (0.064)	0.67 (0.244)		1.17	0.74	151.3
	Wood (g)	102	3.21 (0.174)	1.78 (0.091)	0.87 (0.121)	0.40 (0.072)		1.05	0.93	155.9
PIPO	Branch Length (m)	182	0.30 (0.129)	0.26 (0.013)	0.099 (0.024)	-0.082 (0.015)	0.24 (0.083)	NA	0.87	0.5
	Foliage (g)	51	2.80 (0.575)	1.99 (0.128)	0.16 (0.210)	-0.75 (0.211)	-0.21 (0.181)	1.12	0.91	1262.2
	Wood (g)	51	3.41 (0.172)	2.65 (0.077)	0.086 (0.084)	0.16 (0.148)		1.04	0.98	4810.5
PSME	Branch Length (m)	275	0.51 (0.085)	0.40 (0.015)	-0.011 (0.003)	0.12 (0.037)		NA	0.75	0.5
	Foliage (g)	53	3.34 (0.415)	1.73 (0.126)	0.69 (0.142)	0.40 (0.201)		1.12	0.85	305.8
	Wood (g)	53	3.53 (0.359)	2.45 (0.114)	0.53 (0.115)			1.10	0.93	468.08

* RMSE values are in original units (either m for length or g for foliage and wood; not log transformed)

Table A1.1.4. List of predictor variable rasters considered for mapping biomass and references for each variable.

Predictor Variable	References
Topography and geomorphology	(Evans et al., 2014)
Elevation and slope	(Gesch et al., 2002); (Gesch, 2007)
Eastness and northness	(Kumar et al., 2006)
Compound topographic index	(Gessler et al., 1995)
Heat load index	(McCune and Keon, 2002)
Standard, profile, and planform curvature	(Moore et al., 1991); (Zevenbergen and Thorne, 1987)
Roughness (3x3, 6x6, 9x9,12x12, 15x15, 21x21, 27x27)	(Riley et al., 1999); (Blaszczynski, 1997)
Slope position (3x3, 6x6, 9x9,12x12, 15x15, 21x21, 27x27)	(Reu et al., 2013); (Guisan et al., 1999)
Spectral	
ETM+ bands 1-7	
Soil-adjusted vegetation index (SAVI)	(Huete, 1988)
Normalized difference vegetation index (NDVI)	(Rouse et al., 1974)
Corrected NDVI	(Nemani et al., 1993)
Enhanced vegetation index (EVI)	(Liu and Huete, 1995)
Moisture stress index (MSI)	(Rock et al., 1985)
Second modified soil-adjusted vegetation index (MSAVI2)	(Qi et al., 1994)
Normalized difference infrared index (NDII)	(Hardisky et al., 1983)
Green normalized difference vegetation index (GNDVI)	(Gitelson et al., 1996)
Normalized difference water index (NDWI)	(McFeeters, 1996)
NDWI and NDII with ETM+ band 7 substituted for ETM+ band 5	(Ji et al., 2012)
Tasseled Cap brightness, greenness, and wetness	(Huang et al., 2002)
Tasseled Cap distance	(Duane et al., 2010)
Tasseled Cap angle	(Powell et al., 2010)
Texture	
Mean, variance, homogeneity, contrast, dissimilarity, entropy, second moment, and correlation for ETM+ bands 1, 2, 3, 4, 5, and 7 on a 3x3, 5x5, 7x7, 9x9, and 11x11 window and a (1,1) shift	(Zvoleff, 2016)
Climate (1961-1990 normals)	
Chilling degree-days (degree-days below 0°C)	(Wang et al., 2016)
Growing degree-days (degree-days above 5°C)	(Wang et al., 2016)
Heating degree-days (degree-days below 18°C)	(Wang et al., 2016)
Cooling degree-days (degree-days above 18°C)	(Wang et al., 2016)
Frost-free period	(Wang et al., 2016)
Mean annual precipitation	(Wang et al., 2016)
Mean annual solar radiation	(Wang et al., 2016)
Mean annual temperature	(Wang et al., 2016)
Mean coldest month temperature	(Wang et al., 2016)
May to September precipitation	(Wang et al., 2016)
Number of frost-free days	(Wang et al., 2016)
Mean warmest month temperature	(Wang et al., 2016)
Precipitation as snow between August in previous year and July in current year	(Wang et al., 2016)
Temperature difference between mean warmest month temperature and mean coldest month temperature	(Wang et al., 2016)
Summer heat-moisture index	(Wang et al., 2016)
Annual heat-moisture index	(Wang et al., 2016)

Table A1.1.5. Predictor variables used in the final random forest model for biomass maps made from each set of allometric equations: local (equations presented in this study), Jenkins et al. (2003), and FIA-CRM. Variables are listed by order of importance, with the first variable being the most important. See Table A1.1.4 for acronym definitions.

Allometric Equations	Predictor Variables
Local	ETM+ band 1, NDII, elevation, ETM+ band 5 3x3 second moment, ETM+ band 6, precipitation as snow, northness, EVI, NDVI, mean annual solar radiation, slope position (6x6)
Jenkins et al. (2003)	NDII, elevation, ETM+ band 1, Tasseled Cap angle, May to September precipitation, ETM+ band 1 5x5 entropy, mean annual solar radiation, ETM+ band 4 11x11 homogeneity, EVI, northness
FIA-CRM	NDII, ETM + band 2 5x5 mean, precipitation as snow, elevation, ETM+ band 5 3x3 second moment, EVI, ETM+ band 4 9x9 contrast, northness, slope position (6x6)

Table A1.1.6. Comparison of DBH and height between destructively sampled trees presented in this study (Local trees), trees used from the Legacy Tree database (Legacy trees), and trees measured in the FIA plots. PSME = Douglas fir (*Pseudotsuga menziesii)*; PICO = lodgepole pine (*Pinus contorta*); PIPO = ponderosa pine (*P. ponderosa*)

	Species	Legacy trees	Local trees	FIA Plot Trees
Number of trees sampled	PSME	63	10	811
	PICO	114	20	9601
	PIPO	108	10	593
Mean DBH (cm)	PSME	14.1	24.9	21.5
	PICO	11.4	16.3	19.9
	PIPO	12.7	34.0	23.2
Max DBH (cm)	PSME	39.6	46.6	78.7
	PICO	32.0	29.9	62.0
	PIPO	36.6	61.8	64.3
Min DBH (cm)	PSME	1.5	2.4	2.5
	PICO	1.0	2.5	2.5
	PIPO	0.8	4.9	2.5
Mean height (m)*	PSME	8.0	12.7	11.7
	PICO	7.0	12.2	13.9
	PIPO	6.8	11.3	10.3
Max height (m)	PSME	19.5	19.7	34.1
	PICO	16.2	21.1	31.1
	PIPO	19.2	16.8	29.9
Min height (m)	PSME	1.8	3.2	1.8
	PICO	1.5	3.2	2.1
	PIPO	1.4	3.0	2.1

* Height was not reported for 19 lodgepole pine trees in the Legacy Tree database.

Appendix 1.2: Destructive sampling and oven drying

Tables and figures presenting mass and moisture content of each component from destructive sampling of Douglas-fir, lodgepole pine, and ponderosa pine.

Table A1.2.1. Moisture content for the species and components in this study. Moisture content is presented as a percentage of the wet weight. The "n" for each component is the number of samples oven dried to obtain the moisture content.

Species	Component	n	Mean (%)	SD (%)	Min (%)	Max (%)
Douglas-Fir	Bole	75	44.3	5.2	34.2	54.4
	Bark	75	36.3	8.9	18.4	56.4
	Branch	58	42.2	7.7	21.2	83.8
	Dead Branch	14	8.7	7.3	2.1	33.1
	Foliage	59	53.0	4.3	27.4	60.3
Lodgepole Pine	Bole	132	52.4	7.5	27.9	66.1
	Bark	131	52.0	8.7	28.5	66.6
	Branch	97	44.2	6.6	12.6	67.9
	Dead Branch	10	7.9	0.9	6.9	9.1
	Foliage	97	48.3	6.9	11.2	69.7
Ponderosa Pine	Bole	72	57.6	3.2	47.5	63.4
	Bark	72	33.7	7.3	13.1	57.8
	Branch	60	41.6	9.5	4.9	64.3
	Dead Branch	13	6.7	2.6	3.9	12.8
	Foliage	58	49.6	5.4	25.0	69.0

* A species-specific, whole-tree water percentage was calculated as the mean of each component's moisture content weighted by the percentage of tree biomass in each component (Figure A1.2.1). These values were used to convert trees from the Legacy Database that only reported wet mass to dry mass. The whole-tree water percentages were 44.20% for Douglas-fir, 48.45% for lodgepole pine, and 47.53% for ponderosa pine.
** The subsampled branches from the three smallest lodgepole pine trees were too small to obtain reliable water weights, so were not used in the moisture content calculations. This was also the case for one subsampled Douglas-fir branch and one ponderosa pine branch.

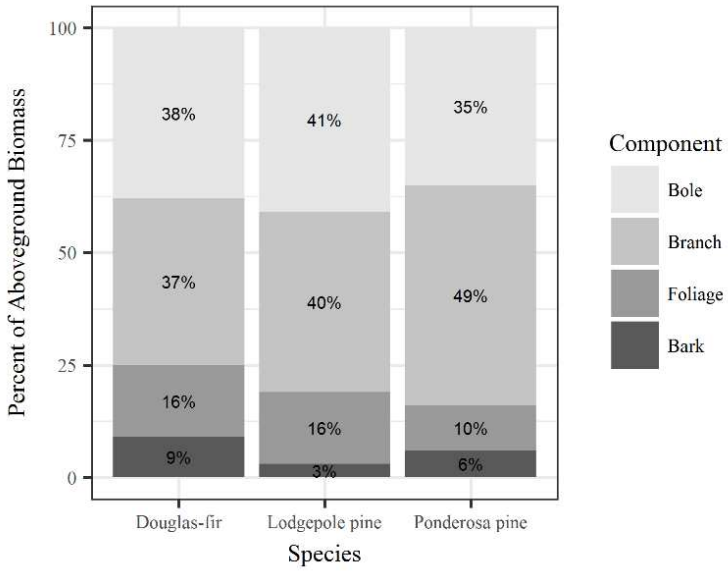

Figure A1.2.1. The mean percentage of aboveground biomass held in each component for the destructively sampled trees.

Appendix 1.3: Biomass variability between allometric equations

Tables and figures characterizing tree and plot-level biomass differences between the three allometric equations evaluated in this study.

Table A1.3.1. Summary of individual tree biomass differences between different allometric equations. Differences are shown for all sizes (All) and by diameter at breast height bins. The denominators for calculating relative differences are the local biomass estimates for "Local-Jenkins" and "Local – FIA-CRM" and is Jenkins biomass for "Jenkins – FIA-CRM."

			Local - Jenkins		Local – FIA-CRM		Jenkins – FIA-CRM	
Species	Component	Diameter Range (cm)	Mean Diff (kg)	Mean Relative Diff (%)	Mean Diff (kg)	Mean Relative Diff (%)	Mean Diff (kg)	Mean Relative Diff (%)
Douglas-Fir (202)	Total	All	-88.9	-34.3	18.8	29.3	107.7	47.8
		2.5 - 20	-17.2	-23.5	24.7	46.3	41.9	56.1
		20 – 40	-97.4	-43.4	19.2	12.8	116.6	39.0
		40 - 60	-487.6	-61.6	-8.3	-1.0	479.3	37.2
		60 - 80	-1605.5	-75.2	-237.7	-9.8	1367.8	37.3
	Bole and Bark	All	-91.7	-47.2	-5.5	17.8	95.2	47.6
		2.5 - 20	-16.4	-28.6	18.8	41.2	38.5	57.7
		20 – 40	-101.2	-63.2	-7.1	-0.2	94.1	38.8
		40 - 60	-508.5	-92.2	-114.7	-21.4	393.9	36.8
		60 - 80	-1658.3	-112.2	-510.3	-33.1	1148.0	37.3
	Branch	All	3.1	0.4	25.7	57.0	22.6	54.8
		2.5 - 20	-0.8	-6.5	10.1	64.4	10.9	65.3
		20 – 40	3.8	6.0	26.3	50.4	22.5	45.6
		40 - 60	20.9	10.2	106.4	51.3	85.5	44.4
		60 - 80	52.9	8.9	272.6	47.0	219.8	41.5
	Foliage	All	1.8	17.7	NA	NA	NA	NA
		2.5 - 20	1.8	22.6	NA	NA	NA	NA
		20 – 40	3.1	15.1	NA	NA	NA	NA
		40 - 60	-3.0	-3.3	NA	NA	NA	NA
		60 - 80	-40.7	-22.7	NA	NA	NA	NA
Lodgepole Pine (108)	Total	All	31.7	18.7	41.7	28.3	10.0	11.6
		2.5 - 20	11.9	18.8	21.3	33.9	9.3	18.2
		20 – 40	51.3	18.2	57.2	20.0	6.0	2.0
		40 - 60	268.9	25.7	417.1	39.6	148.2	18.7
		60 - 80	845.3	32.8	1439.7	55.9	594.4	34.4
	Bole and Bark	All	13.0	-1.2	21.7	12.7	7.6	10.9
		2.5 - 20	-2.5	-9.8	5.2	13.2	7.8	18.5
		20 – 40	26.4	9.9	30.0	11.0	3.6	1.3
		40 - 60	250.8	27.8	368.5	40.6	117.7	17.9
		60 - 80	878.3	37.8	1308.6	56.3	430.3	29.8
	Branch	All	19.7	52.7	22.7	60.5	3.0	15.6
		2.5 - 20	15.6	59.1	18.3	69.7	2.6	24.2
		20 – 40	24.8	46.1	27.3	49.8	2.4	4.6
		40 - 60	18.0	15.1	48.5	38.2	30.5	25.6
		60 - 80	-33.1	-15.4	131.0	61.0	164.1	66.2
	Foliage	All	4.2	39.8	NA	NA	NA	NA

		2.5 - 20	3.9	49.4	NA	NA	NA	NA
		20 – 40	4.8	27.9	NA	NA	NA	NA
		40 - 60	-3.8	-8.1	NA	NA	NA	NA
		60 - 80	-30.4	-42.4	NA	NA	NA	NA
Ponderosa Pine (122)	Total	All	26.3	8.9	101.7	48.8	75.5	43.6
		2.5 - 20	4.2	8.0	31.8	56.4	27.6	52.5
		20 – 40	26.3	8.8	118.9	43.6	92.5	38.1
		40 - 60	152.0	14.3	405.7	39.8	253.6	29.7
		60 - 80	477.3	20.2	405.2	17.1	-72.1	-3.8
	Bole and Bark	All	-46.2	-21.0	15.2	26.8	65.7	42.3
		2.5 - 20	-4.2	-4.3	20.1	46.1	25.5	51.5
		20 – 40	-51.8	-30.9	23.0	18.5	74.8	37.8
		40 - 60	-253.5	-52.6	-43.3	-7.5	210.2	29.6
		60 - 80	-631.5	-66.6	-882.7	-93.1	-251.2	-15.9
	Branch	All	79.0	56.5	95.0	79.3	16.0	49.2
		2.5 - 20	10.4	43.0	17.4	77.0	7.1	58.3
		20 – 40	78.1	63.3	95.9	80.1	17.8	44.8
		40 - 60	405.6	75.4	449.0	84.0	43.4	34.3
		60 - 80	1108.8	81.9	1287.9	95.1	179.1	72.9
	Foliage	All	2.9	-2.7	NA	NA	NA	NA
		2.5 - 20	-0.2	-26.3	NA	NA	NA	NA
		20 – 40	3.1	13.4	NA	NA	NA	NA
		40 - 60	20.1	26.8	NA	NA	NA	NA
		60 - 80	54.7	33.0	NA	NA	NA	NA

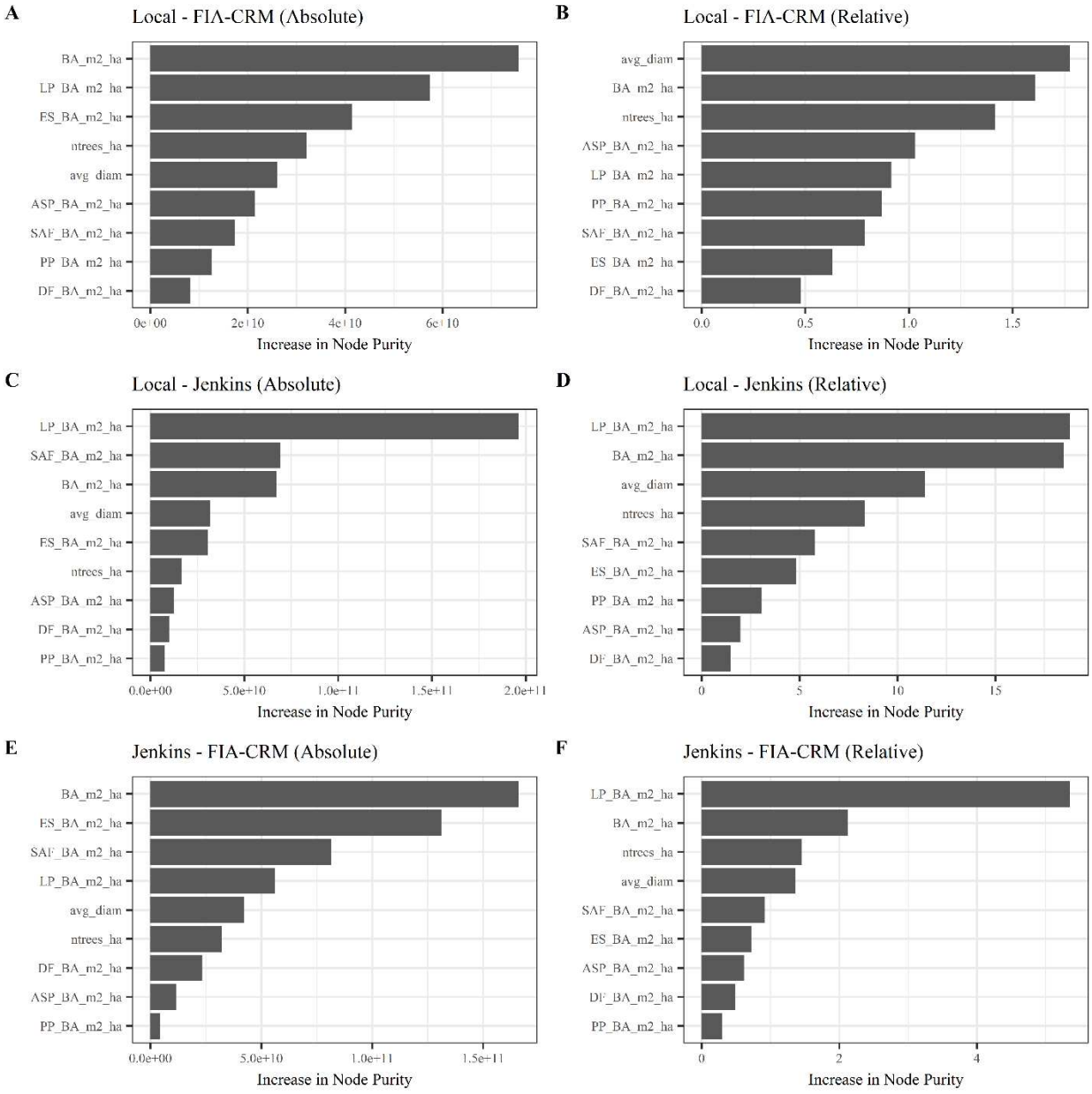

Figure A1.3.1. Variable importance plots for random forests used to model differences in plot biomass estimates between different allometric equations estimates as a function of stand attributes. Both the absolute difference between plot biomass estimates was modeled (left column) as well as the relative difference (right column).
Allometric biomass equations compared: local = allometric equations presented in this study; Jenkins = allometric biomass equations from Jenkins et al. (2003); FIA-CRM = Forest Inventory and Analysis Component Ratio Method allometric biomass equations
Predictor variables considered: BA_m^2_ha = total basal area (m^2 ha^{-1}); ntrees_ha = number of trees ha^{-1}; avg_diam = average tree diameter (cm); LP_BA_m^2_ha = lodgepole pine basal area (m^2 ha^{-1}); PP_BA_m^2_ha = ponderosa pine basal area (m^2 ha^{-1}); DF_BA_m^2_ha = Douglas-fir basal area (m^2 ha^{-1}); ES_BA_m^2_ha = Engelmann spruce basal area (m^2 ha^{-1}); SAF_BA_m^2_ha = subalpine fire basal area (m^2 ha^{-1}); ASP_BA_m^2_ha = aspen basal area (m^2 ha^{-1})

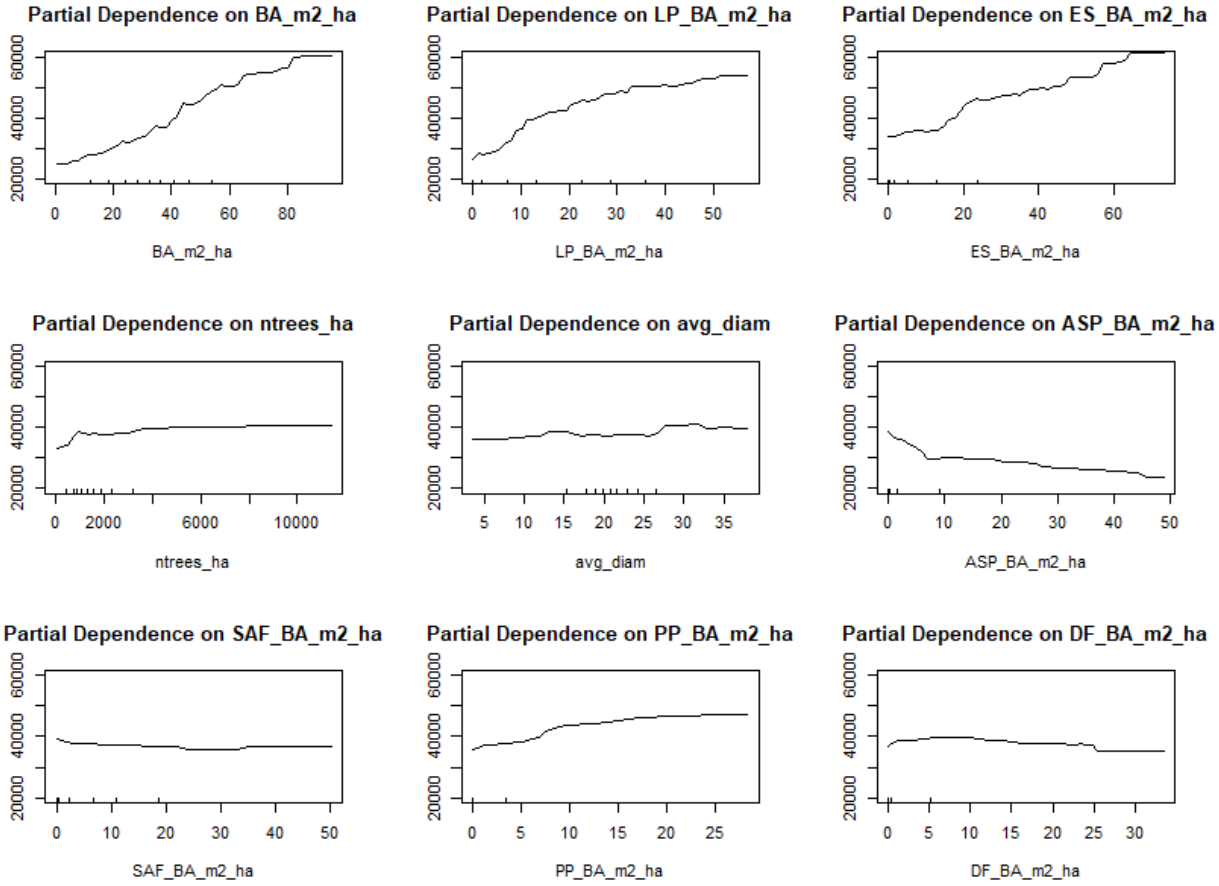

Figure A1.3.2. Partial dependence plot from the random forests model of FIA plot biomass difference between local and FIA-CRM allometric equations as a function of stand attributes. Abbreviations of predictor variables considered are described in caption for Figure A1.3.1.

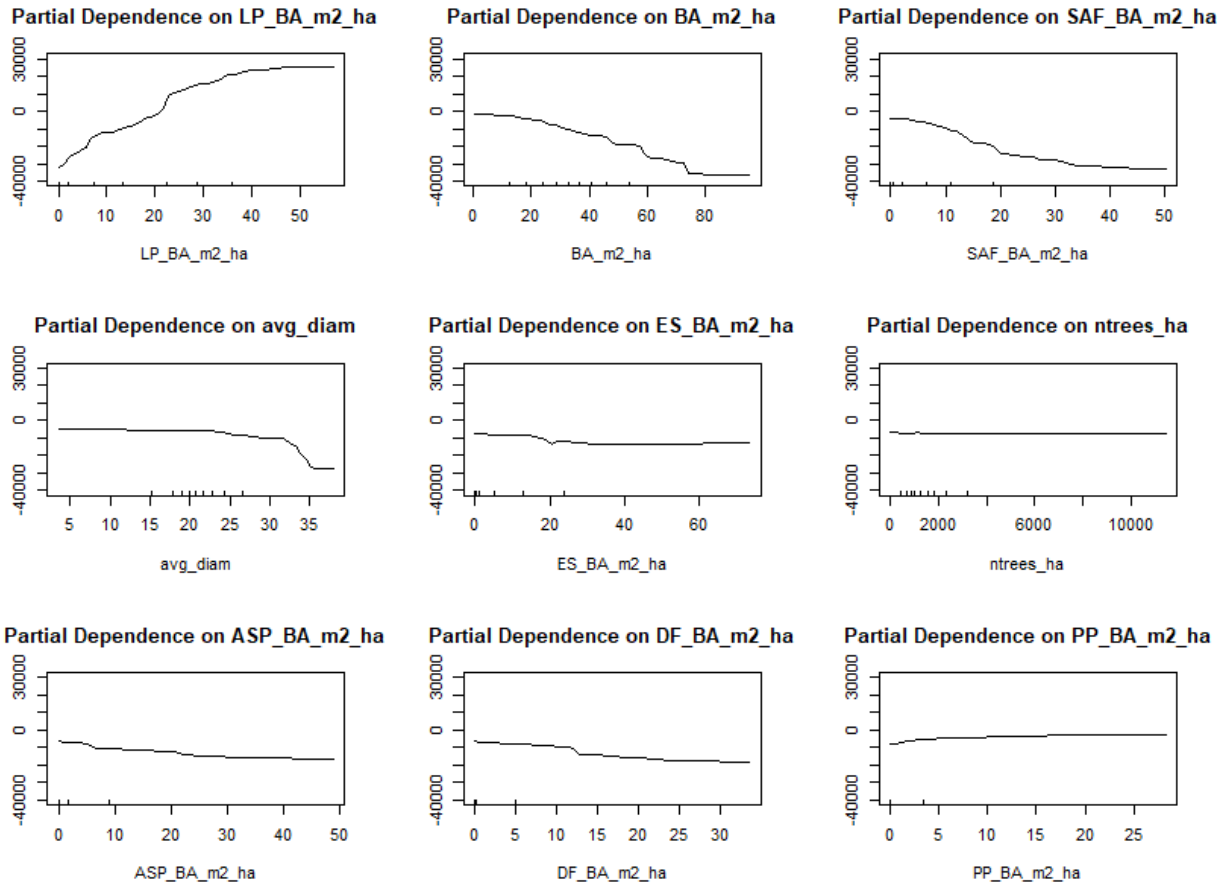

Figure A1.3.3. Partial dependence plot from the random forests model of FIA plot biomass difference between local and Jenkins et al. (2003) allometric equations as a function of stand attributes. Abbreviations of predictor variables considered are described in caption for Figure A1.3.1.

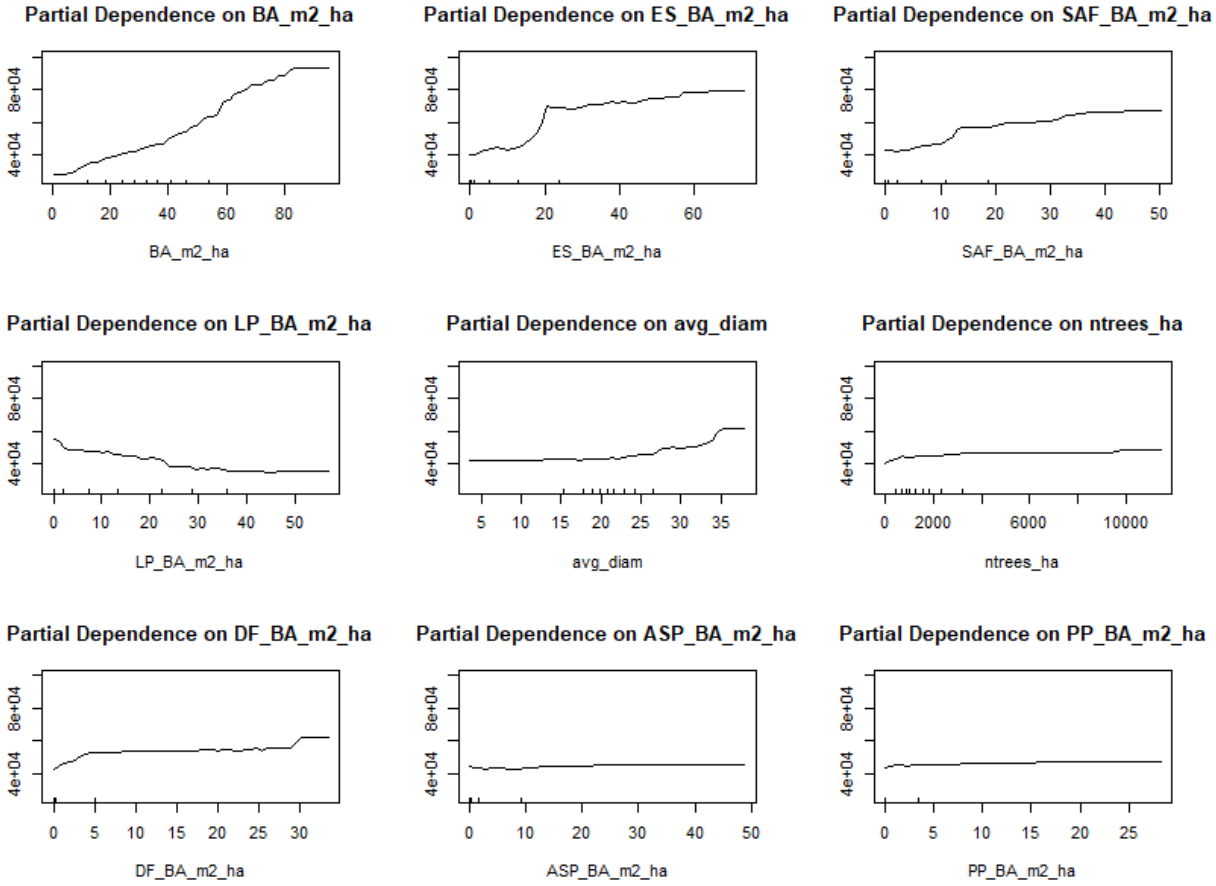

Figure A1.3.4. Partial dependence plot from the random forests model of FIA plot biomass difference between Jenkins et al. (2003) and FIA-CRM allometric equations as a function of stand attributes. Abbreviations of predictor variables considered are described in caption for Figure A1.3.1.

Table A1.3.2. Out-of-bag RMSE, percent RMSE of the mean, and pseudo R^2 for random forests models run with plot biomass difference as the response variable and stand characteristics as predictor variables. Both relative and absolute model differences were modeled for the following allometric equations: local (presented in this study), Forest Inventory and Analysis Component Ratio Method (FIA-CRM), and Jenkins et al. (2003).

Allometric Equations Compared	Relative or Absolute	RMSE	% RMSE (of mean)	Pseudo R^2
Local – Jenkins	Absolute	12.2 Mg ha $^{-1}$	-178.6	.8613
Local – Jenkins	Relative	34.8 %	-267.6	.3903
Local – FIA-CRM	Absolute	17.7 Mg ha $^{-1}$	47.5	.5668
Local – FIA-CRM	Relative	11.7 %	40.6	.4336
Jenkins - FIA-CRM	Absolute	21.4 Mg ha $^{-1}$	48.5	.6633
Jenkins - FIA-CRM	Relative	12.2 %	37.1	.5529

Appendix 1.4: Destructive sampling data

Table A1.4. Data from each tree destructively sampled for this study showing component biomass (kg), diameter at breast height (cm), and height (m) as well as basal area (m^2 ha^{-1}) and tree density (number of trees ha^{-1}) of 7.32 m radius plots measured around each tree.

Species	DBH_cm	Height_m	Bole_kg	Bark_kg	Foliage_kg	Branch_kg	Aboveground_Total_kg	Trees_per_ha	Basal_Area_m2_per_ha
PICO	2.5	3.2	0	0	0.8	0.9	1.7	2139	9
PICO	4.3	4	0	0	1	2.1	3.1	1604	8.2
PICO	6.5	5.2	0	0	2.2	6	8.2	1307	3.7
PICO	8.5	6.4	1	0.1	3.7	10.7	15.6	1010	4.6
PICO	10.2	5.9	4.1	0.5	3.4	11	19	594	13.2
PICO	11	5.9	4.9	0.8	7.5	18.6	31.8	1010	6.2
PICO	12	10	12.1	1	8.1	22.3	43.5	951	7.3
PICO	12.8	7.5	14.3	2.2	8	20.8	45.3	416	2.5
PICO	13.5	8.1	16.7	2.1	10.2	21.7	50.7	1248	5.8
PICO	14.8	14.5	44.2	3.8	6.7	18.4	73.1	1010	31.2
PICO	15	14.6	43.3	3	5.1	17.2	68.6	891	32.5
PICO	17.8	6.9	20	2.7	12.4	35.3	70.4	238	0.5
PICO	19	19.5	105.6	7	5.6	26.1	144.3	1129	39.7
PICO	21.9	13.9	64.2	4.3	15.5	82	166	772	31.5
PICO	22.5	16.2	116.1	11.4	11.2	27.7	166.4	356	17.3
PICO	23.5	19.4	158.8	13.4	16.5	46.1	234.7	772	36.2
PICO	25.8	21.1	174.2	10.3	21.1	46	251.6	951	44.9
PICO	25.9	20.5	206.6	13.3	24.1	72.9	316.9	535	30.7
PICO	27.8	20.5	208.3	14.4	17.1	43.6	283.5	772	14.4
PICO	29.9	21	247.2	15.8	23.3	72.1	358.4	713	31.7
PIPO	4.9	3	0	0	1.5	4.2	5.7	238	23.4
PIPO	12.7	6.3	7.7	3	4.6	17.3	32.6	416	29.7
PIPO	19	9.4	35.3	8.3	6.3	46.5	96.4	416	17.3
PIPO	24	10.3	84.1	16.8	17.9	48.1	166.9	178	13
PIPO	32.5	10.6	126.6	18.4	31.7	135.6	312.3	59	5.5
PIPO	39.3	13.1	286.1	38.2	50.2	377.9	752.4	59	4.7
PIPO	44.9	13.9	308	39.3	41.6	254.9	643.9	59	19.7
PIPO	49	14.5	499.1	60.2	104.3	846.7	1510.2	0	0
PIPO	51.6	16.8	618.5	81.5	79.5	615.9	1395.4	297	20.5
PIPO	61.8	15.4	738.5	89.7	153.9	1206	2188.1	0	0
PSME	2.4	3.2	0	0	1.2	2	3.2	416	14.7
PSME	7.8	6.7	1.9	0.5	4.2	13.7	20.3	535	30.3
PSME	10	8.4	5.3	1.2	5.9	16.8	29.3	535	14.5
PSME	17.8	11.7	30.1	7.3	17.7	35.2	90.4	535	18.8
PSME	24.3	13.5	82	22.7	23.8	51.9	180.3	535	15.5
PSME	27	13.5	100.3	38.7	24.6	50.6	214.2	535	7.9

PSME	30.4	14.8	171.4	44.5	18	58.2	292.2	297	19
PSME	38.2	19.7	355.1	67.6	49.3	126.6	598.5	119	12.4
PSME	44.1	17.5	345.4	66.9	65.1	148	625.4	178	7.2
PSME	46.6	18.4	434.2	81.8	72.1	220.9	809.1	178	15.9

Chapter 2 Appendices

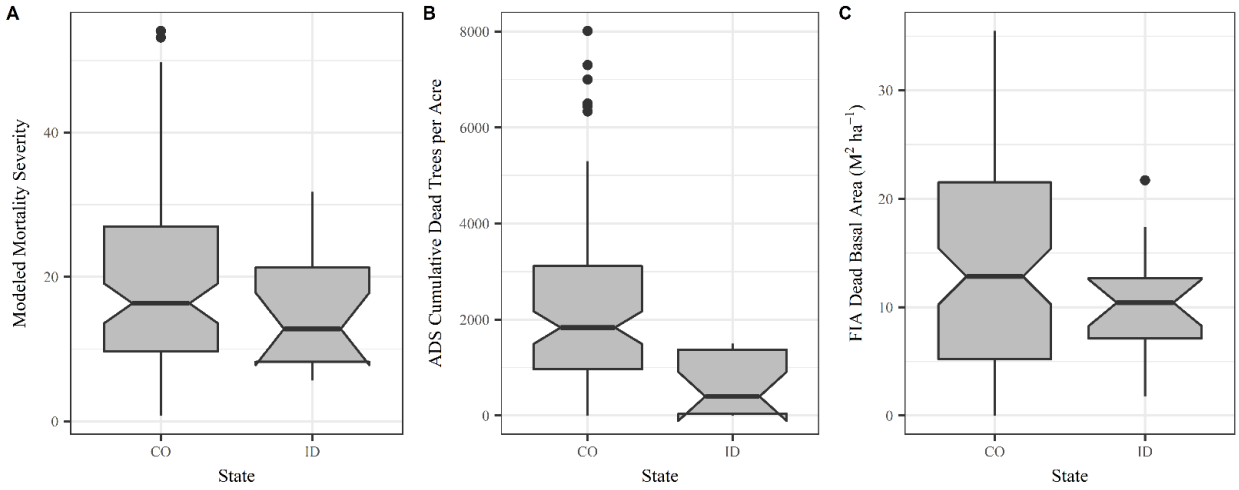

Figure A2.1. The severity of mortality at 99 Forest Inventory and Analysis (FIA) plots in Colorado and 17 FIA plots in Idaho as measured by (A) modeled mortality severity, (B) Aerial Detection Surveys (ADS), and (C) FIA field measurements.

Table A2.1. Assessment of the accuracy of the LANDFIRE lodgepole pine extent mask using Forest Inventory and Analysis (FIA) data. Of the 1,180 FIA plots across all forest types, 821 fell outside the lodgepole pine mask used to define the study area extent and 359 fell within the lodgepole pine mask. Areas that burned between 1984 and 2013 were excluded from the lodgepole pine mask, so some plots falling outside the lodgepole pine mask may fall within a burned area. BA = basal area

	Number of FIA plots	Number of plots without lodgepole pine	% of plots without lodgepole pine	Mean lodgepole pine BA proportion of total BA	Standard deviation of lodgepole pine BA proportion of total BA
Outside lodgepole pine mask	821	522	64	0.13	0.25
Within lodgepole pine mask	359	36	10	0.60	0.36

Table A2.2. All predictor variables considered in developing cumulative lodgepole mortality models. This included elevation, latitude, derived indices of Normalized Difference Vegetation Index (NDVI), Normalized Difference Moisture Index, Tasseled cap greenness, wetness, brightness, and angel, the near infrared (NIR), shortwave infrared 1 (SWIR1), shortwave infrared 2 (SWIR2) and thermal bands from 2013 in addition to the differences of the indices from 2001 and 2013.

Predictor Variable Name	**Sensor**	**Source**
Near infrared band (NIR)	Landsat 8 Operational Land Imager (OLI)	USGS surface reflectance-derived spectral indices (Vermote et al., 2016)
Shortwave infrared 1 band (SWIR1)	Landsat 8 OLI	USGS surface reflectance-derived spectral indices (Vermote et al., 2016)
Shortwave infrared 2 band	Landsat 8 OLI	USGS surface reflectance-derived spectral indices (Vermote et al., 2016)
Thermal band	Landsat 8 Thermal Infrared Sensor (TIRS)	USGS surface reflectance-derived spectral indices (Vermote et al., 2016)
Normalized Difference Vegetation Index (NDVI)	Landsat 8 OLI	USGS surface reflectance-derived spectral indices (Vermote et al., 2016)
NDVI difference (2013-2001)	Landsat 8 OLI (2013) and Landsat 5 Thematic Mapper (TM) (2001)	USGS surface reflectance-derived spectral indices (Masek et al., 2006; Vermote et al., 2016)
Normalized Difference Moisture Index (NDMI)	Landsat 8 OLI	USGS surface reflectance-derived spectral indices (Vermote et al., 2016)
NDMI difference (2013 and 2001)	Landsat 8 OLI (2013) and Landsat 5 TM (2001)	USGS surface reflectance-derived spectral indices (Masek et al., 2006; Vermote et al., 2016)
Tasseled cap greenness	Landsat 8 OLI	USGS top-of-atmosphere reflectance product (Chander et al., 2009)
Tasseled cap wetness	Landsat 8 OLI	USGS top-of-atmosphere reflectance product (Chander et al., 2009)
Tasseled cap brightness	Landsat 8 OLI	USGS top-of-atmosphere reflectance product (Chander et al., 2009)

Tasseled cap greenness difference (2013-2001)	Landsat 8 OLI and Landsat 5 TM	USGS top-of-atmosphere reflectance product (Chander et al., 2009)
Tasseled cap wetness difference (2013-2001)	Landsat 8 OLI and Landsat 5 TM	USGS top-of-atmosphere reflectance product (Chander et al., 2009)
Tasseled cap brightness difference (2013-2001)	Landsat 8 OLI and Landsat 5 TM	USGS top-of-atmosphere reflectance product (Chander et al., 2009)
Normalized burn ratio (NBR)	Landsat 8 OLI	USGS surface reflectance-derived spectral indices (Vermote et al., 2016)
Normalized burn ratio difference (2013-2001)	Landsat 8 OLI and Landsat 5 TM	USGS surface reflectance-derived spectral indices (Masek et al., 2006; Vermote et al., 2016)
C-band Synthetic Aperture Radar Ground Range Detected. Vertical transmit and vertical receive (VV) polarization	European Space Agency (ESA) Sentinel 1A	Sentinel-1 SAR GRD: C-band Synthetic Aperture Radar Ground Range Detected
Elevation	Shuttle Radar Topography Mission (SRTM)	National Elevation Dataset (Gesch et al., 2002; Gesch, 2007)
Latitude	na	na
LandTrendr*	Landsat 5 TM, Landsat 7 ETM+, and Landsat OLI	(Kennedy et al., 2018)
LandTrendr-fitted*	Landsat 5 TM, Landsat 7 ETM+, and Landsat OLI	(Kennedy et al., 2018)

* I tested models using LandTrendr and LandTrendr-fitted predictor variables. LandTrendr and LandTrendr-fitted variables were generated for tasseled cap brightness, greenness, and wetness, blue band, green band, red band, NIR, SWIR1, SWIR2, NBR, NDMI, and NDVI. For these bands and indices, the following metrics were calculated: accumulated minimum, duration of accumulated minimum, duration of the minimum segment, end value of the minimum segment, change of the minimum change segment, slope of minimum slope segment, percent change of minimum segment, slope of minimum change segment, and the start value of the minimum segment.

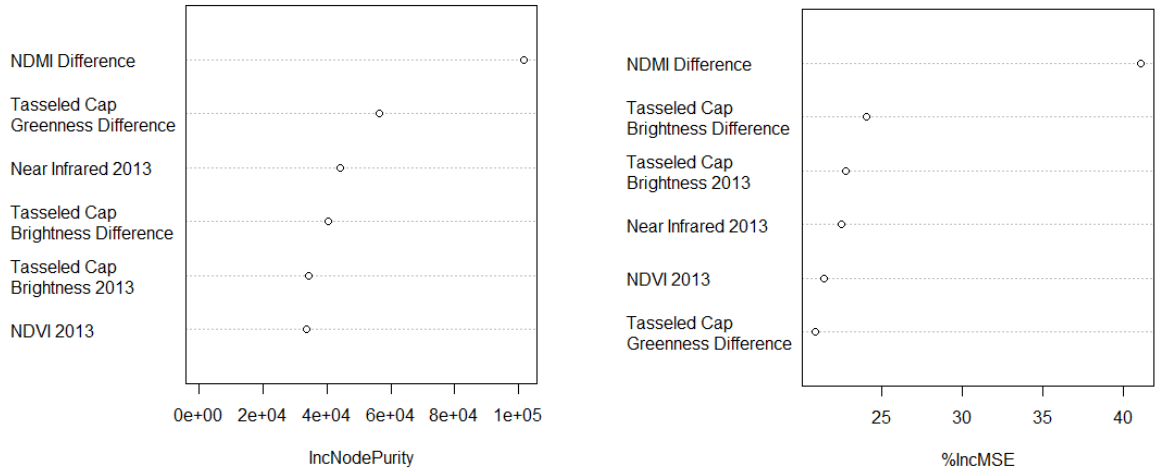

Figure A2.2. Variable importance for the random forest model used to map dead canopy percentage. Differenced variables are the differenced index between 2013 and 2001. (NDMI = Normalized Difference Moisture Index; NDVI = Normalized Difference Vegetation Index)

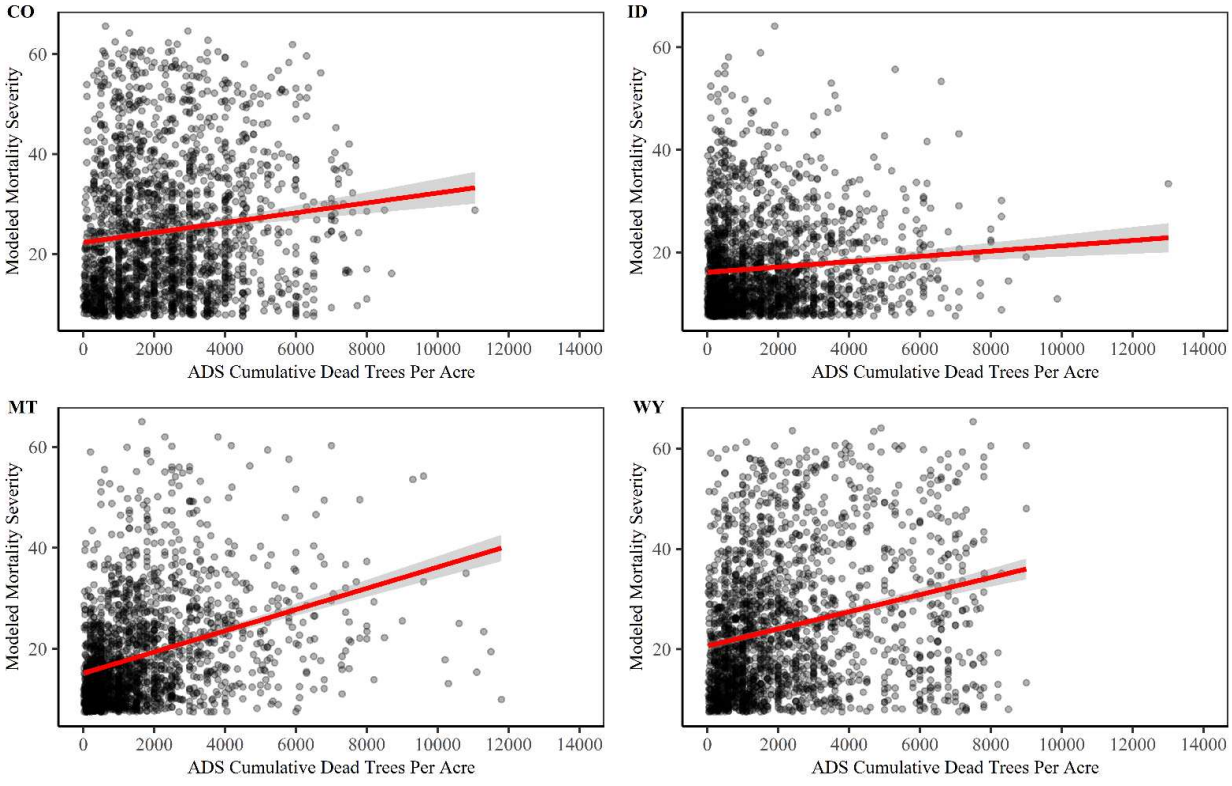

Figure A2.3. Comparison of modeled mortality severity to Aerial Detection Survey (ADS) cumulative dead trees per acre at the 2,000 random points generated in each state.

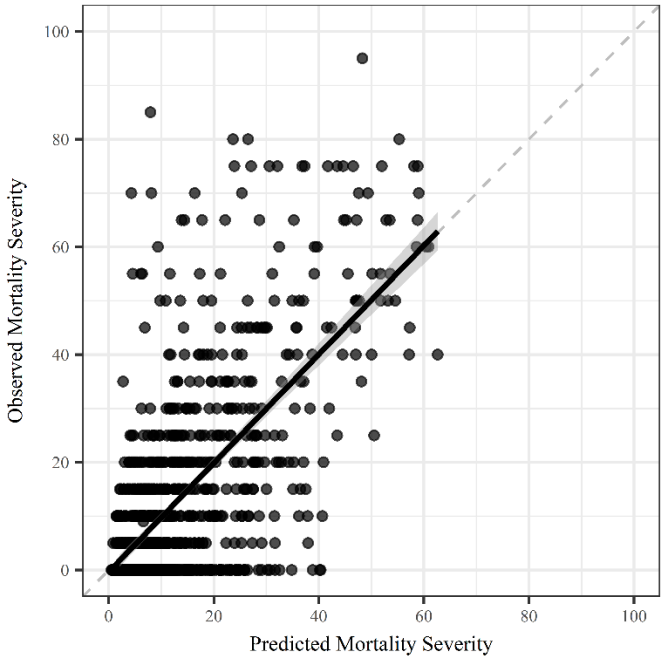

Figure A2.4. Scatter plot showing the relationship between predicted and observed mortality severity values and the 95% confidence interval. The y-intercept was 7.50 (std error=0.35), the slope was 0.4406 (std error= 0.0156).

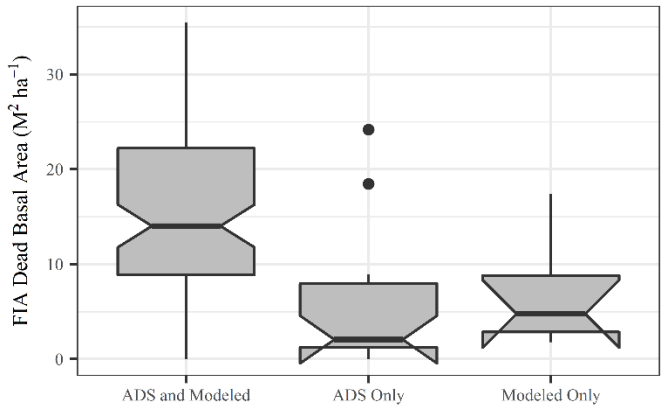

Figure A2.5. Dead basal area measured at Forest Inventory and Analysis (FIA) plots for plots that fall within areas mapped as having mortality by both Aerial Detection Surveys (ADS) and the thresholded mortality severity model ("ADS and Modeled"; N = 88), plots where ADS shows mortality but the thresholded mortality severity model does not ("ADS only"; N = 18), and plots where the thresholded mortality severity model shows mortality but ADS does not ("Modeled Only"; N = 7). Three of the FIA plots fell in areas shown not to have mortality by both ADS and the threshold model—these are not included in this figure due to the small sample size.

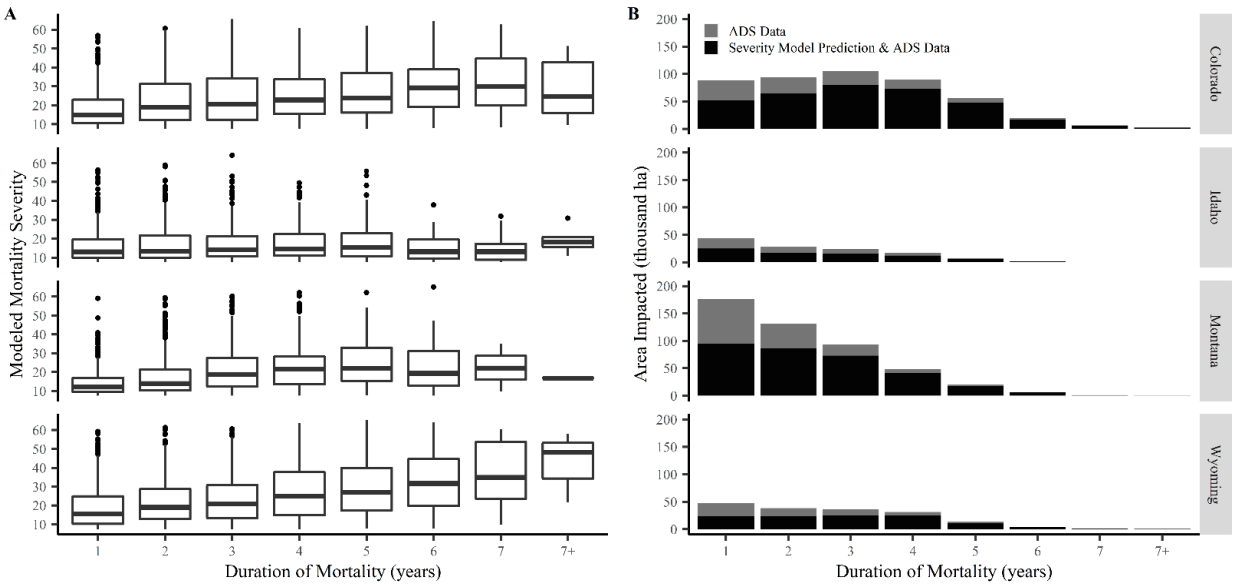

Figure A2.6. Relationship between duration and modeled mortality severity and area impacted at each of the four states.

Chapter 3 Appendices

Table A3.1. The predictor variable rasters used in this study to map dead biomass.

Predictor Variable	References
Forest Structure Products	
Standing aboveground live and dead biomass	(Vorster et al., 2020)
Tree mortality	(Bode et al., 2018)
Topography and geomorphology	(Evans et al., 2014)
Elevation and slope	(Gesch et al., 2002; Gesch, 2007)
Eastness and northness	(Kumar et al., 2006)
Compound topographic index	(Gessler et al., 1995)
Heat load index	(McCune and Keon, 2002)
Standard, profile, and planform curvature	(Moore et al., 1991; Zevenbergen and Thorne, 1987)
Roughness (3x3, 6x6, 9x9,12x12, 15x15, 21x21, 27x27)	(Blaszczynski, 1997; Riley et al., 1999)
Slope position (3x3, 6x6, 9x9,12x12, 15x15, 21x21, 27x27)	(Guisan et al., 1999; Reu et al., 2013)

Climate (1961-1990 normals)	
Chilling degree-days (degree-days below 0°C)	(Wang et al., 2016)
Growing degree-days (degree-days above 5°C)	(Wang et al., 2016)
Heating degree-days (degree-days below 18°C)	(Wang et al., 2016)
Cooling degree-days (degree-days above 18°C)	(Wang et al., 2016)
Frost-free period	(Wang et al., 2016)
Mean annual precipitation	(Wang et al., 2016)
Mean annual solar radiation	(Wang et al., 2016)
Mean annual temperature	(Wang et al., 2016)
Mean coldest month temperature	(Wang et al., 2016)
May to September precipitation	(Wang et al., 2016)
Number of frost-free days	(Wang et al., 2016)
Mean warmest month temperature	(Wang et al., 2016)
Precipitation as snow between August in previous year and July in current year	(Wang et al., 2016)
Temperature difference between mean warmest month temperature and mean coldest month temperature	(Wang et al., 2016)
Summer heat-moisture index	(Wang et al., 2016)
Annual heat-moisture index	(Wang et al., 2016)

Table A3.2. Model performance for other standing dead aboveground biomass models tested. svm = support vector machine

Model	RMSE	R^2
regression trees	38.9	0.23
random forest	33.4	0.43
svm with linear kernels	35.9	0.41
svm with radial kernels	37.8	0.30
svm with polynomial kernels	35.7	0.44
generalized linear model with step AIC feature selection	34.5	0.43
cubist	38.1	0.26
multivariate adaptive regression splines	42.6	0.16
ridge regression	34.0	0.46
k-nearest neighbors	36.7	0.31

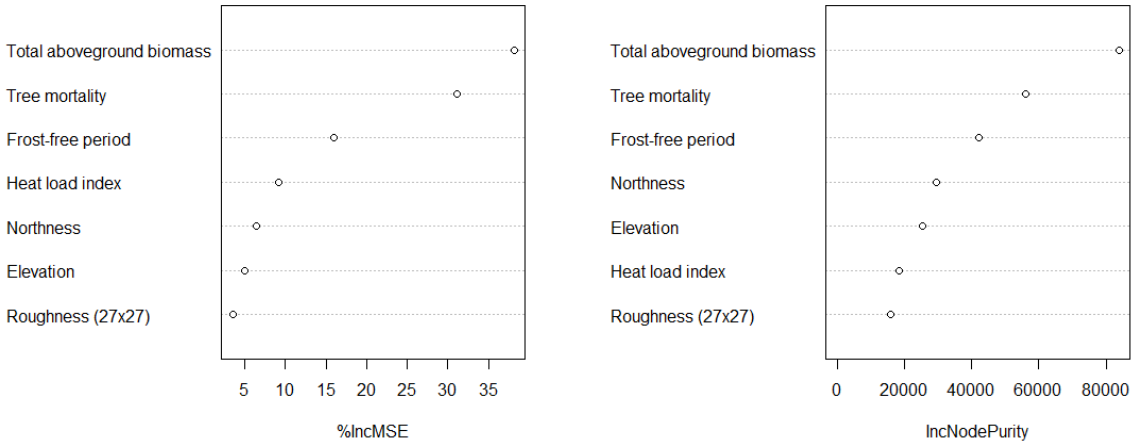

Figure A3.1. Predictor variable importance for the random forest standing dead aboveground biomass model, as measured by the average decrease in mean squared error and the mean decrease in node purity.